The Effect Of Stabilization Heat Treatment On AA5182 Aluminium Alloy

A thesis submitted to the faculty of engineering and the built environment (EBE), at the University of Cape Town, in fulfilment of the degree of Master of Science in Engineering

Prepared by:

Graham K. Morrison

Supervisor: Dr S. L. George

Co-supervisor: Prof R. D. Knutsen

Centre for Materials Engineering

Department of Mechanical Engineering

August 2013

Abstract

AA5182 aluminium alloy is used for the manufacturing of can ends for beverage cans. The alloy selection for this part is based on the formability of the material and its resistance to softening over time. Owing to the intricate design of the can end opening tab, it is vital that the material maintains its strength during its shelf life. The mechanical properties of the AA5182 aluminium alloy are dependent on the microstructural evolution of the alloy during processing and forming. Al-Mg alloys, like AA5182, can undergo a low temperature heat treatment, which has the effect of stabilizing the microstructure and minimizing the subsequent recovery processes during and after coil coating. The effects of these heat treatments have been investigated in order to understand the effectiveness of the stabilization heat treatment on the AA5182 alloy.

This study investigates various stabilization heat treatment temperature profiles, and then aims to characterize the microstructural evolution of the material during a simulation of the coil coating practice that the material is exposed to as the final step in the rolling mill operation. It is during this step that recovery can be experienced in the material that has not undergone a stabilization heat treatment. The microstructure and mechanical properties of as-cold rolled samples after simulated coil coating are compared to those of a stabilized structure after the same coil coating simulation. Mechanical properties, such as yield stress, ultimate tensile stress and work hardening coefficients, are evaluated for all the conditions. These results are then verified by microstructural characterization, using techniques such as electron backscatter diffraction (EBSD) in the scanning electron microscope (SEM) and transmission electron microscopy (TEM).

Detailed investigation was performed on the microstructural evolution during simulated coil coating, with a focus on samples that had undergone a stabilization heat treatment of 150°C for 4 hours, and samples that were in the as-cold rolled condition. The coil coating procedure was simulated by imposing 10% cold work on the samples, followed by a heat treatment at 220°C. After the coil coating simulation procedure, the as-cold rolled samples undergo dislocation recovery by subgrain formation, resulting in reduced mechanical properties compared to the stabilized samples after the same procedure. The strength in the stabilized samples is attributed to the evolution of cell block (CB) structures surrounded by dense dislocation walls (DDWs). These cell blocks form a regular Taylor lattice arrangement with their neighbours. The resulting stabilized AA5182 will retain its strength properties and not age soften to the degree that the as-cold rolled samples do.

During recovery, the stabilized AA5182 retains some of the DDWs and cell structure, while the as-cold rolled samples are seen to have a recovered structure primarily made up of distinct subgrains. These results indicate that a stabilization heat treatment at 150°C for 4 hours has the effect of slowing the recovery processes at coil coating temperatures.

Acknowledgements

I would like to thank the following people for their time and guidance during the duration of my masters:

- My supervisor, Dr. S. L. George, for her technical advice, encouragement, patience, guidance and for all the effort she put into my work.
- My co-supervisor, Prof. R. D. Knutsen, for sharing his wealth of knowledge and for his guidance.
- Mike Shirran, Francois Vlok and the good people from Hulamin for their technical support and funding.
- Paul Evans and Ricky Ricks from Technology Strategy Consultants (TSC) for their technical advice and guidance.
- Penny Park-Ross, Beverley Glass and Liezl Matthews for their support.
- Miranda Waldron, Franscious Cummings, Mohamed Jaffer and the people at the Electron Microscope Unit of UCT for the use of their SEM and TEM microscopes and their understanding with respect to my EBSD and TEM experiments.
- Glen Newins at the mechanical engineering workshop for amongst other things, his machining of required parts for the equipment I used.
- My fellow students in the CME, especially Nicholas Clinning, for amongst other things, checking on my oil bath and helping with the electron microscopes.
- Dr M. Topić, Dr C. Woolard and Prof C. Lang for their guidance over the years.
- The Vogts family for their help and understanding.
- Lastly, I would like to thank my family and friends for all their help in my times of need. I would especially like to thank my brother, Angus Morrison, for all his support.

Declaration

I, Graham K. Morrison, know the meaning of plagiarism and declare that the work carried out in this study is my own, save for the acknowledged content.

Signature.....

Date.....

List Of Abbreviations

- CES - can end stock
- SEM - scanning electron microscope/ scanning electron microscopy
- TEM - transmission electron microscope/ transmission electron microscopy
- EBSD - electron backscatter diffraction
- ECD - equivalent circle diameter
- as-CR - as-cold rolled
- %CW- the degree of cold work imposed on the metal measured in percent
- σ_e - engineering stress
- ε_e - engineering strain
- σ_t - true stress
- ε_t - true strain
- σ_{yield} - yield stress
- σ_{uts} - ultimate tensile stress
- SCCP - the simulated coil coating procedure. AA5182 specimens were 10% cold worked and heat treated at 220°C
- CSHT - the chosen stabilization heat treatment. This is 150°C for 4 hours based on the stabilization used by Hulamin in practice

List of Figures

List of Tables

Contents

Chapter 1

Introduction

1.1 Subject of and Motivation for the Report

This report concerns the effects of stabilization heat treatments on the AA5182 aluminium alloy can end stock (CES) used at Hulamin Rolled Products. A low temperature heat treatment has been found to stabilize the microstructure of the alloy from losing strength at higher temperatures. If the alloy is stabilized, the mechanical properties would not change considerably over time in the finished products which are made from the alloy. The microstructure of the stabilized CES should be investigated to understand the relationship between the microstructural arrangement and the mechanical properties of the CES.

1.2 Background to the Investigation

During the production of the AA5182 aluminium alloy CES sheet used by Hulamin, a stabilization heat treatment is used. This low temperature heat treatment is used to stabilize the microstructure from subsequent softening at higher temperatures. The AA5182 alloy is used primarily to make beverage can ends, which should be stabilized in order to minimize losses in strength over time during subsequent forming steps, such as coating and can forming. The stabilization heat treatment is results in the rearrangement of the microstructure of the AA5182 alloy. The microstructural changes are linked to the stabilization, which counteracts the softening in the alloy, which occurs by processes such as recovery.

1.3 Objectives of the Report

The objectives of this report are therefore to:

- Simulate the stabilization heat treatment used on the AA5182 CES at Hulamin
- Investigate the mechanical properties of stabilized AA5182 CES specimens compared to AA5182 CES specimens without stabilization

- Investigate and describe the microstructure observed in the AA5182 CES after the stabilization heat treatment
- Draw conclusions from the mechanical properties and microstructural investigation of the stabilized AA5182 CES
- Recommend further investigations to be carried out on the AA5182 CES to investigate the effects of the stabilization heat treatments

1.4 Limitations and Scope of the Investigation

Although many variables could have been investigated in this study, this investigation is limited to heat treatments similar to those used by Hulamin in their production of AA5182 CES. A design matrix was thus used based on the heat treatments used at Hulamin on the AA5182 alloy. The AA5182 CES specimens investigated in this study were cut in one direction, the rolling direction (RD), from the CES sheet and thus other directions, such as the transverse direction (TD), were not investigated from the CES sheet. The long-term effects of stabilization on the AA5182 specimens were not investigated due to the time constraints in this study. The focus of this study was on the effects of the stabilization heat treatment, 150°C for 4 hours, on mechanical properties and microstructure in the AA5182 CES, as this treatment most closely simulates the treatment used by Hulamin. The mechanical properties and microstructures of stabilized AA5182 specimens were compared to AA5182 specimens which had not been stabilized, in order to investigate the effect of stabilization on the AA5182 CES.

1.5 Plan of Development

This report begins with a brief description of the experimental procedure employed, which is based on the factors used in industry at Hulamin Rolled Products. The report then focuses on the mechanical properties and microstructural evolution of AA5182 CES specimens. The specimens which have had no heat treatment, the as-cold rolled (as-CR) specimens are first investigated. These as-CR specimens are used as a control for comparison purposes, as they have not been stabilized. The AA5182 specimens heat treated at various times and temperatures, according to the experimental design matrix, are then investigated. The chosen stabilization heat treatment (CSHT) of 150°C for 4 hours is then investigated further. In order to simulate the effects of the coil coating procedure used at Hulamin, the CSHT specimens are treated using a simulated coil coating procedure (SCCP). The mechanical properties and microstructures of these AA5182 specimens are then investigated, with an emphasis on transmission electron microscopy, in order to establish the microstructural arrangements in the alloy. The results of these CSHT specimens with the SCCP are then compared to those of as-CR specimens with the SCCP, to investigate the effect of stabilization on the mechanical properties and microstructure in the alloy. Attention is paid to the testing of strength properties, in the form of yield strength and work hardening

rates. The microstructural information is obtained from electron microscopy investigations using electron backscatter diffraction (EBSD) techniques. Representative micrographs are given for each condition and the information from the other micrographs for each condition are used to obtain average microstructural properties. The average mechanical properties and average microstructures of all the specimens are then summarized and discussed. Conclusions are drawn on the basis of these experimental findings. Recommendations for future work are then made based on these conclusions.

Chapter 2

Literature Review

2.1 Aluminium

Aluminium in its pure form is chemically reactive and thus it is found chiefly in the form of its impure oxide ore, bauxite. Bauxite is often found near the surface of the ground and strip mining of bauxite is therefore employed. The atomic arrangement of aluminium atoms is face-centred cubic (FCC), as shown in the unit cell in Figure 2.1.

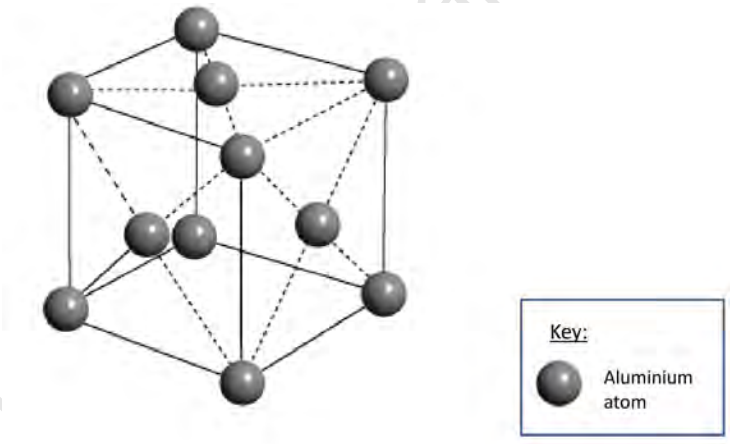

Figure 2.1: Face-centred cubic atomic unit cell representation.

2.1.1 Aluminium's Physical Properties

The physical properties of pure aluminium are summarized in Table 2.1. Compared to other metals, aluminium has a low density, a low melting point and is ductile.

Table 2.1: Physical properties of pure aluminium [1]

Property	Value
Colour	Silvery white
Crystallographic structure	Face-centred cubic
Density at 20°C (kg/dm^3)	2.699
Melting point (°C)	660.2

Unlike materials such as thermoplastics, aluminium is endlessly recyclable without losing its mechanical properties. This recyclability makes the use of aluminium an attractive, environmentally friendly option. Pure aluminium and aluminium alloys form a protective oxide layer on their surface when exposed to air. This oxide layer gives aluminium its superior corrosion resistance when compared to metals such as steel. Further coating, painting or anodizing can give aluminium and its alloys increased corrosion resistance [1].

Although magnesium is the lightest commercial metal, it is often not sufficiently strong enough to be used in engineering applications [2]. Aluminium alloys, however, have good strength to weight properties and are used in engineering applications. The density of pure aluminium is approximately 2.7kg/dm^{3}whereas that of some steels is approximately 2.9 times more at 7.9kg/dm^3[1]. Aluminium is primarily used in the aerospace, packaging, automobile, electrical and building construction industries. Aluminium is typically used where a low weight, non-corrosive, recyclable material is required [3].

2.1.2 Heat Treatable and Non-Heat Treatable Alloys

Aluminium alloys that are wrought or mechanically worked can be placed in the two classes of heat treatable and non-heat treatable alloys, as summarized in Table 2.2. To improve the mechanical properties, heat treatable alloys can undergo heat treatment processes such as solid solution strengthening or precipitation hardening. These processes usually involve solution heat treatment, where soluble elements are put into the solid solution at elevated temperatures in order to create a super saturated solid solution. Rapid cooling (quenching) is then performed on the alloy in order to "lock" the structure as it is.

Solid solution strengthening occurs when lattice strain field interactions occur between dislocations and the alloying atoms. Dislocations are imperfections or line defects in the atomic lattice structure of the metal. They result from a missing row of atoms in at least one layer in the crystal structure. The solute atoms can replace the aluminium atoms in the lattice arrangement of atoms as substitutional atoms. They also can fit in the atomic lattice as interstitial atoms, as shown in Figure 2.2. Substitutional atoms in an aluminium alloy include magnesium, manganese and copper, which have an atomic radii similar to that of aluminium alloys. Interstitial atoms have atomic radii considerably smaller than the aluminium atoms. Since the aluminium atoms have a small atomic radii, the alloying elements do not form interstitial atoms as frequently as

substitutional atoms. The alloying atoms cause a distortion in the aluminium crystal lattice, and these distorted regions impede the movement of dislocations through the alloy and thus strengthen the alloy. This strengthening is solid solution strengthening.

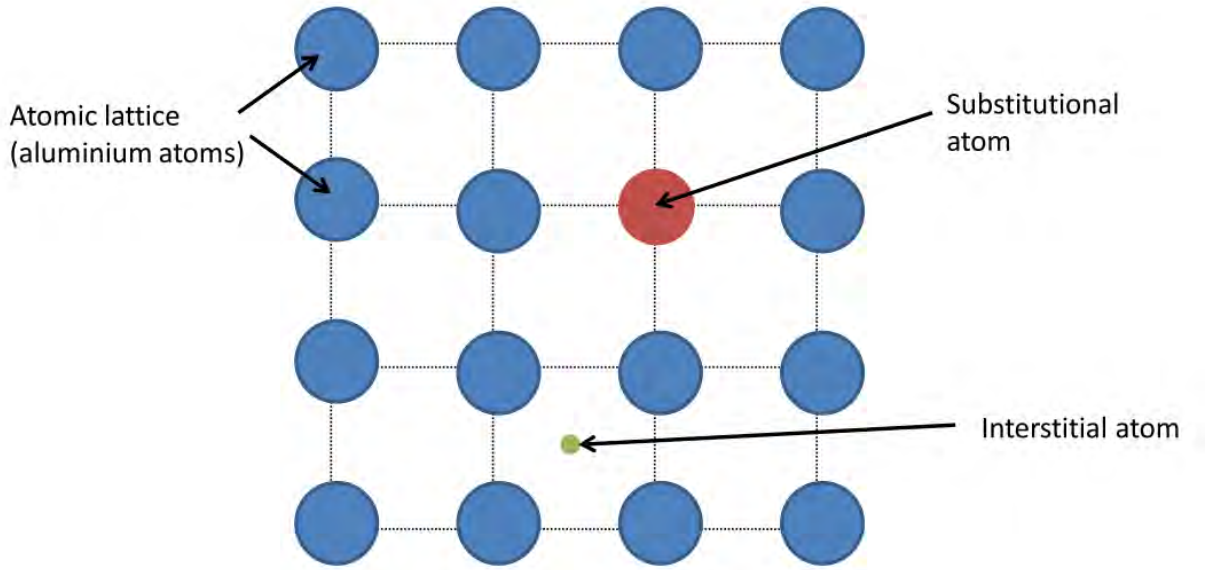

Figure 2.2: Substitutional and interstitial atoms in an aluminium crystal lattice.

The quenched, super-saturated specimens are unstable at room temperature and the constituents precipitate out of the super-saturated solution by a process called "ageing", with the alloy's yield strength increasing in the process [3]. This heating process can be controlled in order for this precipitation hardening to occur. Alloying atoms strengthen heat treatable alloys by solid solution strengthening and similarly, precipitates strengthen the heat treatable alloys by precipitation hardening. The precipitates pin the movement of dislocations, as discussed further in Subsection 2.5.2 . Finely dispersed small precipitates will strengthen the alloy more by precipitation hardening than poorly dispersed larger precipitates will.

Non-heat treatable alloys, however, rely on deformation in order to develop the required structures and mechanical properties in the alloy. This process is known as "work hardening" [1]. The mechanical properties of non-heat treatable alloys, therefore, depend on the amount of cold work introduced, for example, by rolling or drawing, after the last annealing process. The mechanical properties of non-heat treatable alloys are lost if subsequent heating is performed on the cold worked alloy [3].

Table 2.2: The main alloying elements in the wrought aluminium alloy designation system [4]

Alloy	Main Alloying Elements	Description
1XXX	Primarily pure aluminium	Do not respond to any solution heat treatment
		but can be nominally strain hardened
2XXX	Copper	Respond to solution heat treatment.
		Heat treatable
3XXX	Manganese	Do not respond to solution heat treatment.
		Strain hardenable
4XXX	Silicon	Only some alloys are heat treatable depending
		on the amount of alloying elements
5XXX	Magnesium	Non-heat treatable. Strain hardenable
6XXX	Magnesium and silicon	Heat treatable
7XXX	Zinc	Heat treatable
8XXX	Other elements (e.g. tin, nickel or iron)	The characteristics of alloys depend on
		the alloying element(s)
9XXX	Unassigned	

2.2 AA5182 Aluminium Alloy

2.2.1 AA5182 Alloy Composition and Uses

AA5XXX are aluminium alloys with magnesium as their major alloying element. They typically contain trace amounts of elements such as manganese, iron, silicon, copper and zinc (Mn, Fe, Si, Cu and Zn). The addition of small amounts of alloying elements to aluminium can improve its mechanical properties. When aluminium is alloyed with magnesium, a substitutional alloy forms, with the magnesium acting as a solid solution strengthener owing to its atomic misfit in the aluminium atomic arrangement. AA5XXX series alloys are non-heat treatable and thus do not have the ability to obtain maximum mechanical properties when solution heat treated [5]. The coordination number refers to the number of atoms an atom of a certain element can hold as its nearest neighbours. Both aluminium and magnesium have coordination numbers of 12. The metallic atomic radii of aluminium and magnesium are also relatively similar, 0.143nm and 0.160nm respectively, and thus magnesium atoms can substitute aluminium alloys in the atomic arrangement shown in Figure 2.1 [6]. The approximate chemical composition of AA5182 aluminium alloy is given in Table 2.3.

Table 2.3: Approximate chemical composition of the AA5182 aluminium alloy (wt%) [3]

Alloy	Mg	Mn	Fe	Si	Zn	Cu	Al
AA5182	4.0-5.0	0.2-0.5	0.2-0.35	0.03-0.2	0.02-0.25	0.15	Balance

Magnesium is added to aluminium as an alloying element to improve the corrosion resistance and machinability of AA5182, without impairing its ductility [7]. The presence of zinc and magnesium, as well as the protective aluminium oxide layer, make AA5182 very resistant to both atmospheric and marine corrosion [1]. Due to its good combination of strength and formability and its very good corrosion resistance, AA5182 is an industrially important alloy. Silicon is an impurity which is almost always present in Al-Mg-Mn alloys, and it is present in a range of 0.03-0.2wt% in AA5182.

AA5182 is primarily used in the automotive, aerospace and packaging industries [3]. AA5182 alloy is used in beer and beverage can ends for two and three piece can construction [3]. The AA5182 alloy in this study is used by Hulamin Rolled Products for the production of can end stock (CES) for beverage cans. The AA5182 has a melting point range between 575°C and 640°C. AA5182 is selected because of its favourable material properties, such as low density, high corrosion resistance, good recyclability, and the formability necessary for the forming of the intricate tab openings on beverage cans, as shown in Figure 2.3.

Figure 2.3: Can end showing the pull tab opening.

2.2.2 AA5182 Mechanical Properties

The approximate mechanical properties of AA5182 are given in Table 2.4 in a number of conditions at 25°C temperature, (T=25°C). The letter "O" describes the fully annealed state where the alloy

is in the 'soft' condition with the lowest strength properties experienced in the alloy under various conditions. The letter 'H' is used to describe non-heat treatable wrought alloys that have had their strength increased by strain hardening [4]. The first number after H describes the condition, such as '1' for strain-hardened or '3' for stabilized. The second number after H describes the amount of strain hardening in the alloy as a factor of the change in dimensions of the samples with respect to the original dimensions, with the number 8 typically as the hardest condition. The AA5182 alloy used in this study is in the fully hardened condition, designated H18 in Table 2.4. After stabilization heat treatment is performed on the alloy, it is in the strain-hardened and stabilized condition, designated H3X in Table 2.4. The stabilization step is described in detail in Subsection 2.3.3.

Table 2.4: Approximate mechanical properties of AA5182

[8], [3]

T (°C)	Treatment	Tensile Properties	Value
25	H18	Tensile Strength (MPa)	400
	Strain-hardened, fully hard	0.2% Yield Strength (MPa)	375
		Elongation (%)	4
25	H34	Tensile Strength (MPa)	340
	Strain-hardened and stabilized, half hard	0.2% Yield Strength (MPa)	285
		Elongation (%)	10
25	H32	Tensile Strength (MPa)	315
	Strain-hardened and stabilized, quarter hard	0.2% Yield Strength (MPa)	235
		Elongation (%)	12
25	O	Tensile Strength (MPa)	275
	Soft, annealed	0.2% Yield Strength (MPa)	140
		Elongation (%)	25

2.3 The Process Route for the Production of AA5182 Can End Stock (CES)

2.3.1 Ingot casting

An ingot of the AA5182 alloy is first cast using primary aluminium, secondary recycled aluminium and the alloying elements in precisely controlled ratios. The cast AA5182 ingot is scalped to remove a surface layer of metal which may contain defects and impurities of the casting process. AA5182 can end stock (CES) in the Hulamin Rolled Products production is formed from the AA5182 cast ingot by a rolling process.

2.3.2 Rolling

Rolling is the process of passing a metal between metal rolls in order to plastically deform the metal and reduce it's cross-sectional area. Rolling is widely used in the metalworking industry

as it allows high production and close control of the final products [9]. A rolling mill is used to roll metals and the two commonly used rolling mills, two-high and four-high rolling mills, are shown in Figure 2.4. At Hulamin, the scalped AA5182 ingot is rolled to a 23mm thick slab in the preheat hot roughing mill, which is a four-high reversing mill as shown in Figure 2.4.

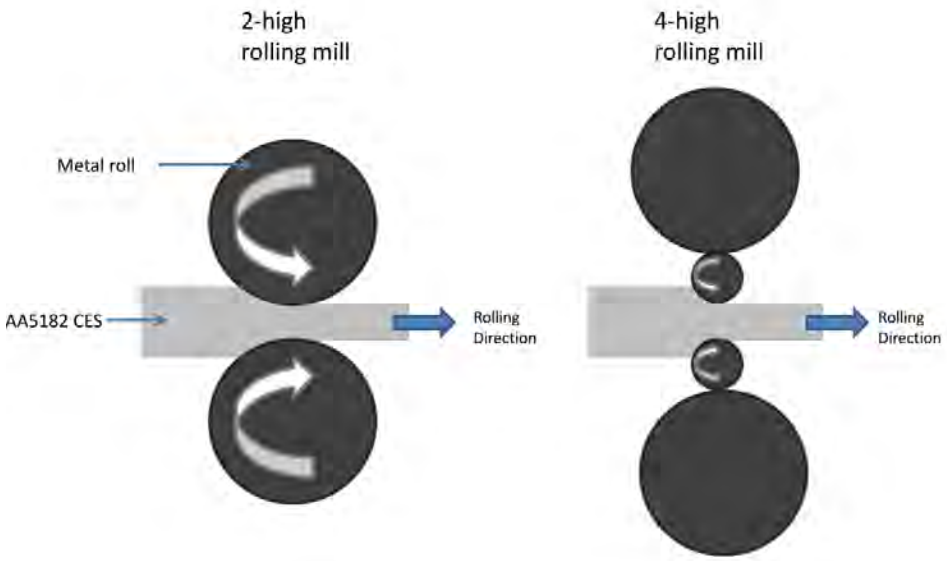

Figure 2.4: Rolling mills.

The CES is then rolled to a 2.7mm coil after 3 passes in a hot finishing mill which is also a 4-high reversing mill. The CES coil is then rolled to 0.77mm in two passes in a cold rolling roughing mill, which is a 4-high mill. The coil is then rolled in two or three passes to a gauge of 0.27mm in a cold finishing 6-high mill. The coil then undergoes a stabilization heat treatment, after which the CES coil is coated and cured. The CES coil then passes through a slitting machine which cuts the coil roll into narrower rolls before it is packed. This final gauge CES is thus stabilized, coated and can then be formed into beverage can ends or used in other industries.

2.3.2.1 Effect of Temperature in the Rolling Process

Rolling and other forming processes are often placed into the two classes of hot-working and cold-working processes. Hot working is deformation performed at temperatures and strain rates such that recovery and recrystallization processes can take place during the deformation process [9]. Cold working causes the metal grains to deform and the dislocations in the metal to multiply and tangle up, as discussed in Section 2.5. Cold working causes a change in the dimensions of the metal and an increase in strength properties and in some instances a decrease in the ductility of the metal.

In Figure 2.5, the as-cold rolled metal is shown with a high dislocation density and high strength. As the temperature of the metal increases, the metal will begin to recover at approx-

imately 195-210°C, approximately a third of the melting point (in degrees Kelvin) of the metal. During recovery, the dislocations, represented by the feint grey lines in Figure 2.5, rearrange to form a network of subgrains and the strain energy in the metal decreases, causing its strength properties to decrease, as described in Section 2.5. If the temperature is increased above a temperature of approximately 195-210°C, these subgrains will increase in size at a faster rate. A further increase in temperature, to approximately 295-310°C, will result in the onset of recrystallization, resulting in the nucleation and growth of new undeformed grains, greatly reducing the number of dislocations and, hence, further decreasing the strength of the metal. To minimize the recovery and recrystallization in CES, hot working steps are generally avoided after the strength properties are obtained from the cold rolling step. A low temperature stabilization process is later employed and is described in Subsection 2.3.3.

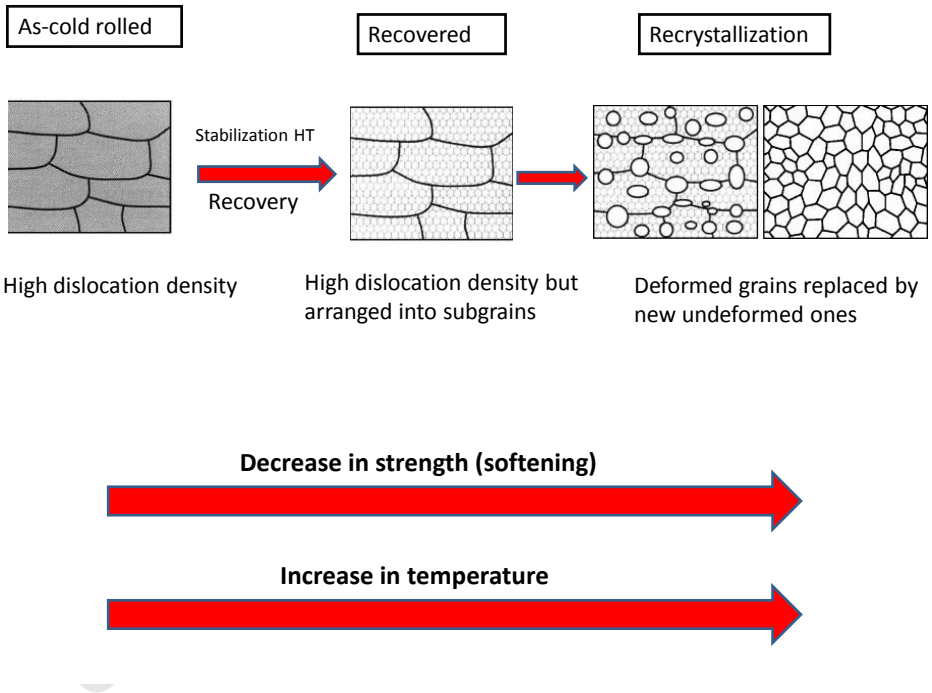

Figure 2.5: Recovery and recrystallization in AA5182, showing a decrease in strength after an increase in temperature (based on Humphreys and Hatherly).

[10]

2.3.2.2 Hot Rolling

AA5182 ingots are initially broken down into billets and blooms by hot rolling. Hot rolling is a rolling operation usually involving the use of four-high rolling mills such as the one shown in Figure 2.4. Hot rolling allows a large amount of deformation on the alloy sheet and large reduction in the thickness to be possible. Hot rolling occurs at temperatures above the recovery and recrystallization temperatures and results in a final product with reduced strength properties

and a recovered or recrystallized microstructure [3], as shown in Figure 2.5. As the temperature experienced by the metal increases, recovery and recrystallization occur in the metal, resulting in an overall decrease in the material strength.

2.3.2.3 Cold Rolling

When the rolling operation is carried out at temperatures below the recovery temperature, such as at about 180-190°C in the AA5182 alloy, it is called cold rolling. Cold rolling is often carried out after the hot rolling process, as shown in Figure 2.7, as it results in a good surface quality and a low thickness tolerance [9]. The strain hardening resulting from the cold work reduction is also often used to give increased strength to the metal. In AA5182 CES, the strength properties are largely obtained from this strain hardening during cold rolling and, therefore, this step is very important in order to obtain the desired final sheet thickness and strength properties. There are several types of rolling mills, but the most versatile and a commonly used one for this AA5182 CES is the four-high single-stand reversing rolling mill, as shown in Figure 2.4. The coiled aluminium CES is repeatedly passed through the four-high rolling mill and then recoiled on the other side of the mill until the final gauge thickness is obtained. Continuous use of alloy specific lubricants, such as certain mineral oils, are required during cold rolling [3]. The mechanical properties after the cold rolling step are close to the final CES required properties. After cold rolling, the CES is not subjected to heat treatments that will allow recrystallization of the metal and a loss of the strength properties through rearrangement of the microstructure. The grains in the heavily cold worked AA5182 alloy are elongated in the rolling direction after the cold rolling step. This is described in Section 2.5.

2.3.3 Finishing Processes

2.3.3.1 Stabilization Heat Treatment of AA5182

Stabilization is a low temperature heat treatment process used to increase ductility and stabilize mechanical properties in the strain-hardened AA5182 alloy [11]. When the AA5182 alloy is in the strain-hardened condition, its strength and hardness decrease, and the ductility increases over time at room temperature [5]. This process, known as "age softening", in Al-Mg alloys increases with an increase in the amount of cold work and magnesium content [11]. In the industrial production of AA5182 CES, the material that is in the strain-hardened condition is subjected to a low temperature stabilization heat treatment in order to complete the age-softening process, or 'artificially age' the alloy. This treatment will provide an alloy with stable mechanical properties [11]. Stabilization heat treatments used in industry for AA5182 are performed at temperatures ranging from 120°C [3][11] to 200°C [12], and for times of approximately 4 hours at 150°C [5].

2.3.3.2 Coil Coating of AA5182 CES

The coiled AA5182 sheet is coated in lacquer after the rolling and the subsequent stabilization processes, as summarized in Figure 2.7. The coating is performed at speeds of approximately 150m per minute and is applied to both sides of the coil with one or two coats per side [3]. During the coil coating process, the CES reaches temperatures of between 250°C and 260°C for up to 3 minutes. The heat curve of coated CES from Hulamin Rolled Products is shown in Figure 2.6. Using this information, the coil coating heat treatment can be simulated in the experiments in this study.

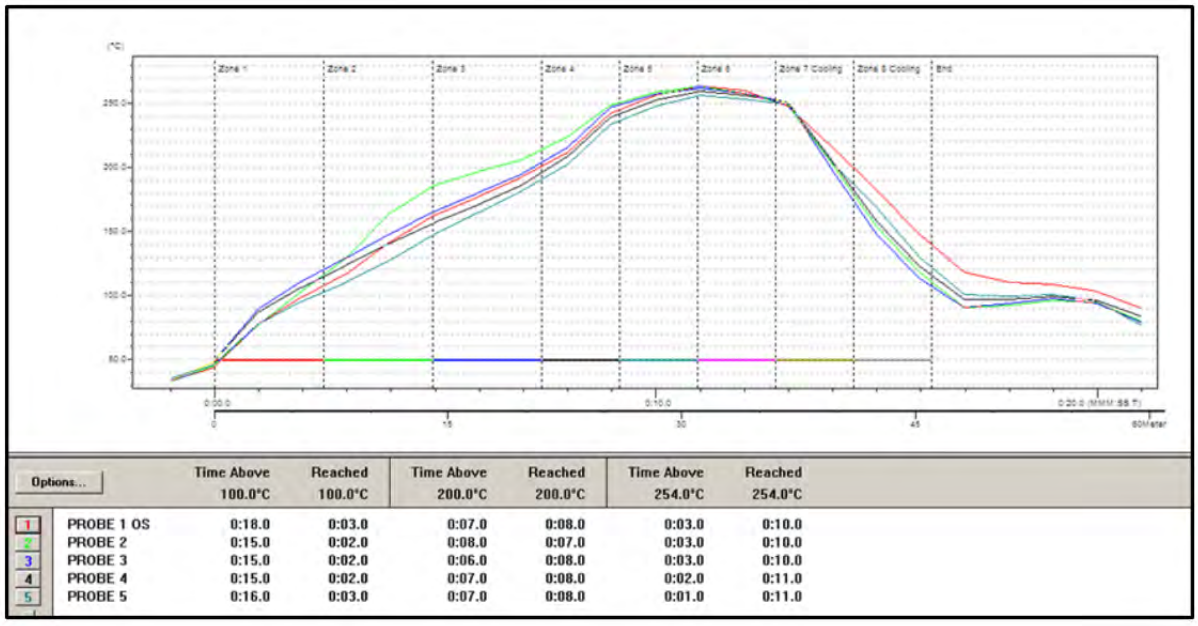

Figure 2.6: Heat curve for AA5182 can end coating on the CES used in this study.

2.3.4 Hulamin AA5182 CES

The CES production process used at Hulamin first involves the casting of an AA5182 ingot which is then scalped. This scalped AA5182 ingot is first hot rolled in a 4-high reversing hot roughing mill to a coil of 23mm thickness. This coil is then hot rolled during at least 3 passes in a hot finishing 4-high reversing mill to a coil thickness of 2.7mm. This CES coil is then cold rolled, in two passes in a 4-high roughing mill, to a 0.77mm thickness. This 0.77mm thick CES coil is then rolled in at least two passes to a the final gauge of 0.27mm in a 6-high cold finishing mill. The CES coil is then stabilized, passed through a lacquer coating stage and cured. The AA5182 CES coil is finally passed through a slitting machine to cut the coil rolls into their required dimensions before they are packed. This production process is summarized in Figure 2.7.

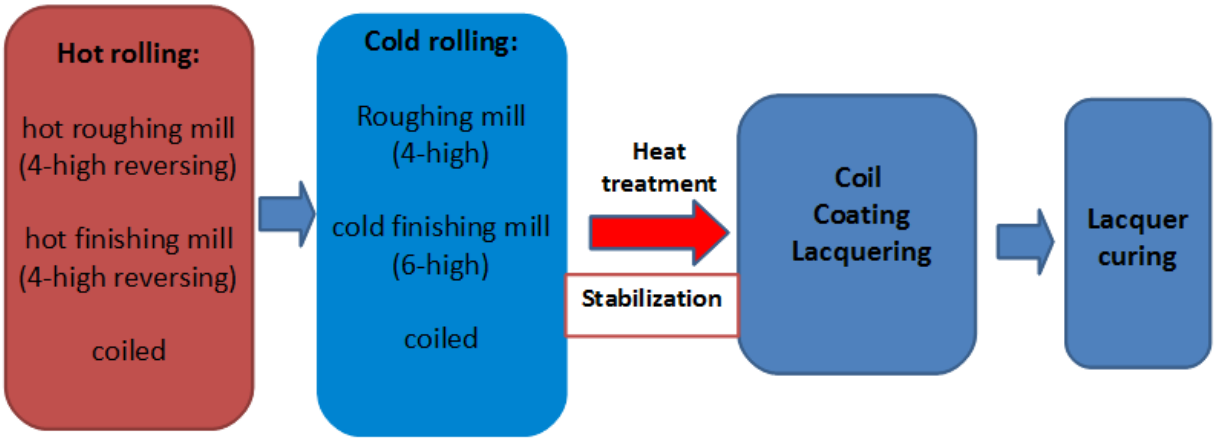

Figure 2.7: Summary of the AA5182 CES rolling process at Hulamin Rolled Products.

2.4 Mechanical Testing of AA5182 Specimens

The mechanical properties of metals are measured by performing tests such as tensile tests. In this study, a specimen in the shape of a dog bone with ends enlarged to strengthen them, as shown in Figure 2.8, is gripped at its ends and then pulled in one axis by a tensile force which gradually increases [13].

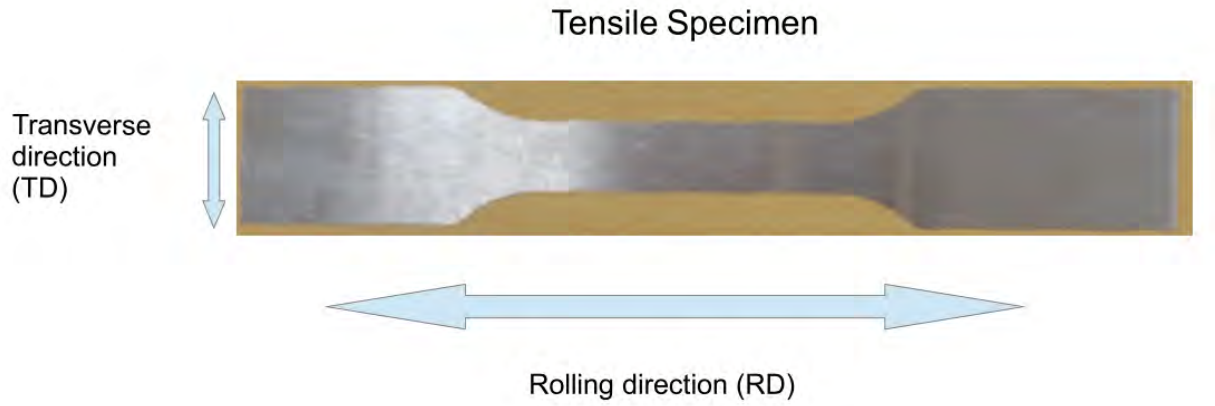

Figure 2.8: Tensile test specimen.

In many ferrous metals, there is a localized, heterogeneous transition from elastic to plastic deformation. This transition results in a sharply defined yield point in the stress-strain curve, where the deformation type changes neatly from elastic to plastic. There is, however, often no sharply defined yield point in non-ferrous metals and thus, a 0.2% proof stress yield point is used to determine the strength of the material [2]. This is illustrated in Figure 2.9 for an as-cold rolled AA5182 specimen. To calculate the 0.2% proof yield stress in Figure 2.9, a line, AB, is drawn

from A, the 0.2% strain value, parallel to the elastic portion of the stress-strain curve. This line cuts the stress-strain curve at B and the stress value corresponding to B is the 0.2% proof yield stress value. The actual elastic limit or yield stress point thus occurs slightly before the point B shown in Figure 2.9.

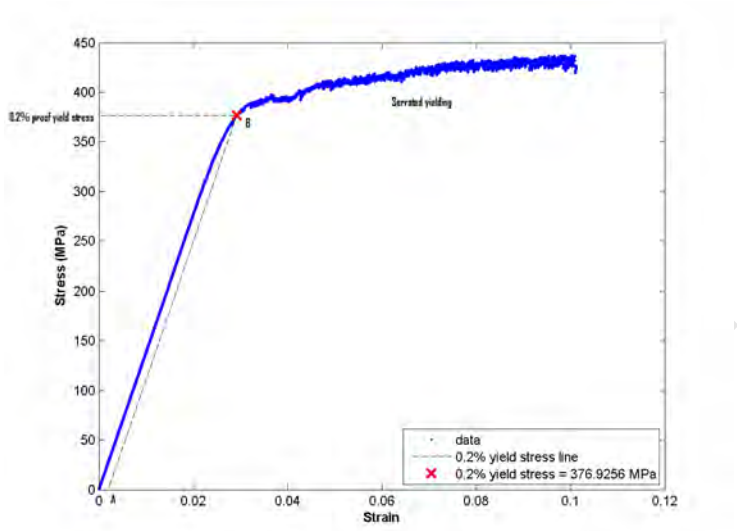

Figure 2.9: Engineering stress-strain curve for as-cold rolled AA5182.

2.4.1 The Portevin–Le Chatelier Effect and Serrated Yielding

Serrated yielding, as shown in Figure 2.9, is also known as the Portevin–Le Chatelier (PLC) effect. The Mg content in aluminium alloys, such as AA5182, is the main factor responsible for the PLC effect in these alloys [14]. The serration magnitude (the difference between the peak and trough in stress) and intensity (the frequency of serrations) both increase with an increase in the magnesium content in the aluminium alloy [15]. A large number of magnesium atoms precipitate out of solid solution in AA5182 specimens tested at low temperatures and thus the magnitude, as defined previously, of the serrations decreases [16]. The time taken for serrations to appear after the yield point is also longer for the specimens in which a large amount of Mg atoms precipitate out of solid solution [15]. During a tensile test of AA5182, there is an increase in the magnitude of serrations as strain increases [15]. An increase in the grain size in the specimen will also result in a decrease in the magnitude of serrations as there are fewer areas of high dislocation density where the mobile dislocations can be pinned [15]. The PLC effect occurs due to dynamic strain ageing at obstacles where the dislocations are pinned. The Mg atoms diffuse to these pinned dislocations and increase the effect of impeding their motion. Dynamic strain ageing is a strengthening mechanism owing to the effect of interstitial and substitutional atoms, such as Mg atoms in AA5182, impeding the motion of dislocations in the material [15]. Since the PLC effect is related to this strengthening mechanism, it results in an increase in strength of the AA5182 but may also result in a decrease in the ductility [14].

As the strain increases from about the point B onwards in Figure 2.9, the stress value fluctuates with increasing strain. A step forms directly after B where strain occurs without an increase in force as numerous dislocations become unpinned from the solute solution. Soon after this phenomenon begins, at about point B on the curve, a number of discrete bands or surface markings can be seen forming at approximately a 45° angle to the tensile axis along the surface of the tensile specimen during the tensile test. An audible pinging sound, or acoustic emission, occurs in AA5182 tensile specimens during tensile tests and this is related to the number of Mg atoms actually physically participating in the dynamic strain ageing process in the specimen. During this process, there is an accompanying formation of these bands, which are shown in Figure 2.10.

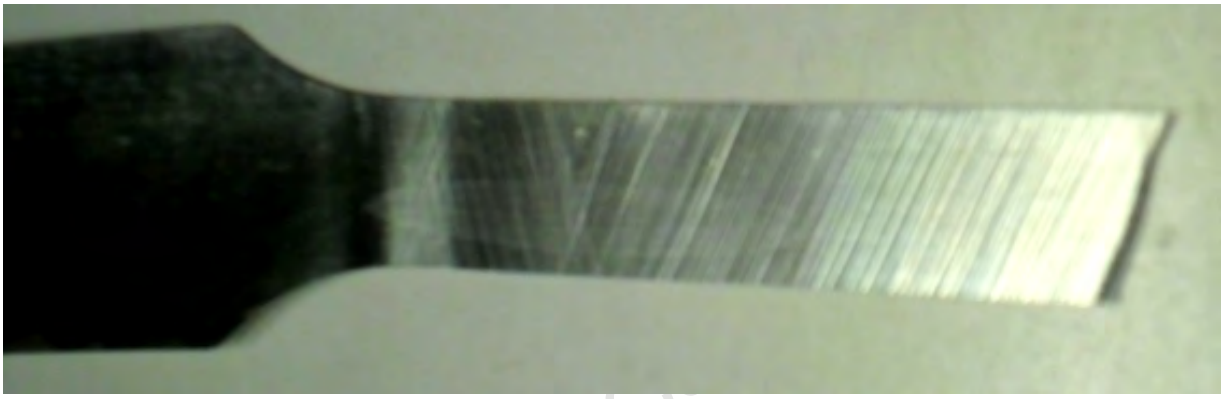

Figure 2.10: Serrated yielding parallel bands on the surface of an AA5182 tensile test specimen pulled in the rolling direction.

When the motion of a dislocation through a material is impeded by forest dislocations or solute particles, it is pinned by these particles or dislocations. The dislocation is also pinned by other dislocations which may diffuse around this dislocation and further increase the effect of impeding the motion. As the stress applied to the material increases, the dislocation will obtain sufficient energy to overcome the obstacles to its motion and one of these parallel surface markings will form. This dislocation will then move through the material until it is impeded once more and the process continues until the tensile specimen fractures under the applied tensile stress. These bands are usually called Lüders Bands and each irregular jog on the stress-strain curve corresponds to the formation of a new Lüders band. Lüders bands are localized regions of plastic deformation. This period of Lüders band propagation is known as serrated yielding. After the Lüders bands have propagated across the entire specimen in other alloys, the stress-strain curve may smooth out, but in the AA5182 alloy the serrated yielding continues until the specimen fractures [9][15]. There are two general types of serrations, Type A and Type B, depending on their magnitude. Type A are continuously propagating curves followed by abrupt drops in the stress values as strain increases, whereas Type B are more irregular serrations or fluctuations of generally lower magnitude [16]. AA5182 has both Type A and Type B serrations. There is, however, a higher magnitude of Type B serrations than Type A serrations in AA5182. The occasional high magnitude Type A serration "spikes" are not obvious in AA5182 due to the

prevalence of Type B serrations. The magnesium concentration is related to the serrations in the AA5182 alloy [16].

2.4.2 Work Hardening

Work hardening, also referred to as strain hardening, is the progressive increase in the resistance of the material to further cold work or deformation. Work hardening occurs during the cold rolling process described in Subsection 2.3.2, and results in an increase in the tensile strength with an increase in the amount of cold work on the material. Work hardening is the principle procedure for strengthening of non-heat treatable aluminium alloys such as AA5182, unlike heat treatable alloys which can, for example, also be precipitation hardened. Although the yield strength of aluminium will increase as the amount of cold work increases, this increase due to work hardening may not be permanent as it is counteracted by the softening due to recovery of the material when heat is generated during the cold working process [11]. Work hardening begins after the CES has yielded and has begun to plastically deform. A logarithmic plot of true stress against true strain results in an n-value slope after the CES has yielded. The work hardening exponent n-values lie between 0.10 and 0.50 for most metals. The n-value relates the ability of a metal to be stretched or formed during metalworking operations [11]. A higher n-value is obtained for a metal with a higher formability, with a n-value of 1 representing a perfectly elastic solid and a n-value of 0 representing a perfectly plastic solid. A high n-value is expected in metals which display a greater tendency for plastic deformation to become uniform when an increase in flow stress is applied to the metal. This n-value is an important indicator as it tells of the formability of the metal and of the maximum uniform reduction in dimensions possible during processes such as cold rolling or deep drawing. The method of work hardening is further discussed in Subsection 2.5.2. The typical n-values for aluminium alloys in the annealed condition are shown in Table 2.5. The n-values for strain hardened alloys will be lower than these values, as previous cold work decreases the ability of the alloy to undergo subsequent cold work.

Table 2.5: The work hardening exponent (n) for aluminium alloys in the annealed condition [11]

Aluminium Alloy	**Work hardening exponent (n)**
AA1100	0.242
AA3003	0.242
AA5052	0.198
AA5086	0.193
AA5454	0.189
AA5456	0.178
AA6061	0.209

The engineering stress-strain curve is based on the original dimensions of the tensile specimen and not the continuously changing dimensions during the tensile test and, thus, it does not

give a true representation of the deformation in the specimen. AA5182 specimens continue to strain-harden from the yield point until they fracture and this is represented properly on a true stress-strain curve, as shown in Figure 2.11. True stress, given in Equation 1, is the force at any instant in the tensile test divided by the cross-sectional area of the tensile specimen at that same instant [9]. True strain values, determined by Equation 2, are the strain values based on the instantaneous strain measurements and, together with true stress values, can be used to draw a true stress-true strain curve.

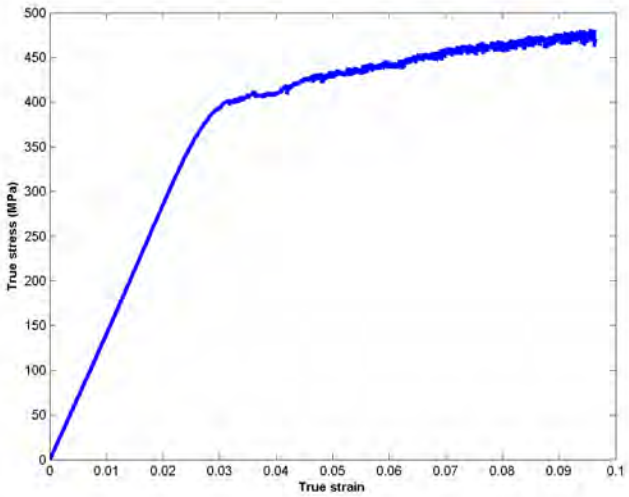

Figure 2.11: True stress-strain curve for as-cold rolled AA5182.

In order to convert the engineering stress-strain curves into true stress-true strain curves and then calculate the work hardening exponent, the following equations are used:

1. True stress, $\sigma_t = \sigma_e(1+\varepsilon_e)$ **Equation 1**
2. True strain, $\varepsilon_t = \ln(1+\varepsilon_e)$ **Equation 2**
3. True stress, $\sigma_t = K\varepsilon_t^n$ **Equation 3**
4. $n = \frac{d\ln\sigma_t}{d\ln\varepsilon_t}$ **Equation 4**

where σ_e is the engineering stress, ε_e is the engineering strain, K is the strength coefficient and n is the work hardening exponent [9]. The work hardening exponent obtained from these curves is limited to the gradient of a straight line and does not follow the serrated pattern present in the AA5182 alloy's stress-strain curve data.

By creating a logarithmic plot of the true stress-true strain data after the yield point, a relationship between true stress and work hardening can be determined, as described in Equation 3. When the logarithmic values of the true stress and the true strain are then plotted, a graph is

obtained, such as Figure 2.12 for the as-cold rolled AA5182 specimens. The gradient of the plastic region (after the yield point) of the curve in Figure 2.12 gives the work hardening exponent, the n value, which is described in Equation 4. As a result of the serrated yielding effect discussed in Subsection 2.4.1, this curve is not a straight line and thus the line of best fit is used to obtain the work hardening exponent, n.

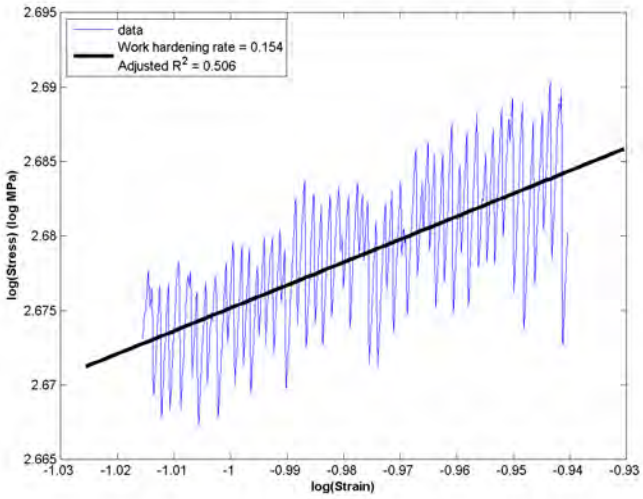

Figure 2.12: The logarithmic true stress-true strain curve for as-cold rolled AA5182 after the yield point.

This plastic deformation portion of the logarithmic true stress-true strain curves may have a "step" phenomena where a rapid increase in strength is observed in the work hardening rate (WH rate). The gradients are labelled "A", "B" and "C" for these stepped curves, as shown in Figure 2.13. The "C" part of the curve is most closely related with the WH rate and is compared in the samples in different conditions. The work hardening property can also be seen in the relative difference between the 0.2% yield stress and ultimate tensile strength in specimens. If these values are wide apart, a higher work hardening is expected compared to if the values are close together.

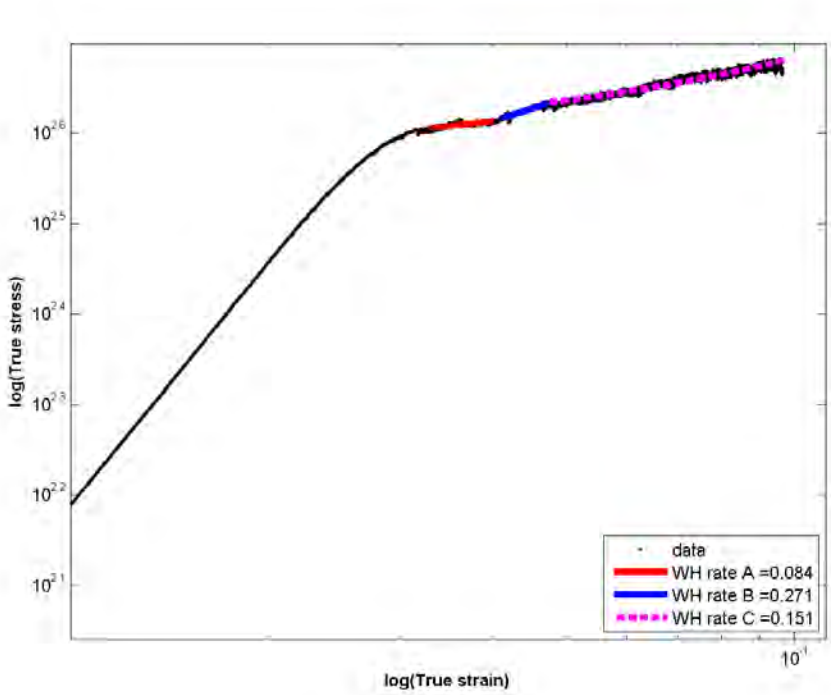

Figure 2.13: Logarithmic true stress-true strain curve for an AA5182 specimen in the as-CR condition showing a stepped work hardening rate with gradients A, B and C.

2.5 Microstructure of AA5182 CES

Cold working of AA5182 results in a deformed microstructure with the grains elongated in the direction of metal flow as shown in Figure 2.15. The as-cold rolled AA5182 grains are elongated in the rolling direction (RD). Plastic deformation in the form of cold work results in an increase in the number of dislocations in the alloy, which by virtue of their interaction, results in a higher state of internal stress in the alloy. Dislocations are imperfections or defects in the crystal lattice of a metal in which there is an extra row of atoms in the crystal lattice. In order to minimize the strain energy in the lattice, the atoms neighbouring this extra row of atoms are displaced, forming the dislocation. An example of a dislocation is shown in Figure 2.14.

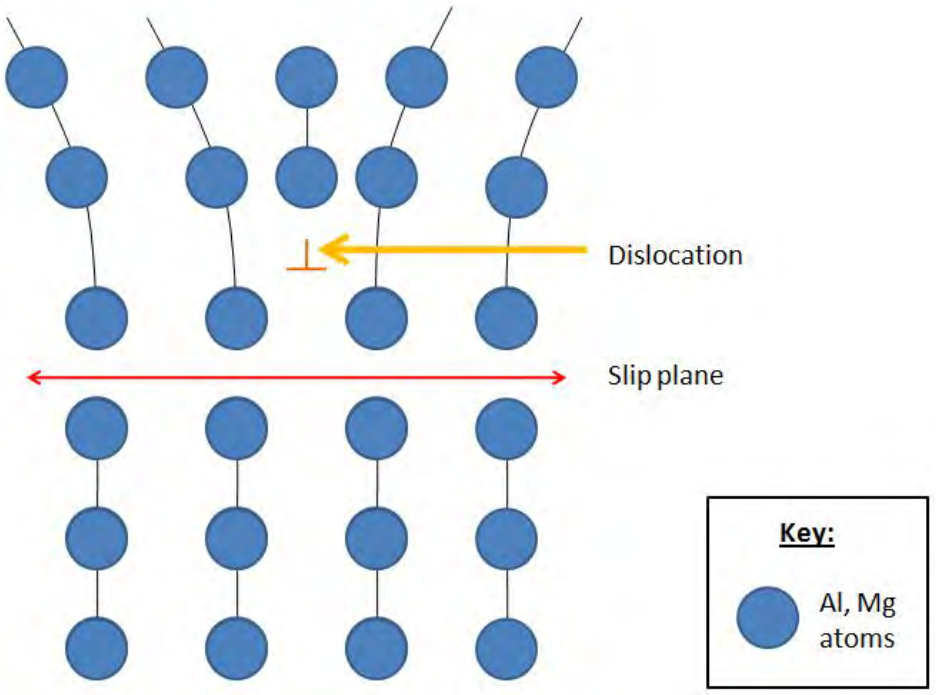

Figure 2.14: Schematic diagram of a dislocation in an Al-Mg alloy

When the metal is cold worked, most of the energy used to deform the metal is lost as heat but some of the energy is stored in the lattice, causing an increase in internal energy in the metal. Much of the stored internal energy in the cold worked metal is due to the generation and interaction of dislocations during the cold working process [9].

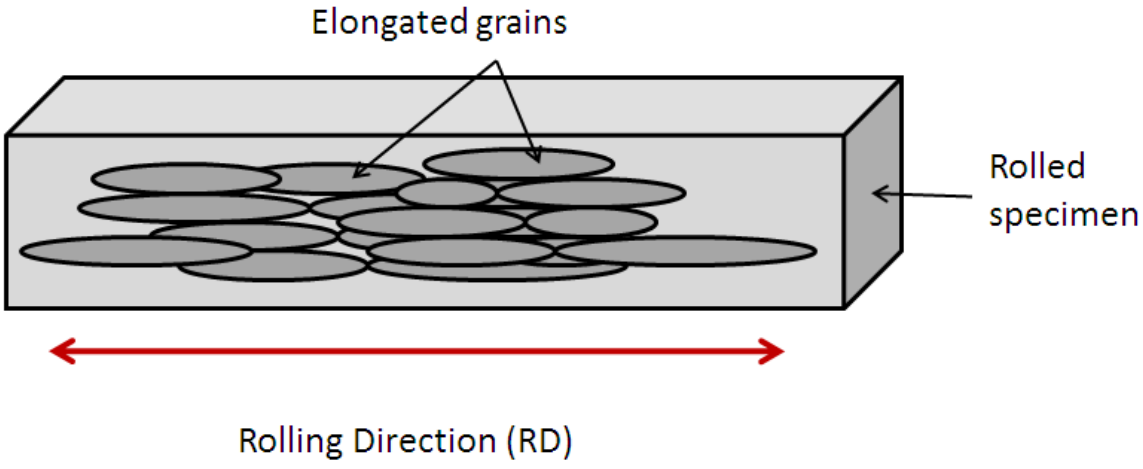

Figure 2.15: Schematic illustration of an elongated microstructure of a rolled metal.

2.5.1 Grain Boundaries

A grain boundary is a boundary between areas of different crystallographic orientations. In effect, when the crystal lattice or atomic arrangement is disturbed, a grain boundary is formed. Grain boundaries are separated into High Angle Grain Boundaries (HAGBs) and Low Angle Grain Boundaries (LAGBs). A HAGB is a grain boundary between two regions with a difference in crystallographic orientation of greater than a chosen threshold value of about 10° to 15°, whereas a LAGB is any other grain boundary between two regions with a difference of about 2° or more in crystallographic orientation [10]. LAGBs are an arrangement of dislocations spaced sufficiently far apart that the dislocation cores do not overlap. Only a fraction of the atomic bonds in LAGBs are highly distorted and thus a lower energy is associated with the LAGBs than the HAGBs. HAGBs have a larger fraction of highly distorted dislocations, broken bonds and free volume due to poor atomic fit across the interface [17].

2.5.2 Work Hardened Microstructure

When a metal has been previously plastically deformed, it has an increased number of dislocations and their interactions, resulting in an increase in the subsequent required stress to cause slip in the metal. The metal in this state is said to be 'work hardened' or 'strain hardened' [9]. The interaction and entanglement of dislocations with each other and with barriers which impede their motion, as shown in Figure 2.16, cause work hardening. These dislocations may be edge or screw dislocations. The dislocations pile up at barriers, forming 'back stress' on the slip planes, and opposing the applied stress [18] [9]. Work hardening also occurs when dislocations moving in one slip plane cut through other dislocations in another active slip plane. These dislocations intersecting the active slip plane are called a 'dislocation forest' [9]. These dislocations in multiple slip planes in the metal result in an appreciable increase in work hardening. Work hardening due to forest dislocations is temperature and strain-rate dependent and can thus be overcome by thermal treatments. Work hardening due to dislocation pile-ups at precipitates and other barriers is less dependent on temperature and strain rate as it occurs over longer distances than dislocation forests. Around the tangled dislocations in the CES are stress fields which interact. To move these tangled dislocations thus requires more stress than if they were not tangled.

Another name for the effect of small particles preventing the motion of dislocations is 'Orowan pinning' [17]. These particles exert a pinning force which counteracts the force pushing the LAGBs and HAGBs. This Orowan pinning has an important influence on preventing recovery, recrystallization and grain growth in a metal. This pinning results in strengthening of a metal by work hardening and prevents softening by recovery. The region of the dislocation boundary nearest the particle is pinned while the other regions of the dislocation continue to move along the slip plane, resulting in a curved dislocation boundary anchored by the particles as shown in Figure 2.16.

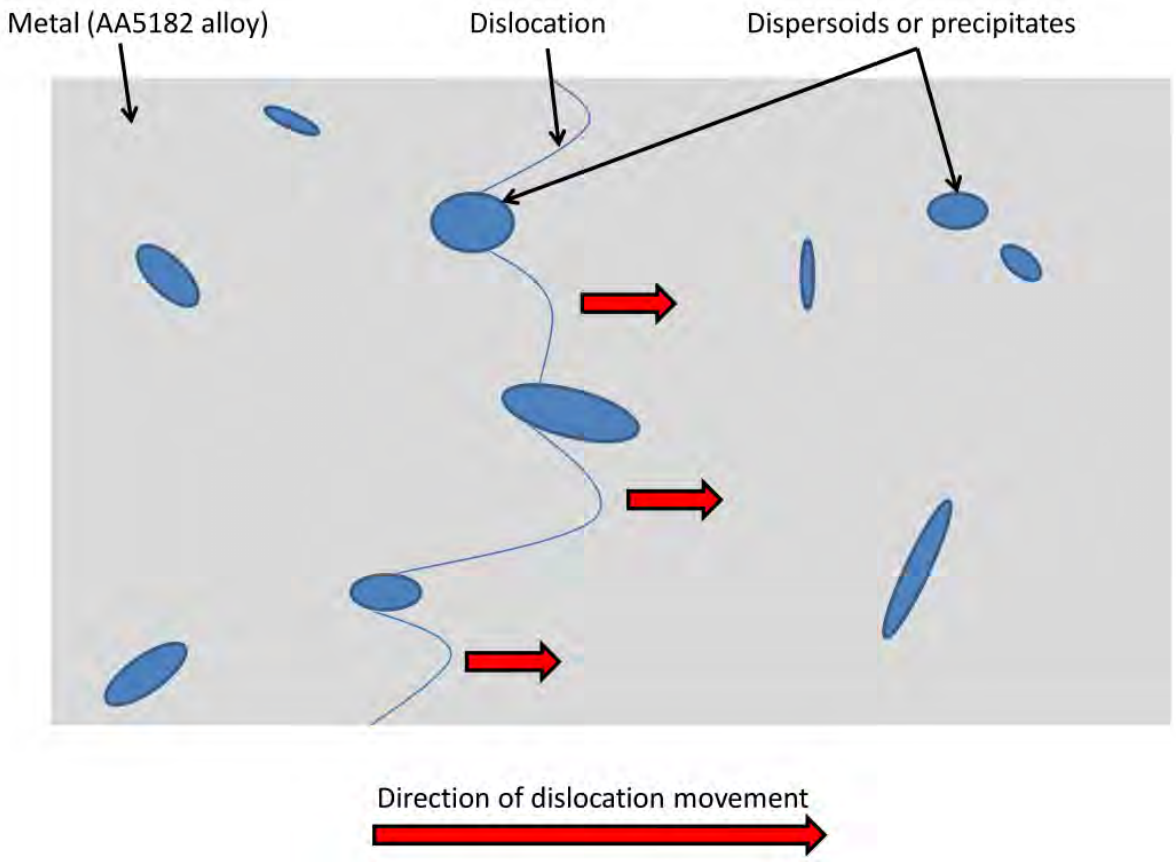

Figure 2.16: Orowan pinning of dislocations by dispersoids and precipitates.

These dislocations are impeded by obstacles, such as dispersoids, but also by other entangled dislocations which are also called 'dislocation forests'. The ability of dislocations in a material to pass around these obstacles to their motion is referred to as 'cross-slip'. The work hardening n-value is low in materials with few entangled dislocations and obstacles, and thus cross-slip is easier in these materials than in materials with high n-values. In metals, a n-value of about 0.1 is relatively low whilst a n-value of about 0.5 is relatively high, as most metals exhibit n-values of between 0.1 and 0.5.

2.5.3 Dispersoids

Dispersoids are arrays of fine particles which precipitate, often during low temperature heating procedures, from an alloy's solid solution. These dispersoids may strengthen the alloy by pinning dislocations as described in Subsection 2.5.2. An example of these dispersoids is shown in the TEM micrograph in Figure 2.17.

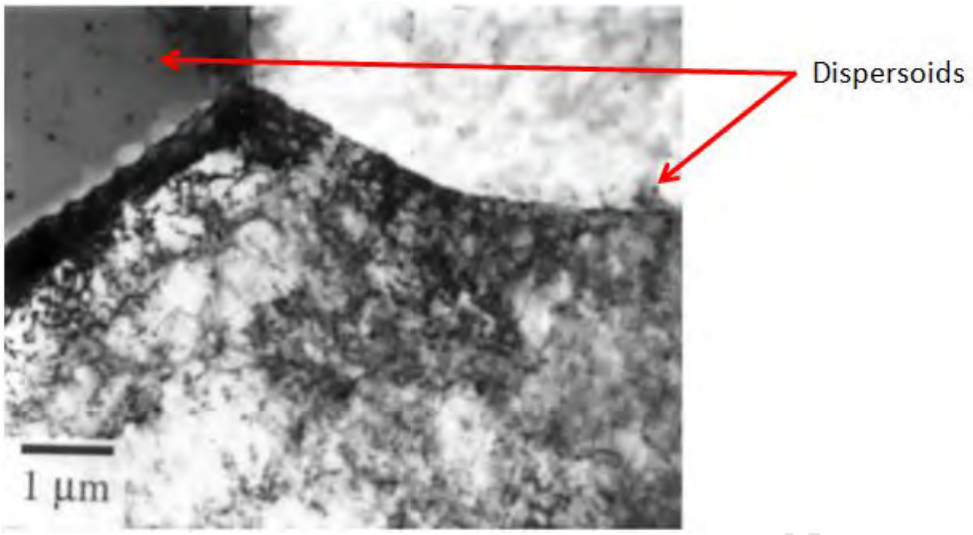

Figure 2.17: A TEM micrograph of an as-cold rolled Al-2.5Mg alloy showing small precipitates in the upper left grain.

[19]

Based on EDS analysis, the rhomboidal, rod and needle shaped precipitates which form in AA5182 aluminium alloys are Al_6(Fe, Mn) phase with a composition of about 16wt%Mn, 6wt%Fe, 47wt%Al [20]. The formula Al_6(Fe, Mn) infers that six aluminium atoms form bonds with either one atom of iron or one atom of manganese. The Al_6Mn phase is shown in Figure 2.18.

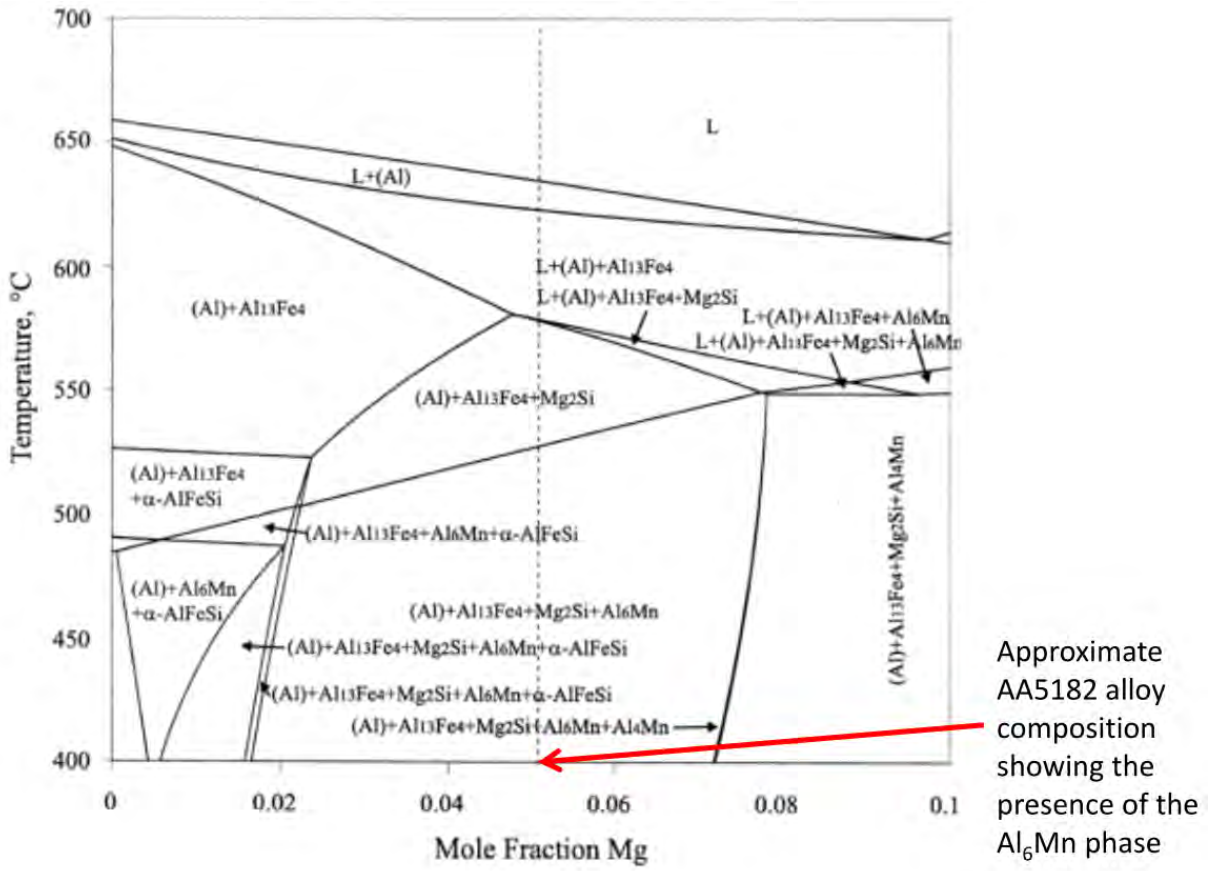

Figure 2.18: A phase diagram calculated for the Al–Mg alloy with fixed values of 0.28wt% Fe, 0.34wt% Mn and 0.1wt% Si (based on work by Yan et al., 2001), showing the Al_6Mn phase for the AA5182 alloy at 400°C.

With an increase in the amount of silicon in the aluminium alloy as an alloying element, Al_6(Fe, Mn)Si dispersoids may also form. There is also evidence that there is the formation of Al_3Mg_2 in AA5182, especially at grain boundaries [14] [20]. These dispersoids may pin the dislocations in AA5182 and thus resist the growth of the subgrains.

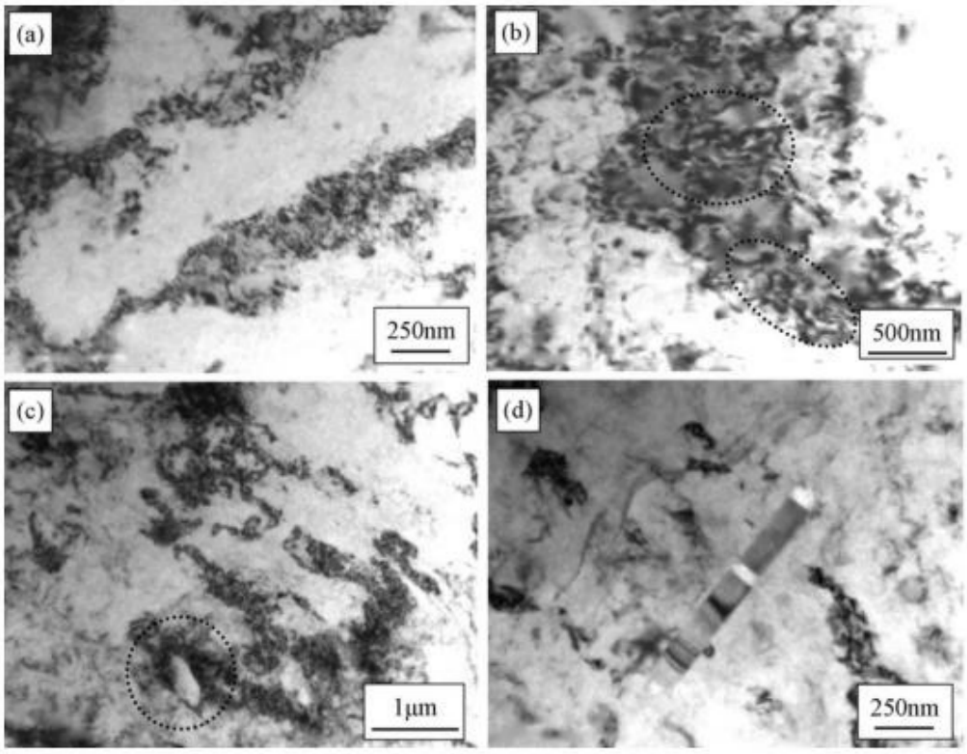

Figure 2.19: TEM micrographs for an Al-4.97wt%Mg-0.74wt%Mn-0.35wt%Er aluminium alloy showing dislocations and the Al_6(Fe, Mn) phase in the sample homogenized at 510°C for 16h, hot rolled, cold rolled and stabilization annealed: (a) substructures; (b) high density dislocations in a dislocation wall; (c) tangled dislocations around Al_6(Fe, Mn) phase; (d) cracked Al_6(Fe, Mn) phase by cold rolling.

[20]

2.5.4 Shear Bands

Shear bands are narrow discontinuity zones of high localized strain in a metal lattice developed during severe deformation. Shear bands are often formed in rolled metal in regions with true strain of more than one (true strain>1) and tend to be orientated at approximately 35° to the RD plane. Shear bands typically cut across many existing grain structures as shown in the AA5182 alloy in (b) in Figure 2.20. An example of shear bands is also shown in Figure 2.21 for the Al-1Mg alloy.

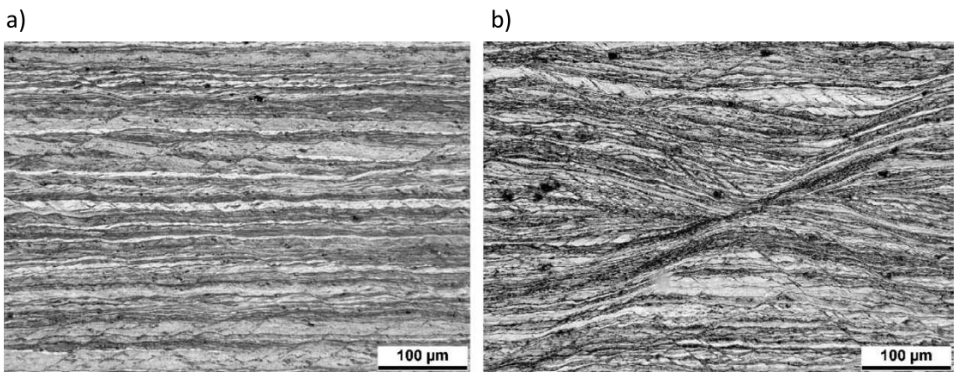

Figure 2.20: Light micrographs after 95% cold rolling showing elongated grains of (a) AA5005 and (b) AA5182 with macroscopic shear bands.

[21]

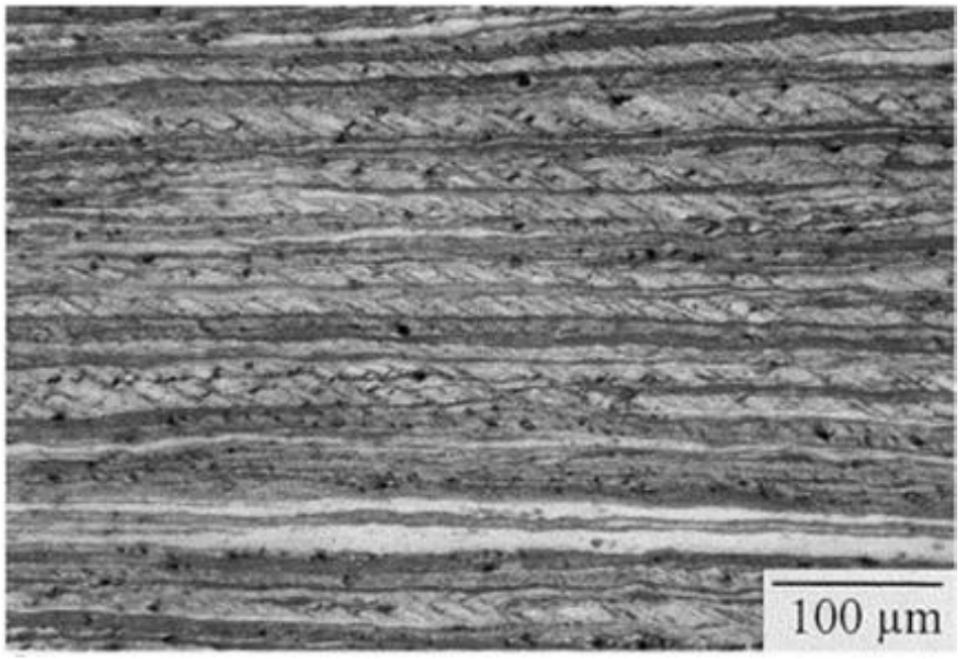

Figure 2.21: Light micrographs showing shear bands in the Al-1Mg alloy for a symmetric flow pattern.

[22]

In Figure 2.20, (b) shows that the AA5182 sample has large macroscopic shear bands cutting through a large section of the sample thickness whereas in (a) the AA5005 sample's shear bands are restricted to a few of the deformed grains. The micrographs in Figure 2.20 also show the presence of second-phase particles in the order of microns in the aluminium alloys. The average size of these particles in AA5182 was found to be about 2.4µm with a volume fraction of 1.1% when the alloy was not cold worked and 2.0µm with a volume fraction of about 1.1% for the AA5182 alloy with a rolling strain of 3 [21].

2.5.5 Deformation Mechanisms and Stacking Faults

Dislocation slip and deformation twinning are the two primary deformation mechanisms exhibited by a crystal lattice to accommodate large strains. These lattice deformation mechanisms are illustrated further in Figure 2.23. In FCC metals such as aluminium alloys, the stress required to form deformation twinning is greater than that needed to form dislocation slip. Aluminium has a high stacking fault energy (SFE) and thus rarely shows twinning [21][9]. Deformation twins have, however, been experimentally observed on the edges of thinned aluminium TEM specimens [23].

Faults or inconsistencies in the stacking sequences can occur in the atomic lattices of metals which have been severely cold worked. Stacking faults are interruptions in the stacking sequence of atom planes on each other and usually consist of one or two layers of atoms. Such stacking faults are represented in Figure 2.22, where the blue circles represent atoms and the dotted red lines indicate a fault lines. These faults can alter the atomic lattice in an area, for example, from face centered cubic (FCC) structures to hexagonal close packed (HCP) structures which differ from each other only in their stacking order. The FCC arrangement shown in Figure 2.22 is represented as the arrangement ABCABCABCABC. Stacking faults in the FCC structure are shown by the dotted red line in Figure 2.22 as a missing A plane for the intrinsic stacking fault (ABCABC_BCABC) and an extra C plane for the extrinsic stacking fault (CABCACBCABCA).

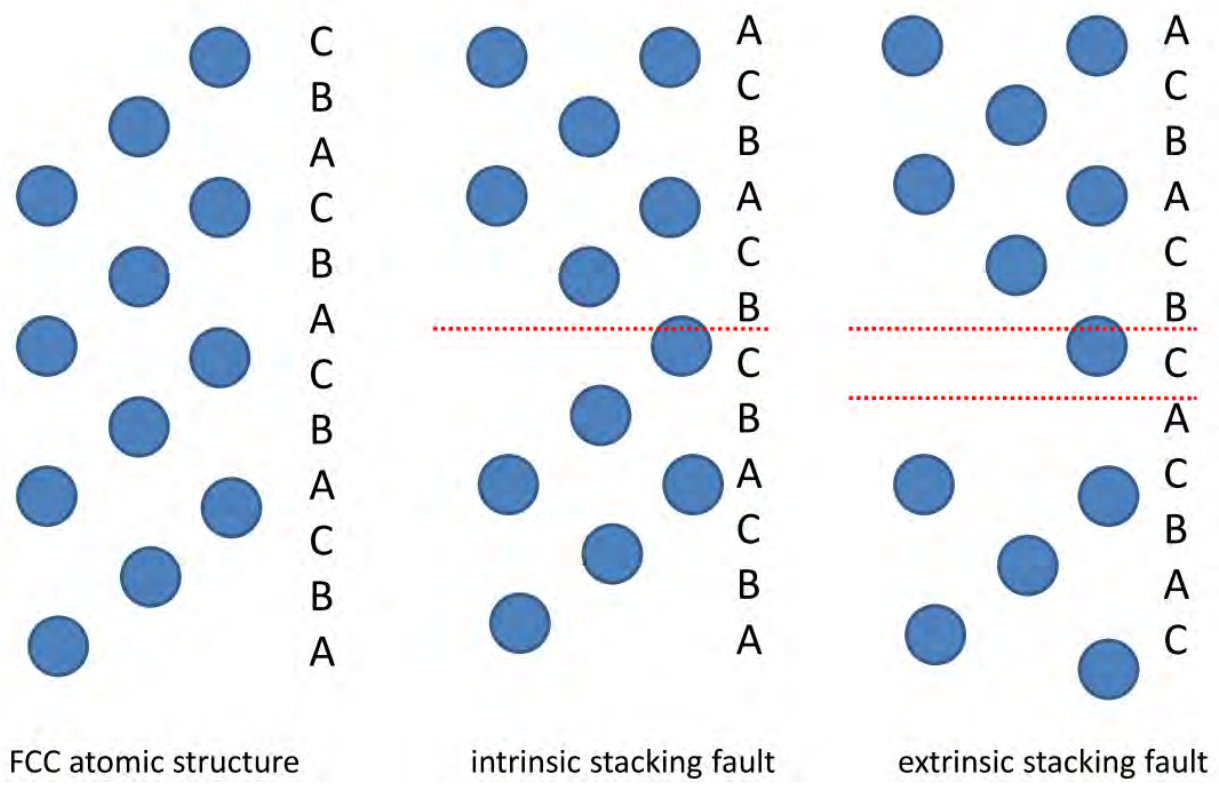

Figure 2.22: Stacking faults in FCC aluminium alloy structures.

A stacking fault which continues over a number of atomic spacings without correcting itself will produce a second stacking fault that is the twin of the first one. A 'twinned structure' is formed when successive adjacent planes are displaced relative to each other in the FCC lattice, forming a reversed stacking sequence. Though twinning usually occurs in BCC and HCP atomic structures, twinning may still occur in the FCC structure of AA5182 under special conditions, such as when thin aluminium foil is annealed or the SFE is very low [24] [25].

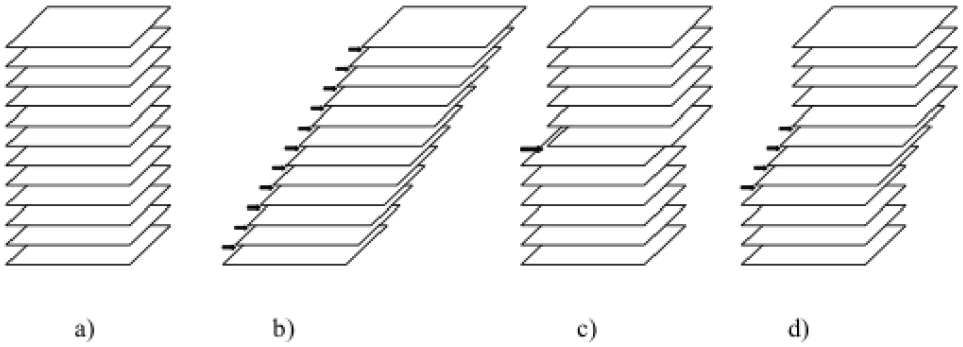

Figure 2.23: Schematic of lattice deformation mechanisms. (a) is the undeformed lattice for comparison to (b) elastic deformation by homogeneous shear strain, (c) plastic deformation by dislocation slip and (d) plastic deformation by deformation twinning.

[25]

2.5.6 Cell Structures

A cellular structure is formed within the grains of some aluminium alloys during deformation instead of twins or stacking faults. The cellular substructure that forms strengthens the aluminium alloys. At relatively low temperatures, these substructures are referred to as 'cells' [26]. These cells have a low misorientation difference between themselves of about 1° and have tangled dislocations for walls. Deformation at higher temperatures, however, results in the formation of 'subgrains' which are bounded by narrower, more well-defined walls with a higher misorientation between each other. Recovery in the alloys results in the change from cells to subgrains [26]. During recovery in cold worked metals such as AA5182, the microstructure transforms through many steps from tangled dislocations to the formation of cell structures and eventually the formation and growth of subgrain structures [10]. These dislocation recovery steps occur to relieve the stored stress in the cold-worked material. Two dislocations moving parallel to eachother may annihilate eachother when they change their cross slip planes, resulting in the change from b) to c) shown in Figure 2.24. All the microstructural changes are displayed schematically in Figure 2.24. These steps often interlap and are not found in as clearly defined steps as are shown in Figure 2.24.

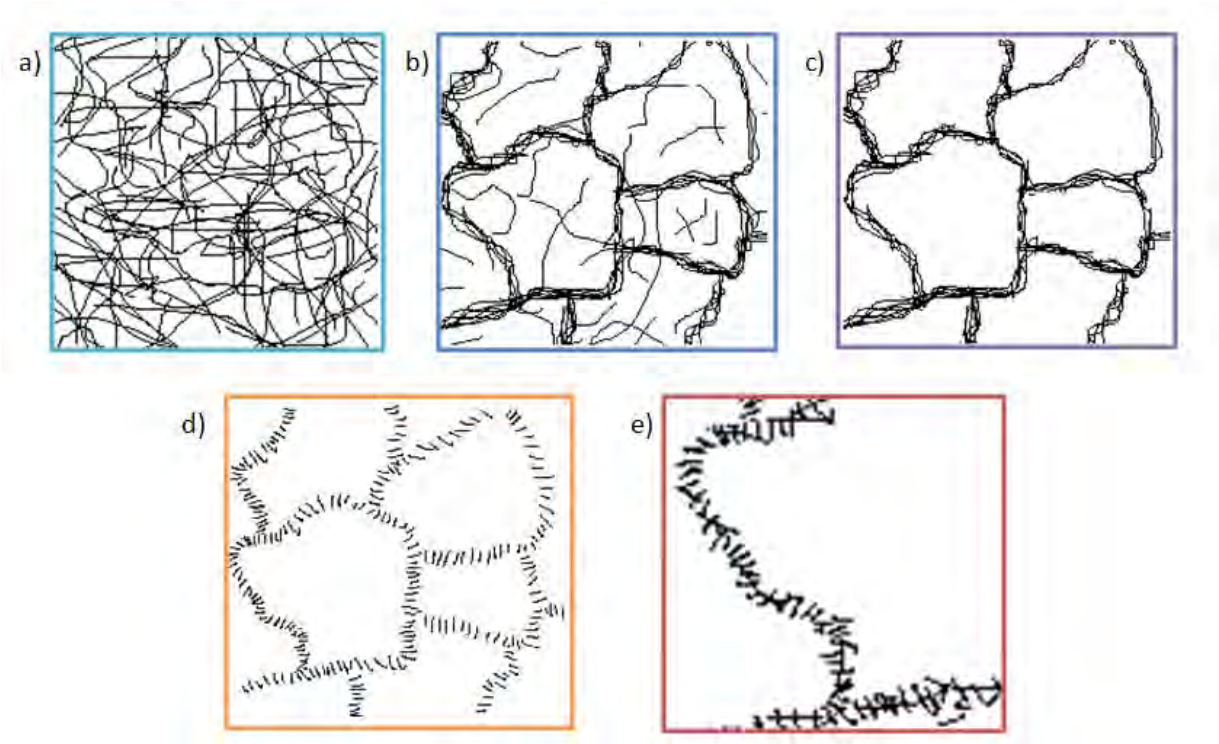

Figure 2.24: Dislocation recovery steps in cold worked metal showing a) tangled dislocations b) the formation of cell structures c) the annihilation of the free dislocations within the cell structures d) the formation of subgrains and e) the growth of subgrains.

[10]

Cold worked samples investigated with transmission electron microscopy (TEM) showed no distinctive cell formation [27]. Specimens with 60% cold work showed entangled dislocations which formed poorly defined elongated cell structures [27]. After 90% cold work, however, high dislocation density walls were found to show a tendency towards the formation of a near cellular structure [27], as illustrated in Figure 2.25. These poorly defined cells or near cellular structures, formed from entangled dislocations, were observed in all AA5182 grains after 90% cold work [27].

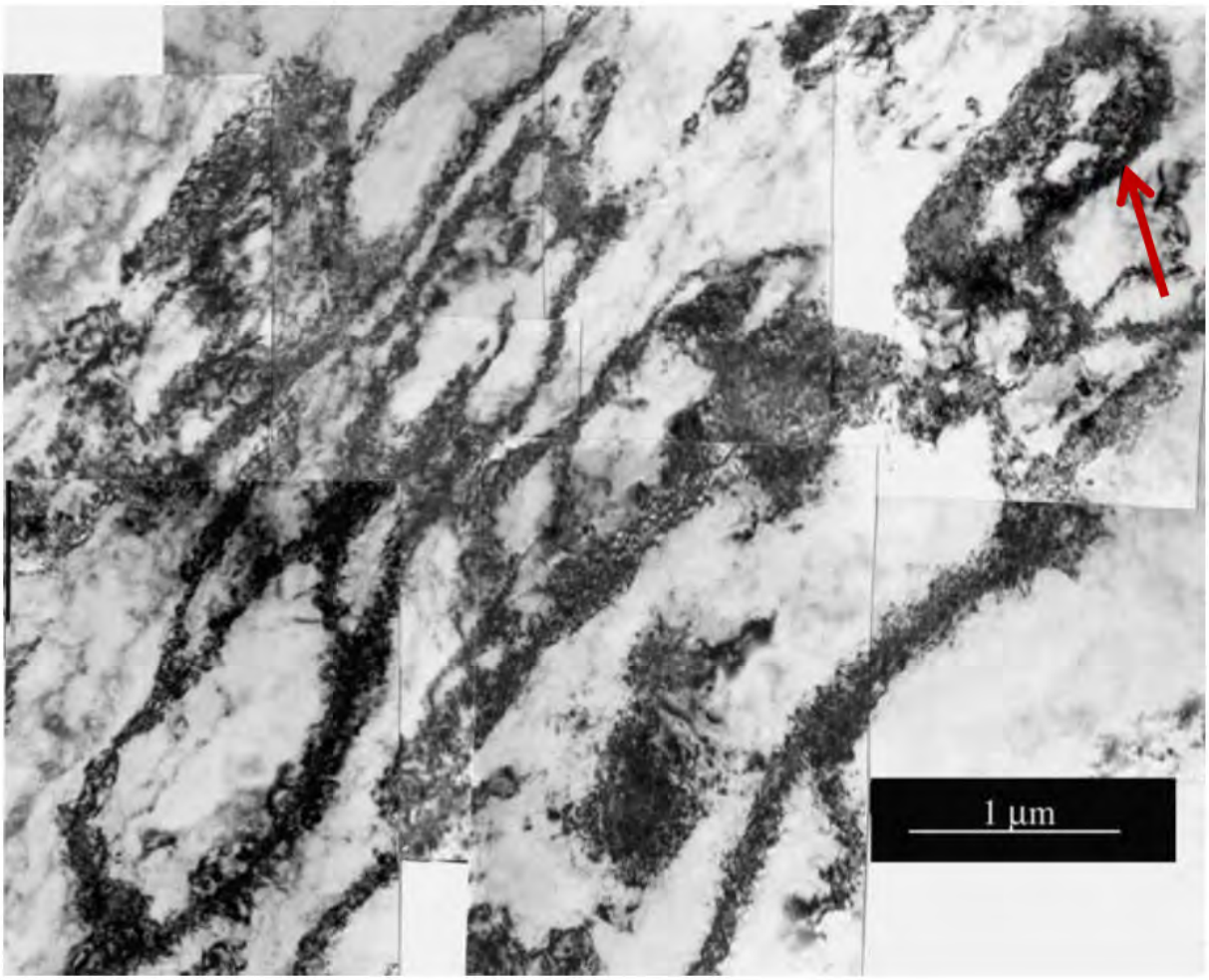

Figure 2.25: TEM micrograph of AA5182 cold rolled specimens ($\varepsilon = 2.4$), showing a tendency towards the formation of cells, as marked with an arrow.

[27]

Shear bands were observed in the microstructure of AA5182 after 90% cold work. At high strains levels, these shear bands were found to intersect [27], as shown in Figure 2.26.

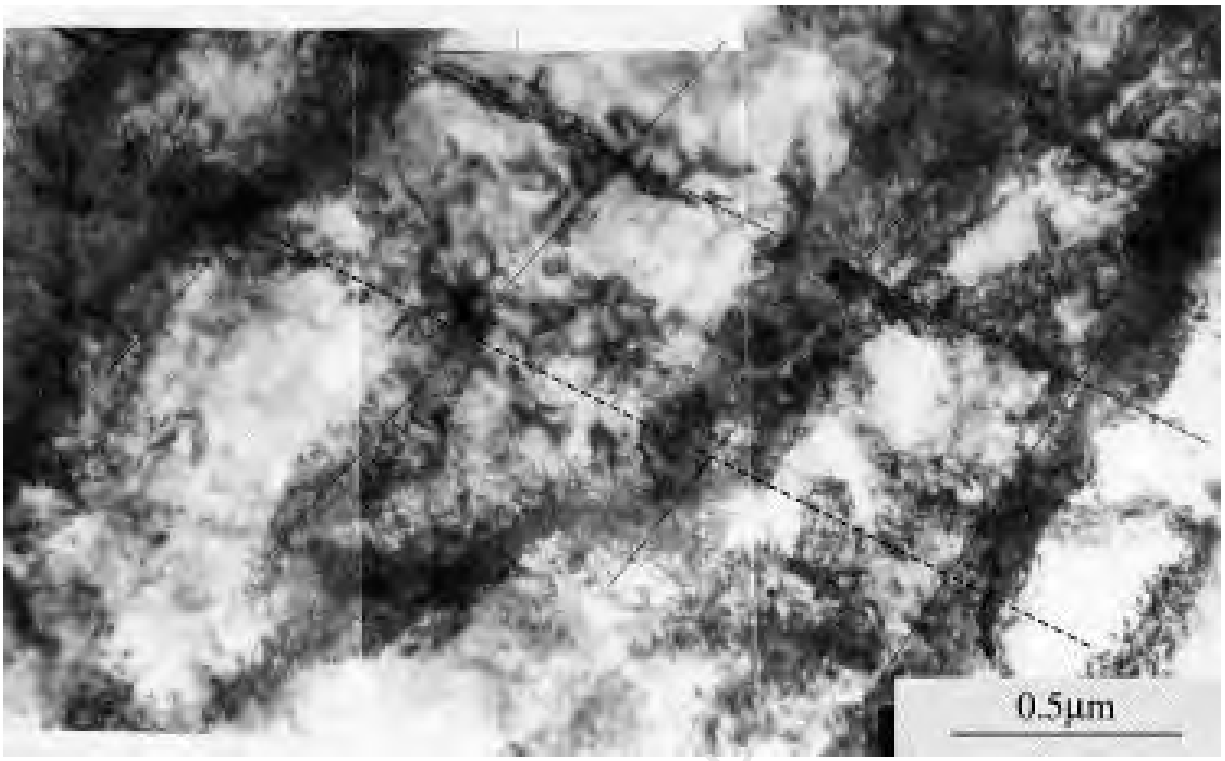

Figure 2.26: TEM micrograph of AA5182 specimens ($\varepsilon = 1.6$) showing intersections of shear bands as dotted lines.

[27]

2.5.7 Deformation Texture Models

The classical approach to determining the plastic deformation route in metals is using Taylor's (1938) model. This model assumes that in each grain, the strain is homogeneous and that the overall polycrystalline strain is equal to this strain. This model is extended to the self-consistent scheme suggested by Kroner in 1961 or the relaxed Taylor model suggested by Honnef and Mecking in 1978. In the relaxed Taylor model, the material is stabilized when the grain shape changes from equiaxed to flat grains, allowing relaxation of the shears [27][28]. The other models, based on work by Taylor and Godfrey in 1938, are shown in Table 2.6.

Table 2.6: Deformation texture models based on work by Taylor and Godfrey (1938).

Model	**Lamel**	**Alamel**	**GIA**	**CPFEM**
Full Name	Lamellar structure	Advanced Lamel	Grain Inter-Action	Crystal Plasticity
				Finite Element

The models in Table 2.6 were designed to improve on the Taylor models but still only consider the crystal structure of the material and not other material properties [27]. The Alamel model, for instance, was designed to better predict deformation texture. The GIA model takes the deformation behaviour of eight grains in a homogeneous surrounding into consideration [27].

These models describe the intergranular inhomogeneities of the deformation modes, but do not describe the strain fields within the individual grains themselves and the plastic deformation is assumed to be homogeneous (Taylor assumption) [29]. Taylor-type texture models have been used to estimate the deformation texture of the AA5182 alloy but these have been found to have a low accuracy in simulating the rolling texture. This is perhaps due to the presence of microstuctural heterogeneity, including shear bands, dislocation formations and second phase particles in the alloy [21] [29]. Shear banding has been hypothesized as a deformation mechanism for certain alloys, such as aluminium AA5182 alloys [29]. Shear banding plays a major role in the plastic deformation of AA5182 alloys and substantially decreases the strength properties of the rolled texture [30]. In general, these models are not fully predictive of the deformation texture in AA5182 and need to be improved for aluminium alloys [28].

2.5.8 The Effect of Temperature on AA5182

AA5182 can soften by various processes, such as the recovery process illustrated in Figure 2.5, and thus lose its strength properties when subjected to a thermal treatment. AA5182 CES will age soften if it is not stabilized or stored at sub-zero temperatures. Controlled thermal treatments used on the AA5182 alloy developed a desired microstructure and properties. As was stated in Subsection 2.5.2, work hardening due to forest dislocations is temperature dependent and can thus be overcome by thermal treatments. Highly strained AA5182 studied with electron microscopy techniques have previously exhibited no measureable change in the dislocation density during the age softening process [11]. The internal strain energy in AA5182 appears to be relieved by the changing in tangled dislocation interactions and relaxation without a measureable decrease in the actual numbers of dislocations being observed in the alloy with techniques such as transmission electron microscopy (TEM) [11].

2.6 Microscopy Techniques

2.6.1 Polarized Light Microscopy

Polarized light microscope (PLM) can be used to determine the overall qualitative microscopy of the AA5182 alloy. The aluminium alloys need to be electrolytically anodized and examined under polarized light [31]. This reveals the contrast between individual grains throughout the sample's structure. The preparation of samples for PLM investigation of grain structures first involves grinding and polishing of a sample, which is then electrolytically anodized. This anodizing process forms a layer or film of Al_2O_3 on the surface of the aluminium alloy, where the thickness of this layer on each grain varies as a result of each grain's crystallographic orientation. When polarized light passed through a filter is incident on the Al_2O_3 surface layer, the plane of polarization rotates depending on the orientation of the underlying grain. This rotation in the polarized light results in various shades of grey being produced in the light micrograph, as shown in Figure

2.27. The light micrograph produced can also be converted to a colour contrast micrograph by inserting tint plates or filters into the polarized light microscope [31].

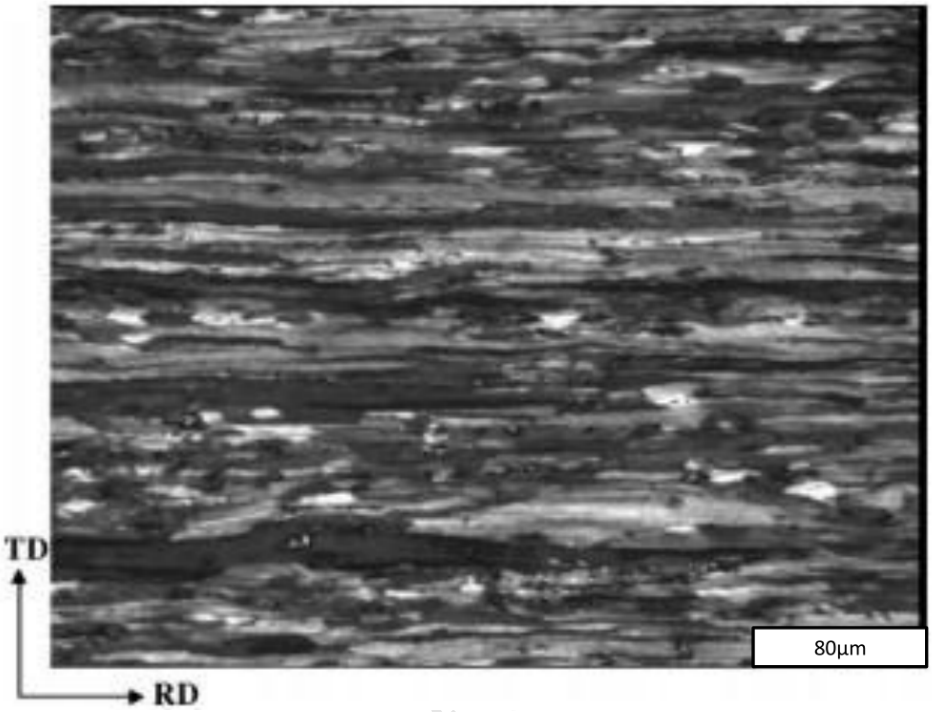

Figure 2.27: Light micrograph showing grain structures in continuous cast AA5182 in the hot band condition.

[31]

2.6.2 EBSD

Electron backscatter diffraction (EBSD) is a technique performed in the scanning electron microscope (SEM), as summarized in Figure 2.28.

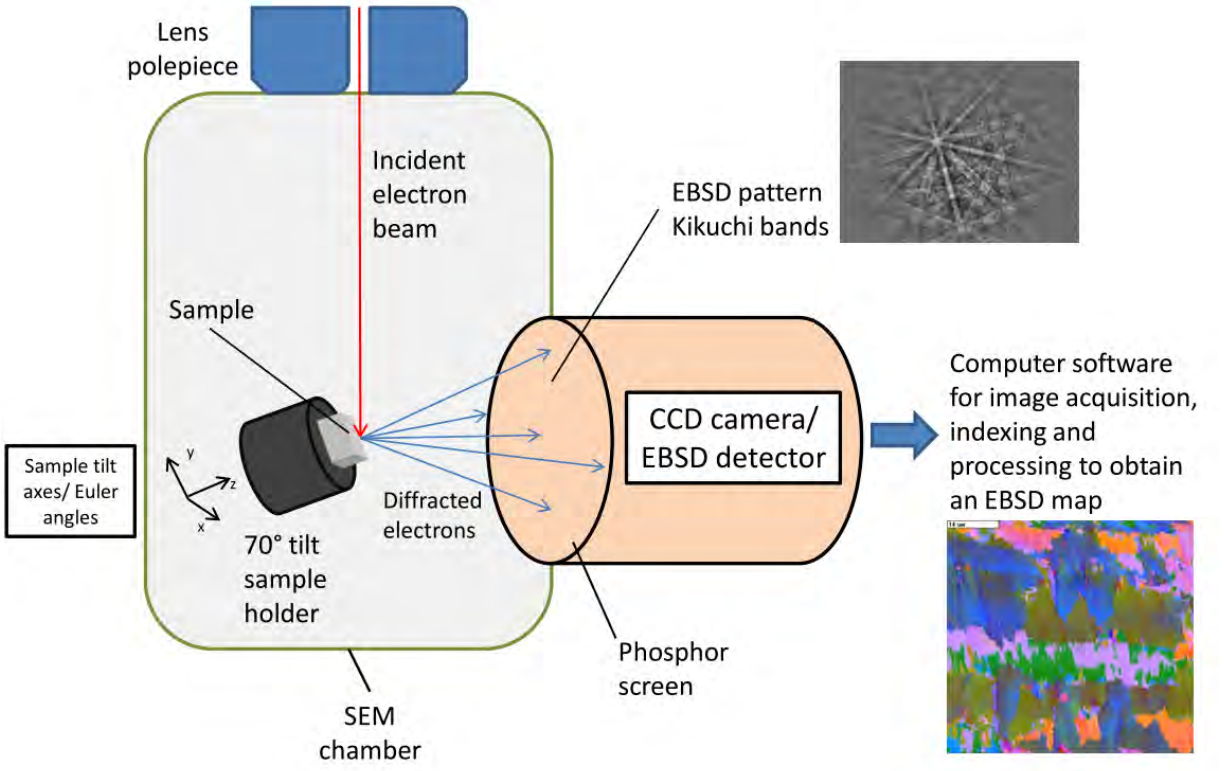

Figure 2.28: Schematic of the EBSD apparatus and process.

The EBSD technique can be used to quantitatively investigate the crystallographic orientation of grains, and to obtain grain and subgrain size data. Textures and microstructures can be analyzed using the electron backscatter diffraction (EBSD) technique. Diffracted electrons fluoresce the phosphor screen on the sensitive charge coupled device (CCD) camera used in the SEM under vacuum. In the current study, the LAGBs are defined as between 2° and 10° of misorientation and HAGBs as above 10° of misorientation, as described in Subsection 2.5.1. High quality EBSD diffraction patterns, such as the one shown in Figure 2.29, obtained from each pixel in a specified scan area, can be used to produce an EBSD map. Each pixel for an indexed point is compared to its nearest eight neighbours to obtain a relative orientation for each point. The EBSD map may be obtained as an Euler map in colour, where a colour is assigned to each pixel in the map with respect to its relative orientation, as shown in Figure in 2.30. This orientation is with respect to three Euler angles assigned to the three axes for the sample (x, y and z axes), as shown in Figure 2.28. The EBSD map may also be a greyscale map with the shade of grey also determined by the relative orientation of each pixel in the EBSD map. EBSD maps, when processed with software such as the Vmap programme or the Channel 5 HKL Tango programme, can be used to determine the average size of subgrains in the aluminium alloy. These subgrains, as discussed in Subsection 2.3.2.1, will generally grow in size at higher temperatures, resulting in a decrease in strength with a reduction in the pinning effect of the dislocations forming these

subgrain boundaries, as described in Subsection 2.5.2.

Though a diffraction pattern can be obtained in less than a second, a longer scan time is often used to obtain improved EBSD image quality [32]. In order to obtain good diffraction patterns needed to produce high quality EBSD maps with a good confidence level, the samples used must be clean from contamination and relatively strain-free.

The low atomic number of aluminium results in inefficient generation of backscattered electrons from an aluminium sample and thus the solution of the Kikuchi pattern may be difficult to obtain [32]. A high quality Kikuchi diffraction pattern is shown in Figure 2.29, with an easily visible pattern which should be indexed by the Channel 5 HKL programme. Each indexed Kikuchi pattern results in an indexed point in the EBSD map, which, when generated, is the final image result of the EBSD technique. EBSD diffraction patterns are also generally more difficult to generate on a heavily cold worked aluminium alloy sample than on a commercially pure aluminium sample due to the distorted nature of the heavily cold worked sample's crystal lattice. For these reasons, the sample preparation method should be carefully controlled to obtain the highest possible quality of EBSD maps. The best sample preparation method usually involves the use of colloidal silica as the final abrasive polishing step [32]. The non-indexed points in the EBSD maps appear as green points in the colour maps and black points in the greyscale maps.

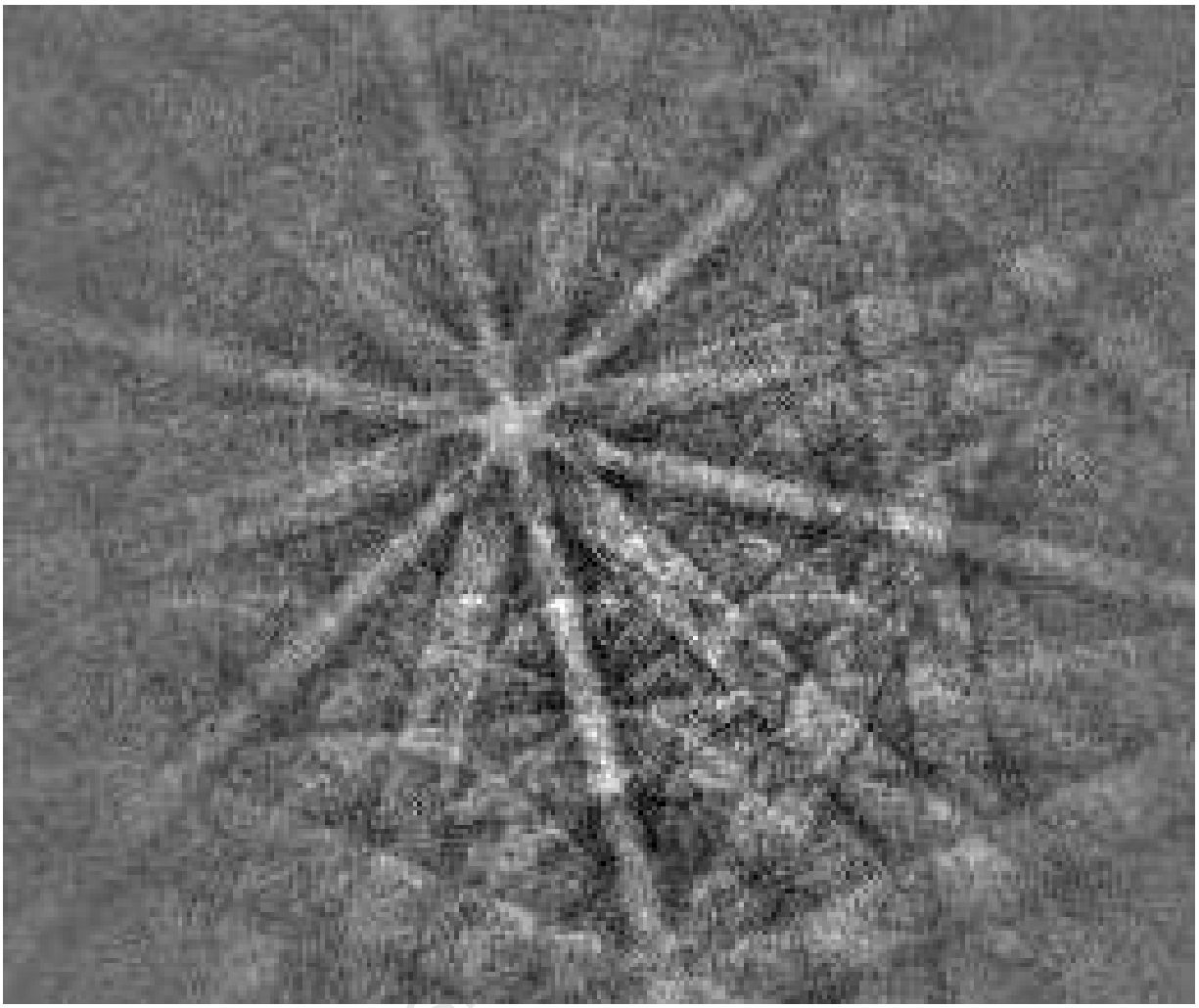

Figure 2.29: EBSD Kikuchi diffraction pattern for mild steel with a pattern quality indexing of more than 80%.

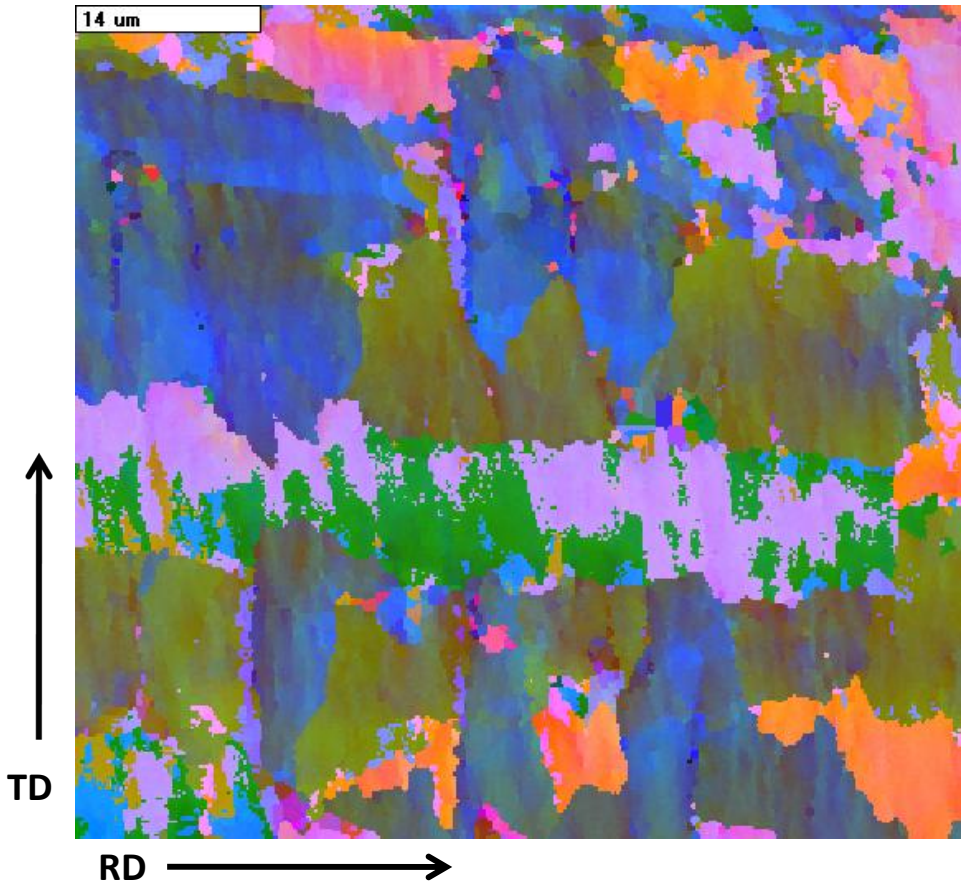

Figure 2.30: EBSD map for AA5182 CES in the as cold-rolled condition showing, in Euler colours, the elongated grains in the rolling direction as well as some elongation in the transverse direction.

2.6.3 TEM

The transmission electron microscopy (TEM) technique can be used to investigate the different microstructures obtained for aluminium alloys subjected to various conditions. The subgrain structure can be identified qualitatively at a high magnification and phases, in the micrometer and nanometer scale, can be studied. This microstructure may include shear bands, stacking faults, dispersoids, dislocations, dislocation forests, cell structures, grain boundaries and other precipitates, as described in Section 2.5.

The morphologies of precipitates and dispersoids in Al-Mg aluminium alloy samples, after they are preheated at different temperatures for 4 hours, are shown in Figure 2.31. This alloy is Al-4.97wt%Mg-0.74wt%Mn-0.098wt%Zr-0.016wt%Ti-0.35wt%Er-0.18wt%Fe-0.12wt%Si [20]. When the preheating temperature was lower than 400°C, as shown in Figure 2.31, various phases were found to form in rhomboidal shapes (labelled A), script shapes (labelled B), rod shapes (labelled C) and needle shapes (labelled D). These phases were found to mainly be distributed at grain boundaries but were also found in the aluminium matrix [20] . The phases, as discussed in Subsection 2.5.3, were determined by EDS analysis to be mainly Al_6(Fe, Mn) and Al_3Mg dispersoids.

These dispersoids pin dislocations, resulting in microstructures such as those shown in the TEM micrographs in Figure 2.19.

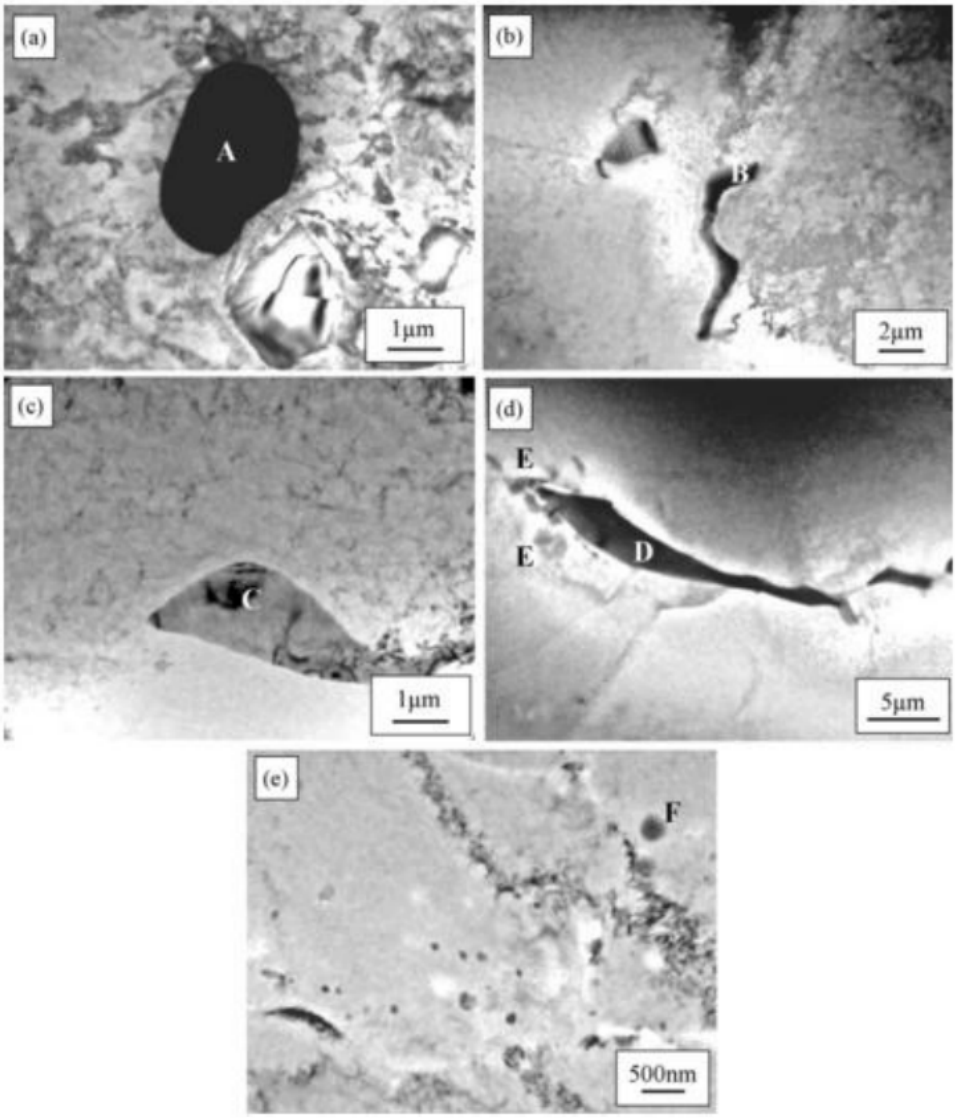

Figure 2.31: TEM micrographs showing the morphologies of precipitates (A-F) in Al-Mg alloys preheated at different temperatures for 4h: (a) 200°C; (b) 250°C; (c) 300°C; (d) 350°C; (e) 400°C. [20]

Where a crystalline lattice structure is rotated in relation to another, Moiré fringes may be observed in the TEM micrographs. Moiré fringes can be likened to the effect of looking at an angle at a similar mesh structure behind another and seeing the parallel lines with a slight overlap effect caused. This effect occurs similarly with atomic lattice structures as the "mesh" and the electron beam being the "observer" at an angle in this example. These Moiré fringes can be observed in TEM images for AA5182 alloys and are evidence of dislocations forming subgrain walls in this study. An example of Moiré fringes observed in an Al-Mg alloy TEM micrograph is

shown in Figure 2.32.

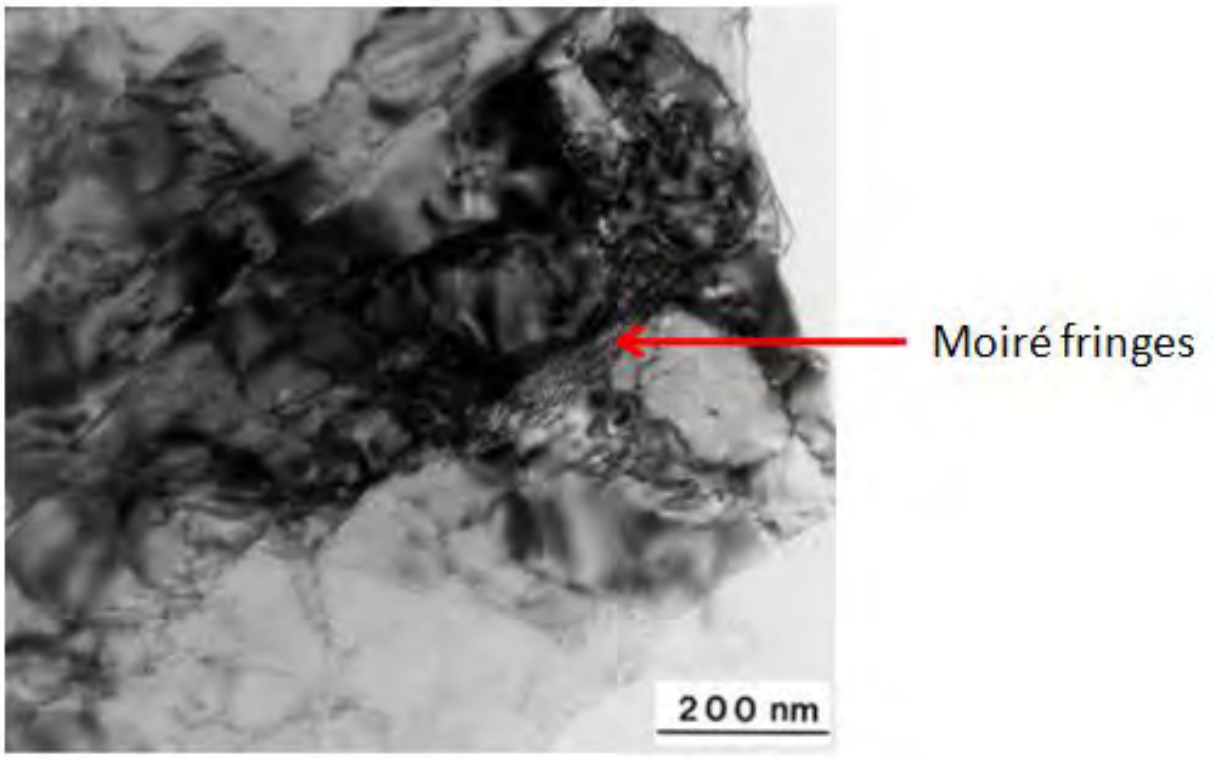

Figure 2.32: Moiré fringes displayed in a typical view of Al–1.5% Mg alloy. [33]

Chapter 3

Experimental Procedure

The following chapter describes the experimental procedure that was followed during this research. A summary of the experimental procedure used is shown in the flow chart in Figure 3.1.

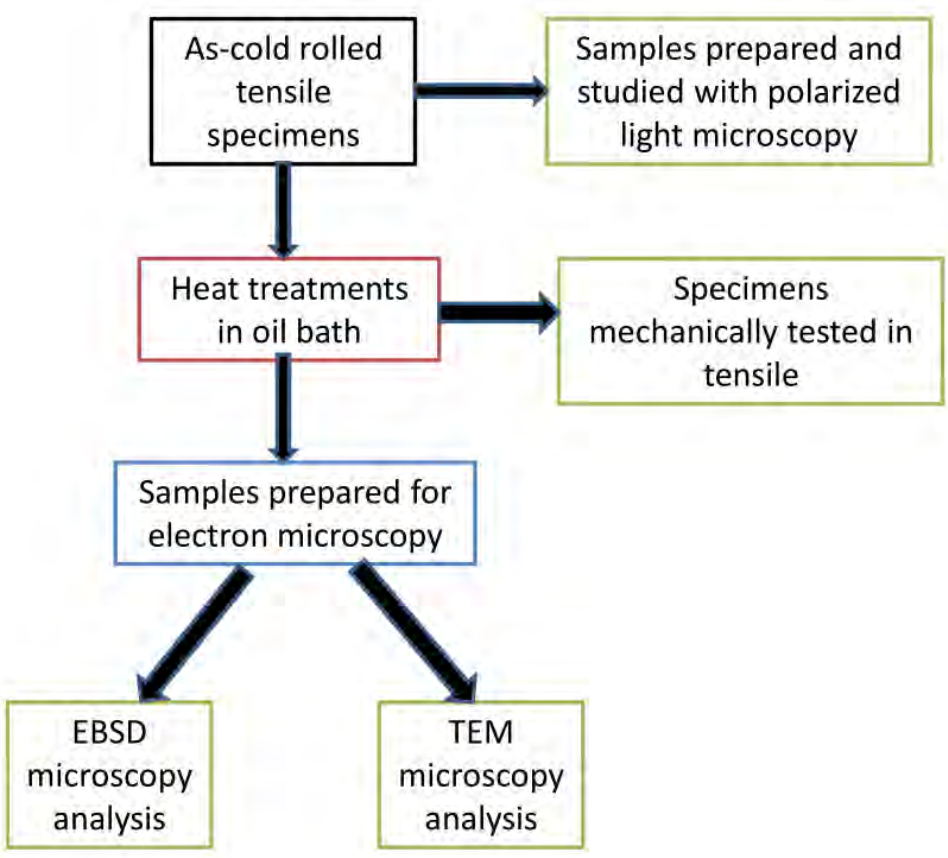

Figure 3.1: Summary flow chart of the experimental procedure.

3.1 As-received Material

The material used in this study is the AA5182 aluminium alloy which has an approximate composition of 4.0 to 5.0wt% magnesium as its major alloying element, as described in Table 2.3. The material is in the form of 0.27mm thick tensile specimens with dimensions shown in Figure 3.2. These tensile specimens were cut from the CES sheet after the cold rolling process and before the coil coating process, shown in Figure 2.7. The tensile specimens used in this study were cut from the CES sheet in the rolling direction and were pulled in tension in this orientation, as shown in Figure 3.2.

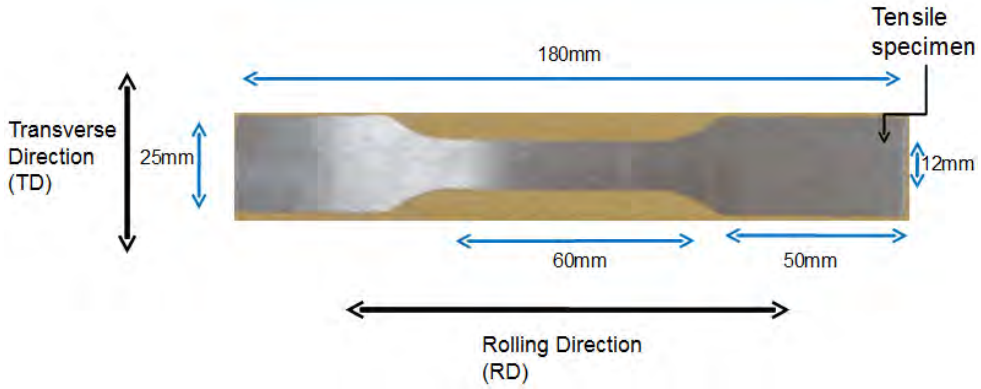

Figure 3.2: AA5182 tensile specimen with dimensions.

3.2 Heat Treatments

3.2.1 Initial Heat Treatments

The as-cold rolled specimens were received in the H18 condition, in the form of flat tensile specimens. These specimens were then subjected to heat treatments designed to simulate the stabilization process shown in Figure 2.7. The design matrix shown in Table 3.1 was chosen. The temperatures selected were 120°C, 150°C and 200°C, for times of 1 hour and 4 hours.

Table 3.1: Heat treatment design matrix

	1 hour	4 hours
120°C		
150°C		
200°C		

A temperature controlled oil bath, shown in Figure 3.3, was used to heat treat the tensile specimens. Three specimens were taken for each of the six heat treatments shown in Table 3.1. These specimens were placed into the steel wire basket in the oil bath to heat to the required temperatures described in the design matrix. The oil bath is temperature controlled

and is mechanically mixed to ensure that the oil temperature is kept at a uniform temperature throughout.

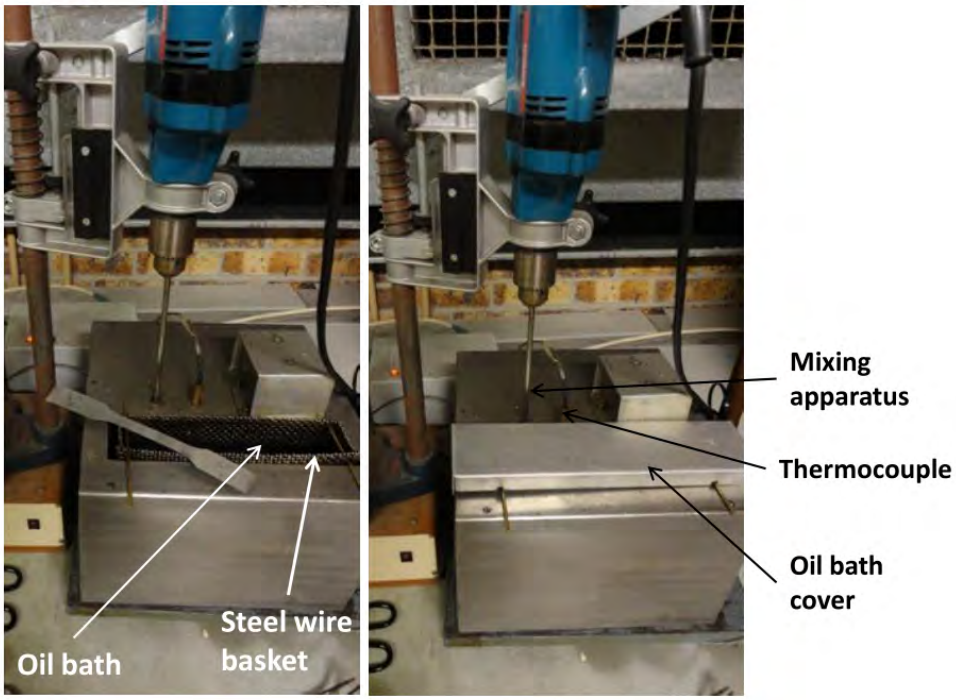

Figure 3.3: Temperature controlled oil bath without the lid on the basket (left) and the lid on the basket (right).

Once the three tensile specimens for each condition in Table 3.1 have remained in the oil bath for the required amount of time, they are removed from the oil bath wire basket and allowed to cool to room temperature. This is repeated for all of the heat treatments in the design matrix in Table 3.1. This stabilization heat treatment simulation procedure is summarized in Figure 3.4.

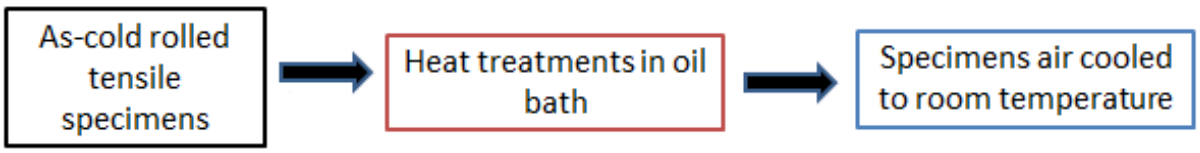

Figure 3.4: Summary of the simulated stabilization heat treatment procedure.

3.2.2 Simulated Coil Coating Procedure

After the initial stabilization heat treatments were investigated on the AA5182 specimens, the effect of the coil coating procedure was investigated. This simulated coil coating procedure

(SCCP) mimics the coil coating step used at Hulamin, shown in Figure 2.7.

Eight more tensile specimens were prepared for the heat treatment of 150°C 4 hours and eight more for the as-cold rolled condition. The stabilization heat treatment of 150°C 4 hours was found to most closely simulate the conditions experienced at Hulamin. It was therefore used for a more detailed investigation into the combination of stabilization and the effect of the subsequent coil coating process. These results were then compared to the as-cold rolled samples also exposed to the lacquering process. Two specimens were prepared for each of the eight secondary conditions shown in Table 3.2.

Table 3.2: Simulated coil coating procedure (SCCP) design matrix

	10%CW	10%CW 220°C		
		4 minutes	30 minutes	4 hours
150°C 4hours				
as-cold rolled				

These specimens were prepared in the oil bath in a similar way to that shown in Figure 3.4. These tensile specimens were then cold worked using a rolling mill to reduce their thickness by 10% to introduce 10% cold work (10%CW) into the specimens. After the cold working step, specimens were exposed to the secondary heat treatments of either 220°C for 4 minutes or 220°C for 30 minutes. The cold work step and the secondary heat treatments were used together to simulate the effect of coating the AA5182 CES in lacquer and curing it after the rolling and stabilization steps, as shown in Figure 2.6 and Figure 2.7.

Using the coil coating heat curve in Figure 2.6 as a guide, the AA5182 specimens were heated in the oil bath to a temperature of 220°C over 40 minutes and then held at that temperature of 220°C for 4 minutes and 30 minutes. In order to investigate the effect of extended time at this elevated temperature, specimens were also held at 220°C for 4 hours.

The as-CR specimens were used as a reference to demonstrate the effectiveness of the stabilization heat treatment of 150°C 4 hours on specimens when compared to specimens in the as-CR state without stabilization. The design matrix shown in Table 3.2 was used. The secondary cold work and lacquer simulation procedure heat treatments are summarized in Figure 3.5 and Figure 3.6.

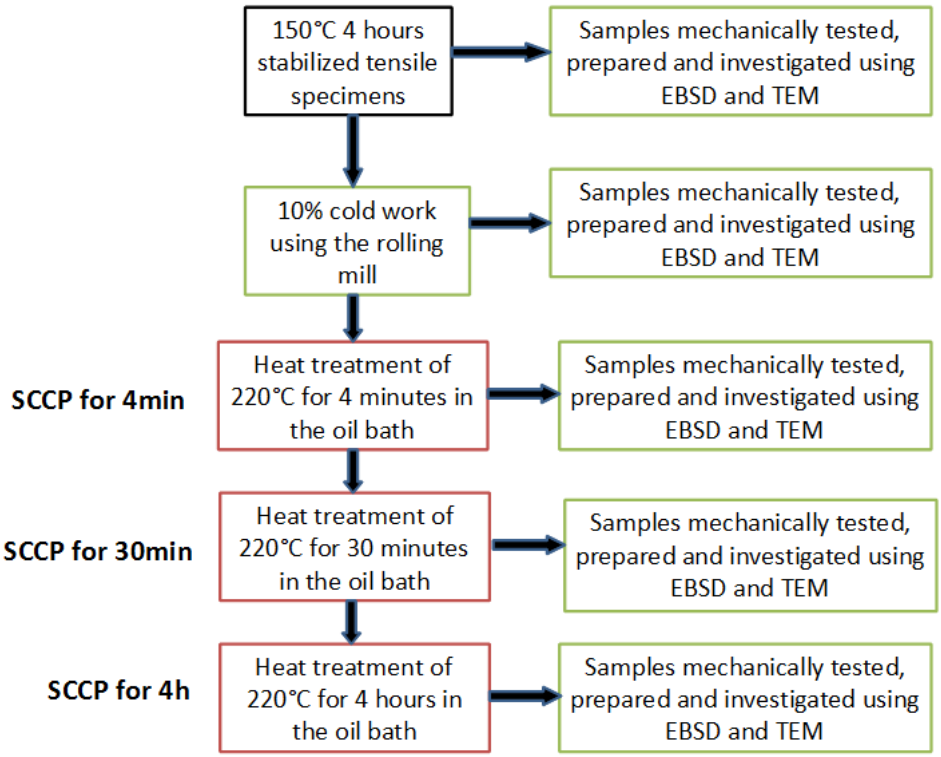

Figure 3.5: Summary of the simulated coil coating procedure (SCCP) on specimens heat treated at 150°C for 4 hours.

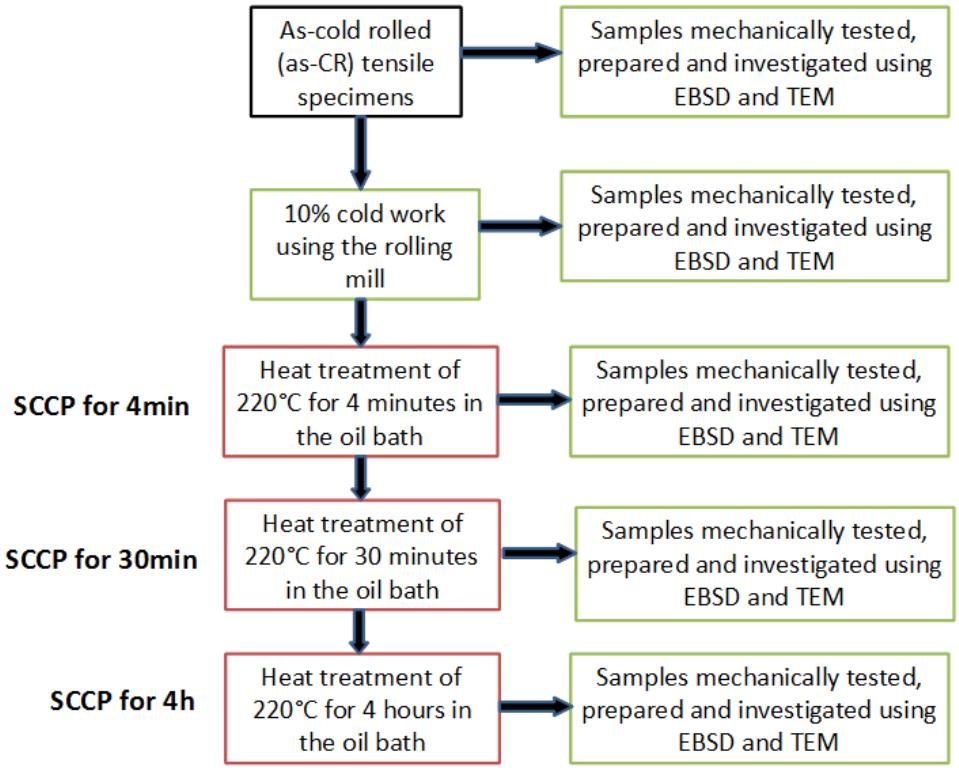

Figure 3.6: Summary of the simulated coil coating procedure (SCCP) on as-CR specimens without stabilization.

3.3 Tensile Testing

Tensile tests were performed to determine the mechanical properties of the AA5182 specimens. Tensile tests were carried out on all the stabilization heat treated and the as-cold rolled tensile specimens using the Zwick tensile tester shown in Figure 3.7. The 10kN grips were used instead of the conventional 100kN grips. The smaller grips held the thin sample better and so were chosen so as to avoid the slipping of the thin tensile specimens out of the grips during the tensile test and having to linish the specimens. Since there is anisotropy in the microstructure in the cold rolled AA5182, the samples are only tested in the rolling direction, shown in Figure 2.8, to allow for simple comparison of tensile properties in the different specimens. A low strain rate of 6.7×10^{-4} s^{-1} was used to capture in detail the shape of the stress-strain curves so that these changes could be compared between specimens, The force and extension data was converted into true stress-true strain curves in order to determine the mechanical properties of the AA5182 specimens under each condition shown in Table 3.1 and Table 3.2. Two specimens were prepared for each tensile test.

Figure 3.7: Zwick tensile testing machine.

3.4 Polarized Light Microscopy

The polarized light microscopy technique was used to reveal the general microstructure of the as-cold rolled AA5182. 10mm square samples were cut from the tensile specimens as shown in Figure 3.8.

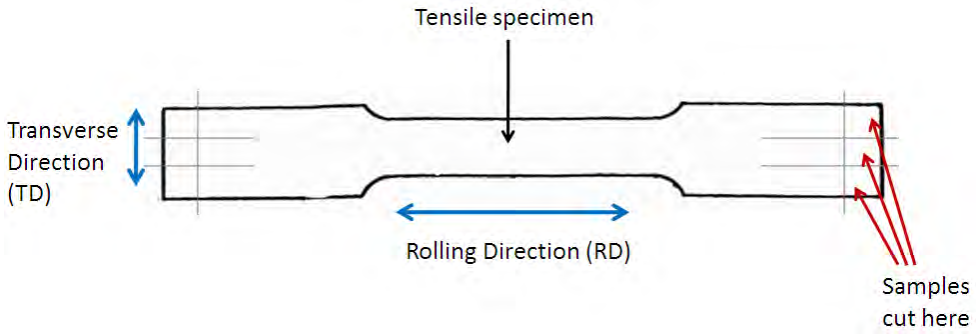

Figure 3.8: Schematic of positions samples were sectioned from the AA5182 tensile specimens.

These samples were ground and polished using the procedure described in Subsection 3.5.1. The samples were cold mounted in resin to avoid thermal effects on the aluminium microstructure which may be caused by hot mounting the samples at temperatures above 100°C. These samples were then anodized in Barker's solution containing HBF_4 and distilled water in a 3:97 ratio for 10 seconds using a 40V setting. The anodized samples were then viewed through a polarising lens in a Reichart MeF3A Polymatic inverted light microscope shown in Figure 3.9.

Figure 3.9: Reichart MeF3A inverted light microscope fitted with a polarized lens.

3.5 Sample Preparation for the Scanning Electron Microscope

Samples for microstructural investigation were sectioned from the ends of the tensile specimens in the plane with the rolling direction (RD) and transverse direction (TD) in it, as shown in Figures 3.8 and 3.10.

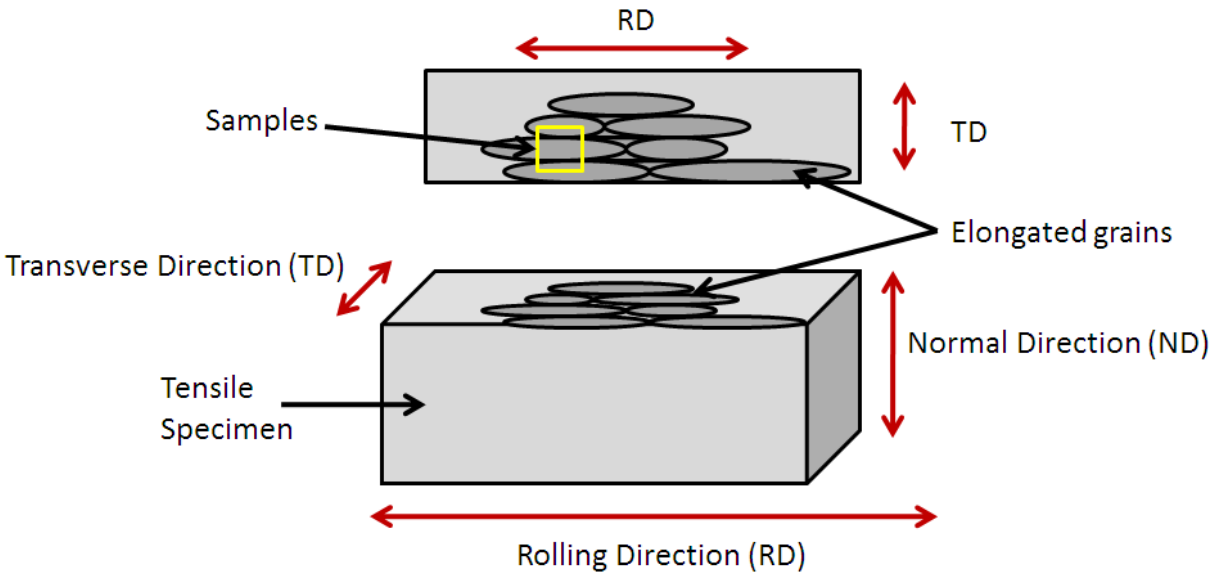

Figure 3.10: Schematic of the elongated grains on the AA5182 tensile specimens.

A resin ratio of 7:1 for Specifix Resin to Specifix-20 curing agent was mixed, poured over samples in Vaseline greased polymer pots and left to cure for 12 hours. The apparatus used is shown in Figure 3.11. These cold mounted samples were prepared for metallographic examination using the polishing conditions described in Table 3.3.

Figure 3.11: Cold mounting reagents and apparatus.

3.5.1 Grinding and Polishing

The rough ends of the cold mounted samples were flattened using a 1200 grit grinding paper on a manual grinding wheel. The samples were then ground and polished using the Struers TegraForce-1 automatic polisher, as shown in Figure 3.12. The lubricant and conditions used in the grinding and polishing methods are shown in Table 3.3. Once these steps were completed, the samples were washed using warm water, ethanol and dried. The samples were then inspected under the stereo light microscope for large, non-uniform scratches. If these scratches were present, the OP polishing step was repeated. Once the samples were polished, they were removed from their cold mounts.

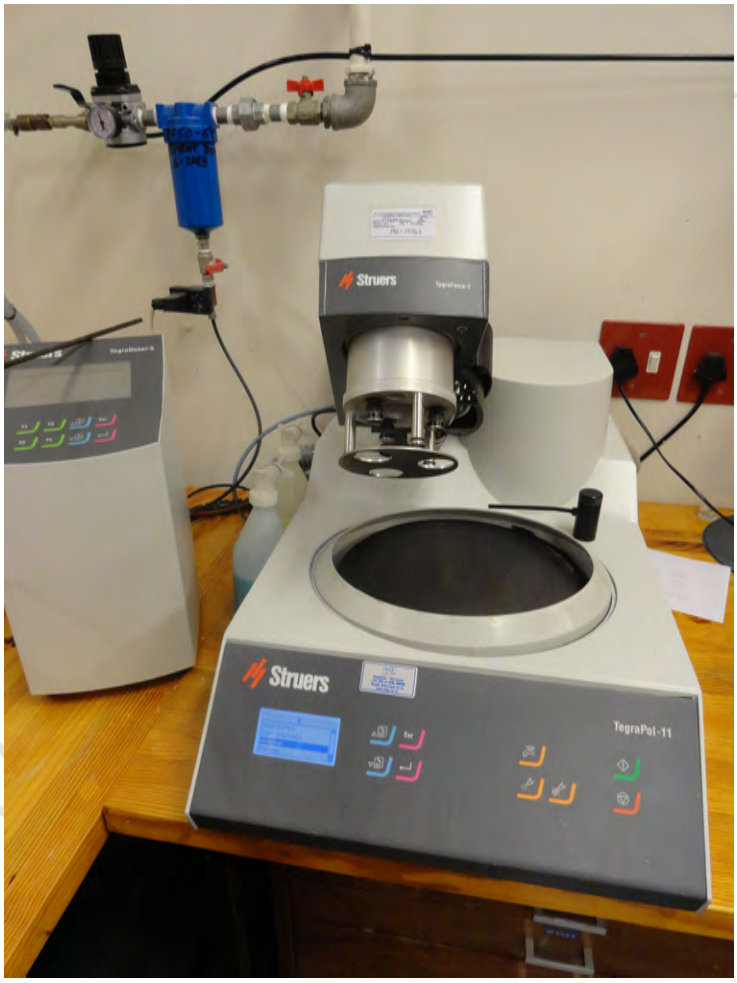

Figure 3.12: Automatic polishing machine.

Table 3.3: Summary of the conditions used in the polishing method

Step	Pad	Force	Lubricant	Time (minutes)
Grinding	1200 grit	10N	Water	2 to 3
Polishing	Mol 3μm	10N	Mol 3μm Suspension	4 to 16
Polishing	NAP	10N	OP Colloidal Silica Diamond Paste	3 to 6
Polishing	NAP	10N	Warm water	2

3.5.2 Chemical Polishing

In order to improve the surface finish and remove the deformation layer, the AA5182 samples were chemically polished. A beaker with 15g NaOH pellets, 85g distilled water and a teaspoon of table sugar was prepared and mixed. A second beaker was filled with 10ml nitric acid and 90ml distilled water. The polished samples were picked up with tweezers and dipped into the 15% NaOH solution for 20 seconds to chemically polish them. The samples were then dipped into the second beaker of 10% nitric acid solution for 10 seconds to wash off the NaOH solution. The chemically polished samples were then carefully washed with warm water, fine cotton wool, ethanol and then dried. The polished samples were each mounted on a SEM stub using a small quantity of silver dag solution, as shown in Figure 3.13. This silver dag is then left to dry for 24 hours to ensure that the samples are securely glued onto the stubs with the dried silver dag. These samples were then taken to the Nova NanoSEM for microstructural investigation.

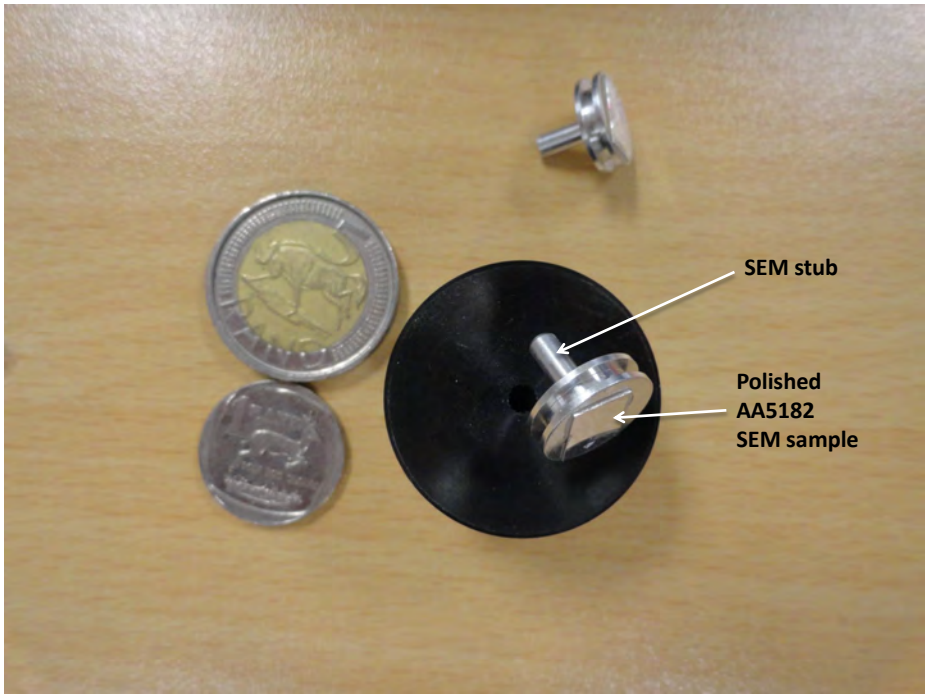

Figure 3.13: Polished AA5182 SEM samples mounted on stubs.

Figure 3.14: Struers Tenupol-3 twin jet electropolishing equipment.

3.6 Sample Preparation for the Transmission Electron Microscope

3mm disks were punched from the ends of one of the three tensile specimens prepared for each heat treatment condition. The 3mm disks were ground down using 1200grit grinding paper with water as a lubricant. The thickness of these disks was reduced from 0.27mm to less than 0.1mm.

3.6.1 Twin Jet Electropolishing

The 3mm AA5182 disks, with a thickness of less than 0.1mm, were placed into the twin jet electropolishing machine holders shown in Figure 3.14, to have their thickness further reduced by electropolishing to be thin enough to use in the TEM. The conditions that were used in the twin jet electropolishing machine are shown in Table 3.4. The electrolyte was cooled with liquid nitrogen as the reactants undergo a highly exothermic reaction.

Table 3.4: The conditions used in the twin jet electropolishing machine

Condition/ Setting	**Value Used**
Electrolyte used	75volume% methanol: 25volume% nitric acid
Flow rate used	4
Temperature of electrolyte	-30°C to -20°C
Photosensitivity	10
Ammeter range	0.5A
Voltmeter range	40V
Electropolishing stop time	Switched off

After electropolishing, the 3mm disks were carefully washed by gently dipping them into each of two beakers of ethanol to remove the electrolyte. These samples were left to dry on filter paper and then carefully stored to be used in the TEM. A schematic of the electropolished TEM disks is shown in Figure 3.15.

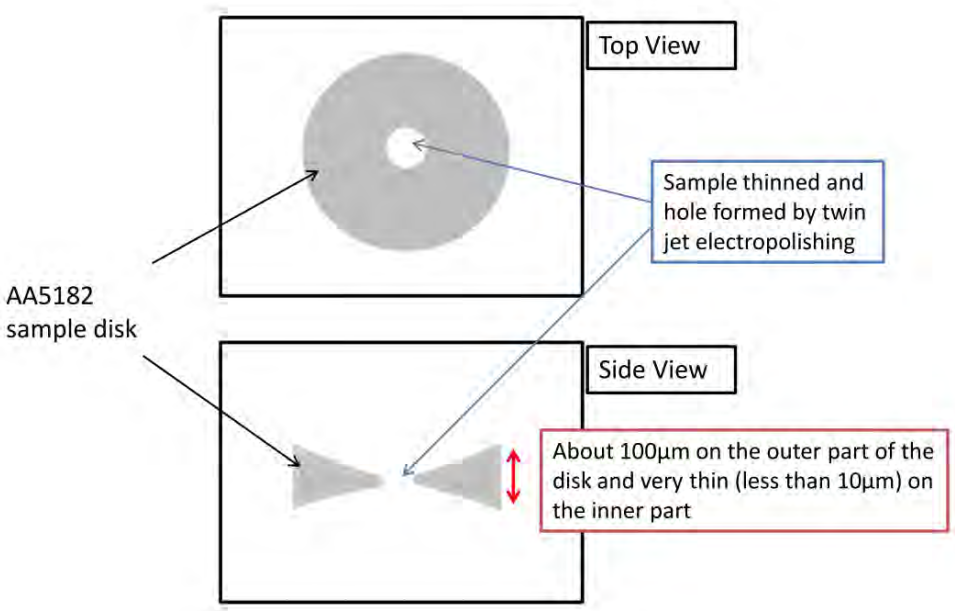

Figure 3.15: Schematic of the 3mm AA5182 disks thinned by twin jet electropolishing.

3.7 Electron Backscatter Diffraction

The electron backscatter diffraction (EBSD) technique was used to determine the average subgrain sizes of the samples and track the microstructural evolution in the samples. EBSD maps were generated for samples of each heat treatment condition. The FEI FEG Nova NanoSEM machine, shown in Figure 3.16, was used to perform the EBSD mapping technique. The Vmap program was used to analyze the data and generate microstructural information in the form of average subgrain sizes, described as Equivalent Circle Diameters (ECD), from each EBSD map. An average ECD from 10 representative EBSD maps was generated for each sample. Only maps with an above 50% indexing rate were considered. This was done in order to obtain a representative average for each sample. The experimentally determined conditions used for the EBSD are shown in Table 3.5. The LAGBs and HAGBs were defined as 2° and 10° of misorientation respectively, as described in Subsections 2.5.1 and 2.6.2.

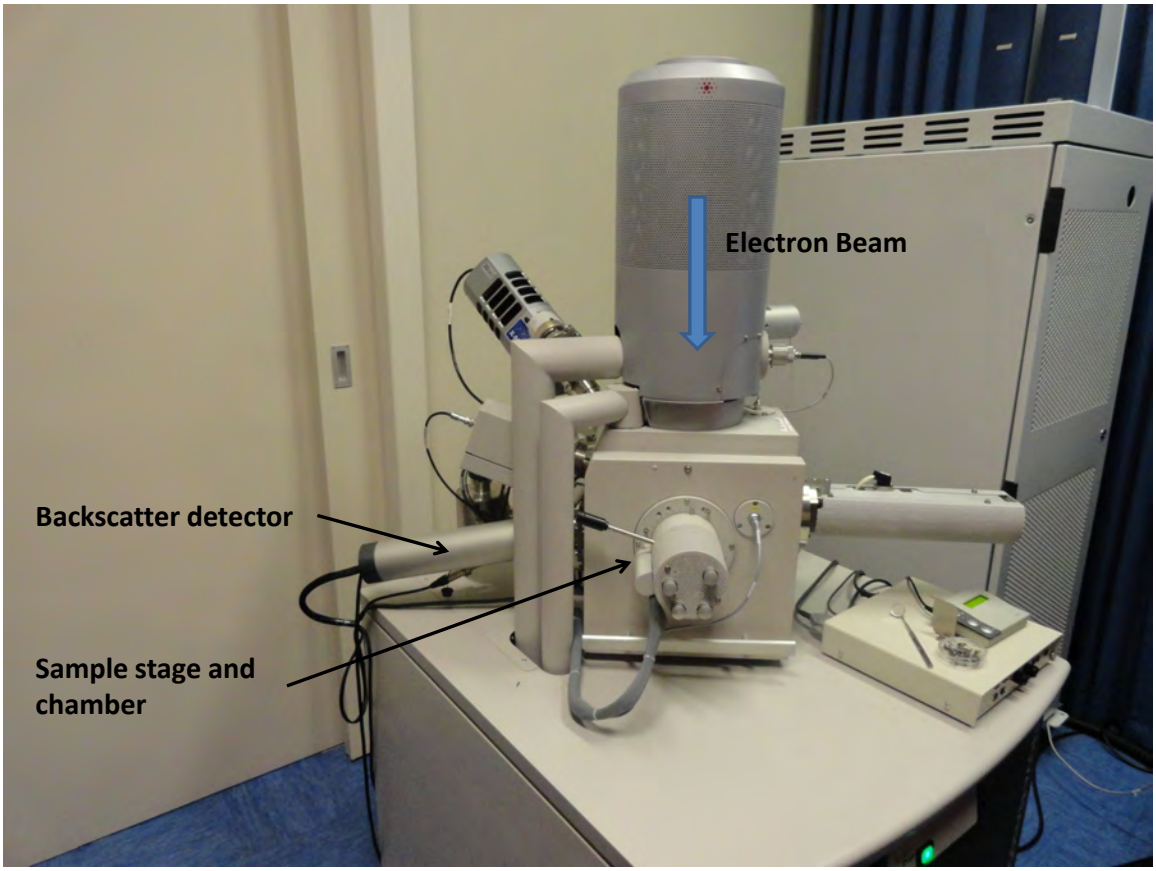

Figure 3.16: Nova NanoSEM with backscatter detector for EBSD.

Table 3.5: Conditions used for the EBSD maps in the FEG NanoSEM

Condition/ Setting	**Value Used**
Electron Beam	20kV
Magnification	x7500
Working distance	10mm
Map grid size	160 x 150
Step-size	0.2μm
Binning	2 x 2
Gain	High
Timing per frame (at least)	40ms
Sample tilt angle	70°
Number of bands detected	4 and 6

3.8 Transmission Electron Microscopy

The 3mm TEM sample disks were placed in the TEM single tilt holder, shown in Figure 3.17, to enable the samples to be viewed from multiple tilt angles.

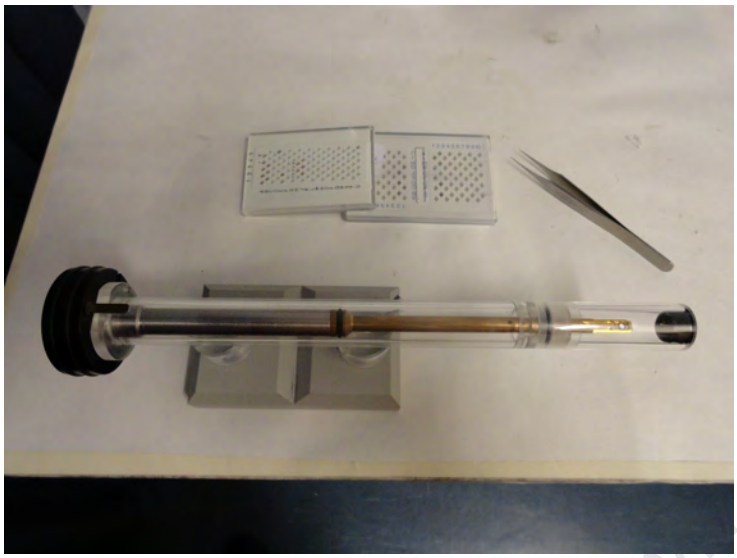

Figure 3.17: TEM single tilt sample holder.

The FEI Tecnai T20 transmission electron microscope (TEM) operating at 200keV, shown in Figure 3.18, was used to investigate the microstructure of the electropolished 3mm disks from each of the conditions shown in Table 3.2. The Gatan image filtering system was incorporated with the CCD camera to allow for energy filtering of the images acquired. The microstructures in these samples were determined for each condition from TEM micrographs taken from areas thin enough for representative and informative TEM micrographs to be acquired.

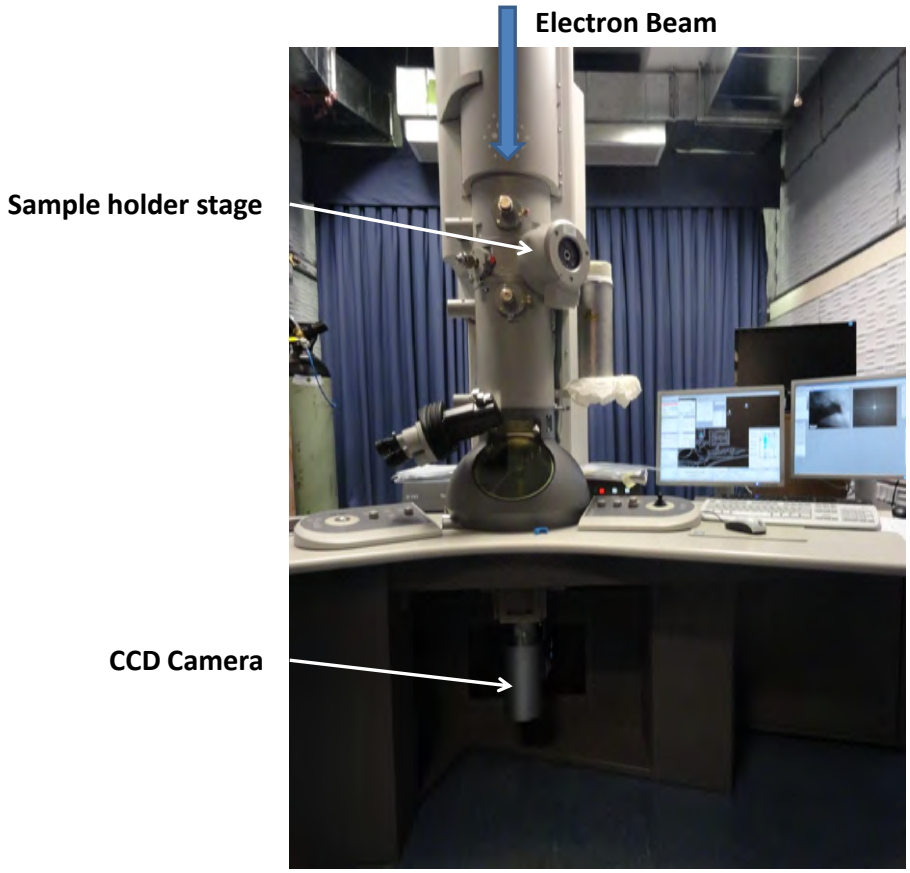

Figure 3.18: FEI Tecnai T20 TEM.

3.9 Experimental Procedure Summary

The experimental procedure used in this study is summarized in Figure 3.1. Mechanical tests were carried out in the form of tensile tests and microstructural studies were performed using light microscopy, EBSD and TEM. The as-cold rolled AA5182 specimens were tested in order to provide a control. The specimens were then heat treated to simulate the conditions of stabilization at Hulamin, and were tested at these conditions. The chosen heat treated specimens were then subjected to a further heat treatment procedure which simulated the coil coating procedure used at Hulamin. The specimens were then mechanically tested at these conditions and their microstructures were investigated.

Chapter 4

Results and Discussion

4.1 Introduction to the Results

The following results have been obtained following the methodology described in Chapter 3. In order to determine an overview of the AA5182 microstructure, light microscopy images were first obtained. The results are then presented for the mechanical testing and microstructure investigations on the as-cold rolled (as-CR) AA5182 specimens. These as-CR results were then used to compare the subsequent test results to. The results for the heat treated specimens, described in Table 3.1, and the specimens after the simulated coil coating procedure, described in Table 3.2, were then obtained. Two AA5182 specimens were mechanically tested for each condition. These results are discussed in each section and are summarized in Section 4.4.

4.2 Light Microscopy

In order to investigate the general microstructure of the as-CR AA5182, anodized samples were investigated using polarized light microscopy. A representative light micrograph is shown in Figure 4.1. The AA5182 grains are elongated in the direction of metal flow during rolling, the RD, as discussed in Subsection 2.5.2. This elongation is expected in these severely cold rolled samples, as the surface investigated includes the RD and TD, as described in Figure 3.8. The average grain sizes observed fell into the range of between 140μm and 160μm in length elongated in the RD and between 12μm and 20μm in the TD direction, as described in Figure 3.10. There were no noticeable shear bands observed in the grains of the samples investigated. Within these grains, however, structures such as subgrains may form, and the size of these was investigated using the EBSD technique in the SEM, as described in Section 4.3.

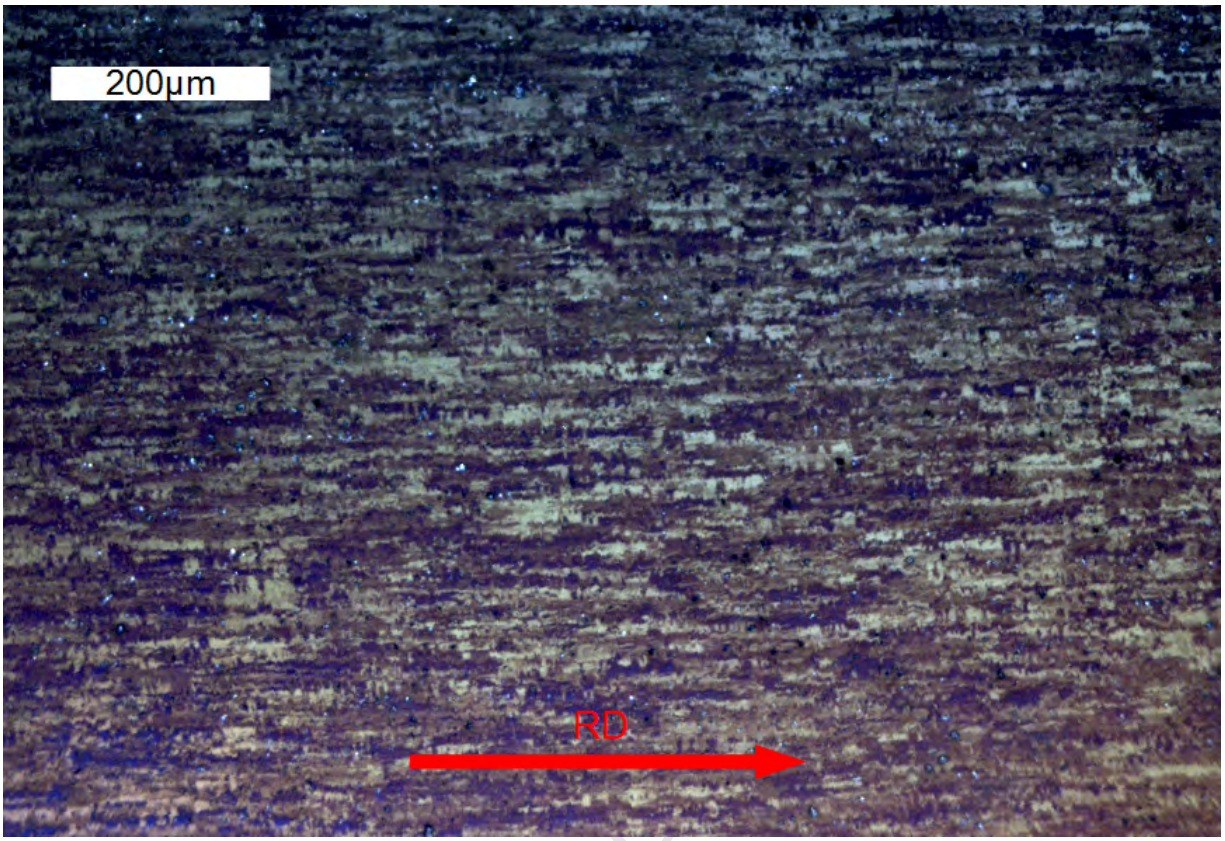

Figure 4.1: A representative polarized light micrograph for an as-cold rolled AA5182 specimen.

4.3 Stabilization Heat Treatment Design Matrices

4.3.1 As-Cold Rolled Specimens

Mechanical testing was performed on the as-cold rolled (as-CR) AA5182 tensile specimens to provide a reference against which the results of the heat treated specimens could be measured. The as-CR 0.2% yield stress, shown in the bottom right hand corner of Figure 4.2, was 368MPa and the average value obtained from two tensile tests was 373MPa.

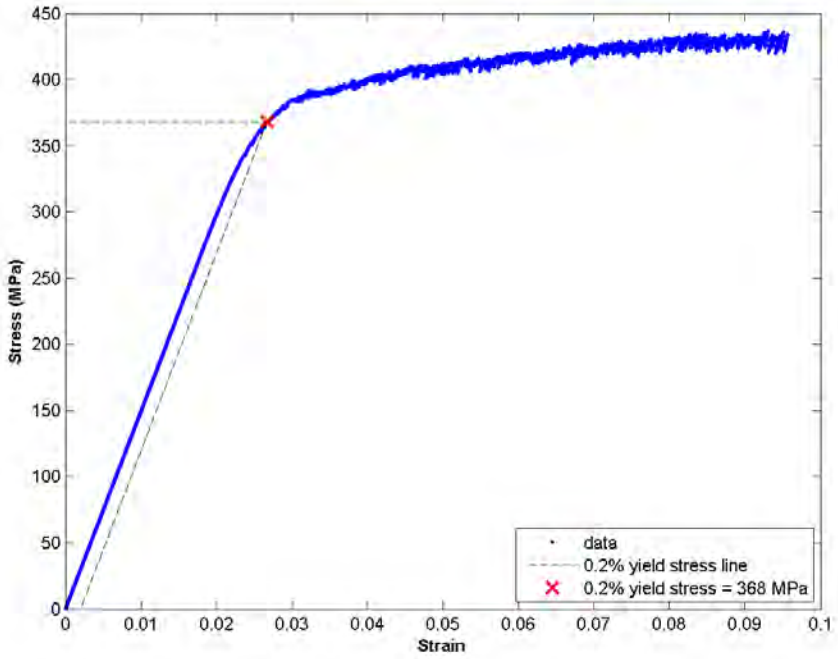

Figure 4.2: Stress-strain curve for an as-CR specimen.

This 0.2% yield stress value is only 2MPa less than the expected H18, strain-hardened, fully hard condition's 0.2% yield stress value of 375MPa, as shown in Table 2.4. This as-CR average 0.2% yield stress value is 88MPa larger than the value of 285MPa for the H34, strain-hardened and stabilized condition, as shown in Table 2.4 also. The average ultimate tensile strength (UTS) for the as-CR samples is 427MPa, which is 27MPa higher than the H18 condition value of 400MPa, as shown in Table 2.4. As shown in Table 2.4, the % elongation in Figure 4.2 is approximately 9.7%, which is 5.7% greater than that of the H18 condition at 4%. The mechanical properties of the as-CR AA5182 specimens were thus such that the 0.2% yield stress was comparable to that of the H18 condition, while the % elongation and UTS values were both greater than the H18 condition values.

The true stress and true strain values were determined, as described in Subsection 2.4.2, for the as-CR specimens. The true stress-true strain values are shown in Figure 4.3a). The logarithmic values of the true stress and true strain values are then plotted in Figure 4.3b) in order to obtain the work hardening coefficient, as described in Subsection 2.4.2.

a) b)

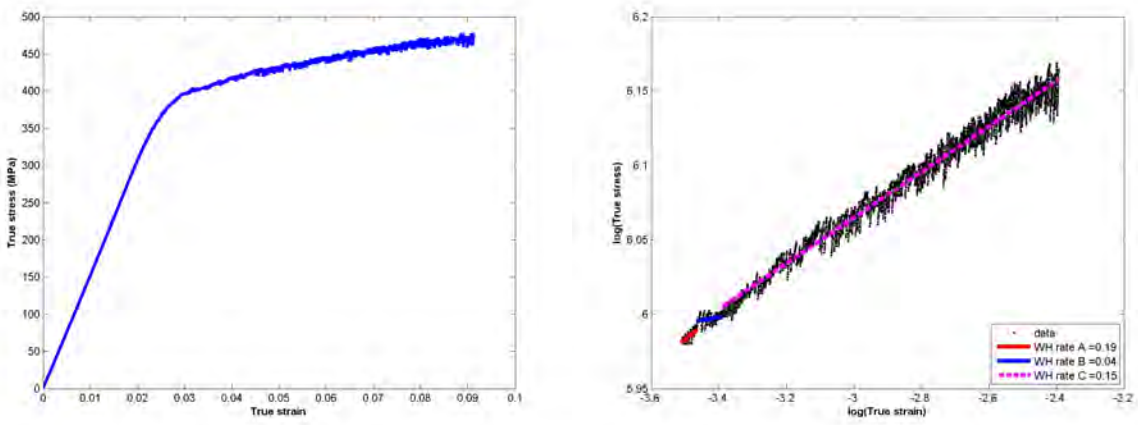

Figure 4.3: True stress-true strain curves showing work hardening for an as-CR specimen.

The work hardening rate is expected to be between 0.1 and 0.2 for metals such as the AA5182 specimens, as described in Table 2.5. This work hardening often occurs as a step in three parts, as described in Figure 2.13 as gradients A, B and C. It can be seen from Figure 4.3 that the work hardening exponents are 0.19, 0.04 and 0.15 for the gradients labelled A, B and C respectively. The n-value for at least one of these regions in the graph is in the expected range of 0.1 to 0.2. The n-value for C is 0.15, for example, as summarized in Table 4.1. This value is in the expected range but is relatively low when compared to a typical n value of about 0.2 for aluminium alloys [11]. AA5182 CES with a high n-value has a greater capacity to be formed during the subsequent can forming processes, than CES with a low n-value. The cold rolling mill imparted strain on the CES and thus it has a lower capacity to undergo additional straining. The as-CR CES has a lower formability than if it had been cold worked to a lesser extent. The CES does, however, have a high 0.2% yield stress, a high UTS and a % elongation higher than the H18 value. The as-CR specimens were not stored at sub-zero temperatures during this study and therefore age softening did occur. This may have resulted in the mechanical properties, such as the 0.2% yield stress value, being lower than expected. A sample size of two tensile tests per condition was used due to time and material constraints, and this may not have reduced the variation of the average results. The AA5182 specimens, however, do have favourable strength properties and % elongation values, when compared to the H18 AA5182 values shown in Table 2.4, and these are desirable for the CES produced.

The electron backscatter diffraction (EBSD) map shown in Figure 4.4 is a greyscale map. The shades of grey indicate separate subgrains in the sample, defined as areas with misorientation of 2° or more, as described in Subsection 2.6.2. The black points in the greyscale map indicate non-indexed points where no crystallographic information could be determined due to poor quality Kikuchi patterns, as described in Subsection 2.6.2.

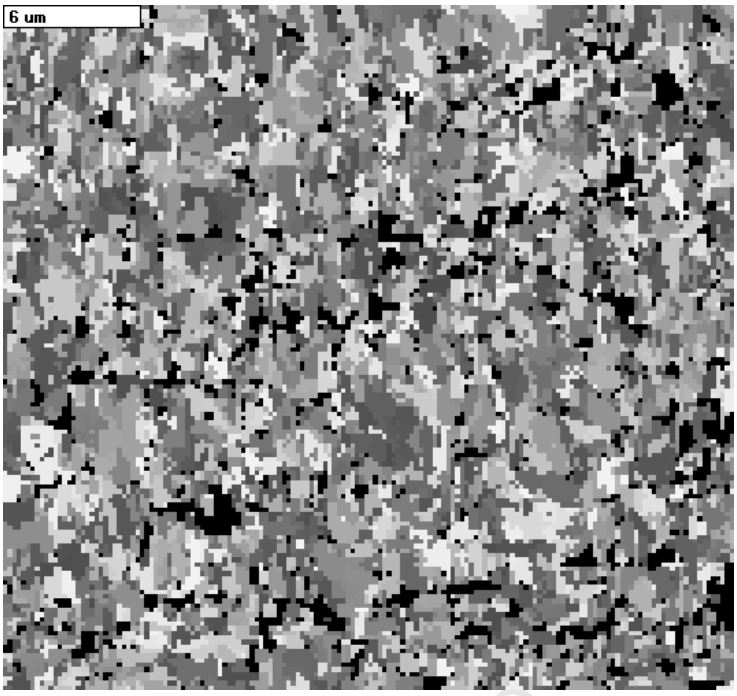

Figure 4.4: A representative EBSD map of an as-CR sample.

The average size of these subgrains was determined from 10 EBSD maps with high indexing rates where greater than 50% of the points were indexed. The theory in Subsection 2.5.2 explains that regions with high dislocation density, such as at subgrains, will impede the motion of dislocations through the material and thus will result in an increase in yield strength due to strain hardening. This average subgrain size is described as an equivalent circle diameter (ECD), as each subgrain is approximated to a circle. This average ECD value was 0.62μm from the 10 chosen high quality EBSD maps for the as-CR samples. These ECD values and mechanical properties obtained for the as-CR samples are summarized in Table 4.1 and will now be compared to the values obtained for the heat treated specimens.

Table 4.1: Mechanical properties and ECD values for the as-CR specimens

Condition	σ_{yield}	σ_{uts}	**n values**			**average**
	(MPa)	**(MPa)**	**A**	**B**	**C**	**ECD (μm)**
as-CR	368	437	0.19	0.04	0.15	0.62
	377	437	0.05	0.30	0.15	

4.3.2 120°C Heat Treatments

The 0.2% yield stress values, shown in the bottom right hand corners of Figures 4.5 and 4.6, were 380MPa for the 120°C for 1 hour and 366MPa for the 120°C for 4 hours heat treatments. The average 0.2% yield stress values were calculated as 378MPa and 366MPa for the heat treatments for 1 hour and 4 hours respectively.

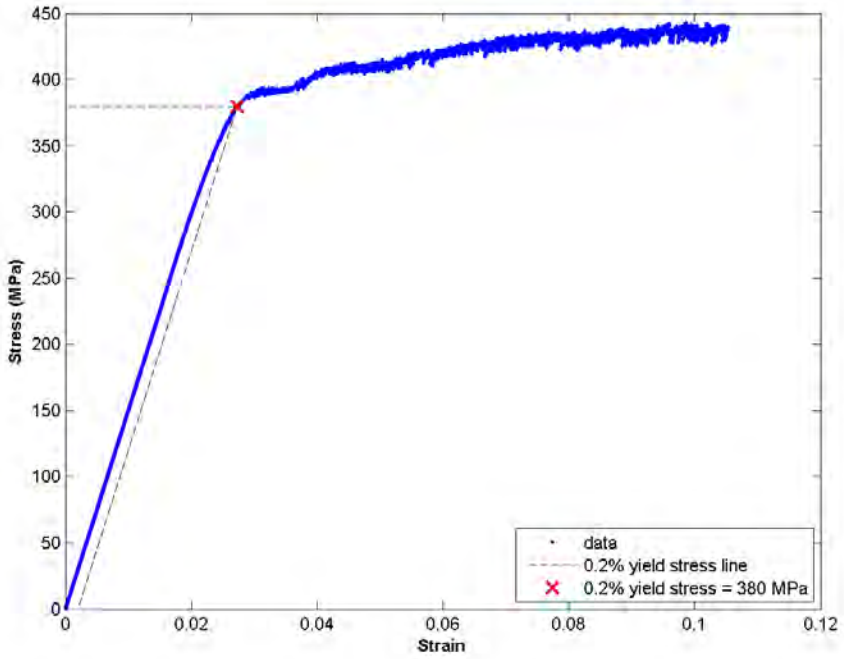

Figure 4.5: Stress-strain curve for AA5182 heat treated at 120°C for 1 hour.

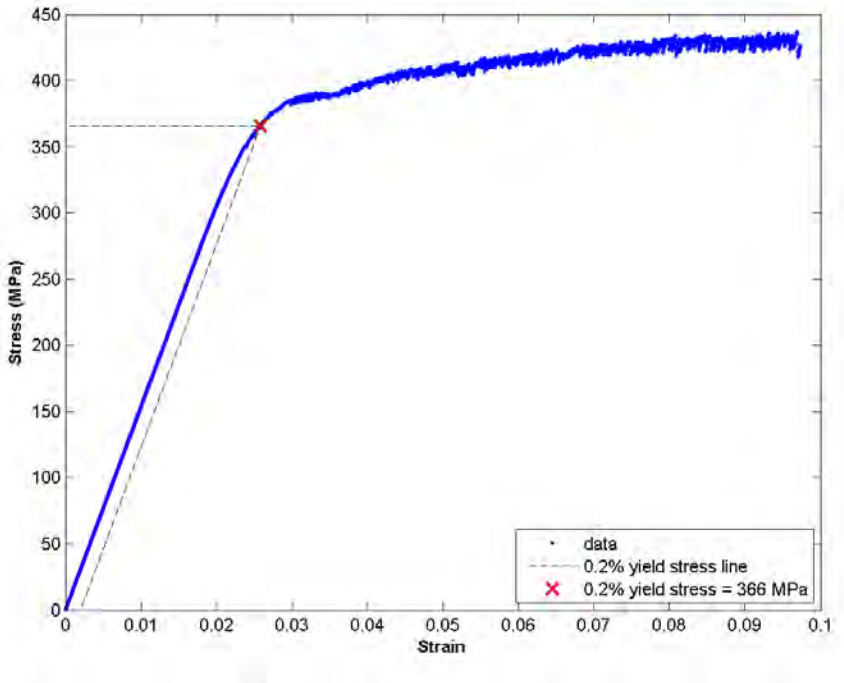

Figure 4.6: Stress-strain curve for AA5182 heat treated at 120°C for 4 hours.

For a stabilized specimen, it is expected that the 0.2% yield stress value decreases to about

285MPa, as shown for the H34 condition in Table 2.4. The H34 condition specimens are strain-hardened and stabilized. The average 0.2% yield stress values for the 120°C heat treatments, however, were comparable to values of the as-CR specimens at 373MPa, and not to the expected values of the H34 condition at 285MPa. These average values suggest that the heat treatment time of 1 hour at 120°C did not sufficiently stabilize the AA5182 specimens, as the 0.2% yield stress was similar to that of the as-CR sample with a difference of 5MPa greater. The average values also suggest that the heat treatment for 4 hours at 120°C does not sufficiently stabilize the specimens but perhaps causes some softening due to recovery in the alloy. The average 0.2% yield stress is 7MPa lower than that of the as-CR specimens. The average 0.2% yield stress values for both 120°C heat treatments are considerably higher than the H34 value of 285MPa, shown in Table 2.4. This also suggests that a temperature of 120°C for either 1 or 4 hours does not result in sufficient stabilization of the AA5182 specimens. The average UTS values for the 1 hour and 4 hour heat treatments are 439MPa and 432MPa respectively. These strength values are 12MPa and 5MPa greater than the as-CR value of 427MPa respectively, and are comparable to that of the as-CR specimens.

The true stress and true strain values were determined, as described in Subsection 2.4.2, for the 120°C heat treated specimens. The true stress-true strain values are shown in Figures 4.7a) and 4.8a). The logarithmic values of the true stress and true strain values are then plotted in Figures 4.7b) and 4.8b), in order to obtain the work hardening coefficient, as described in Subsection 2.4.2.

a) b)

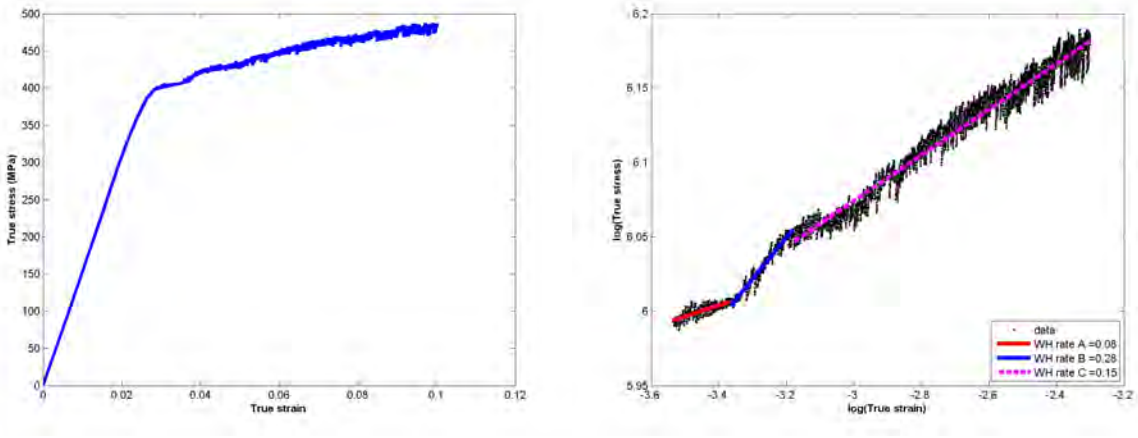

Figure 4.7: True stress-true strain curves showing work hardening for AA5182 heat treated at 120°C for 1 hour.

a) b)

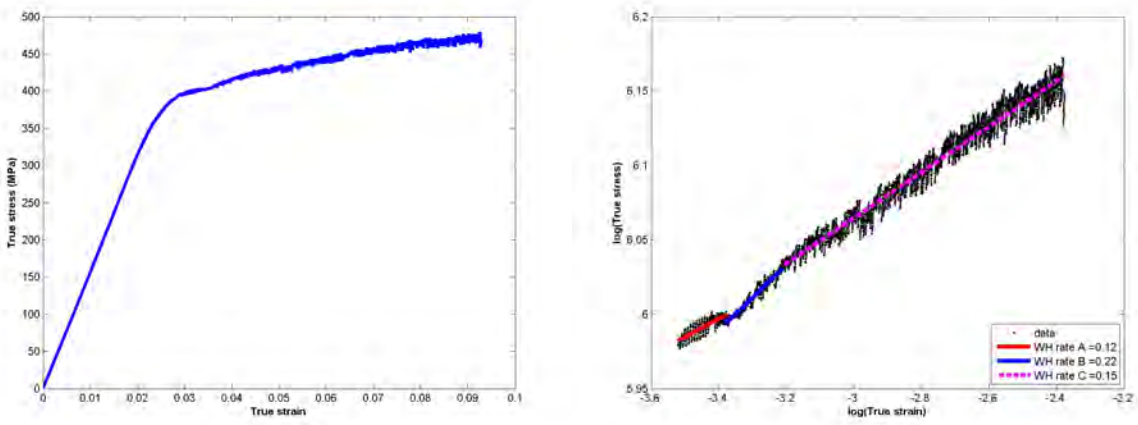

Figure 4.8: True stress-true strain curves showing work hardening for AA5182 heat treated at 120°C for 4 hours.

As was described in Subsection 4.3.1, the expected work hardening rate is between 0.1 and 0.2 for the AA5182 specimens. This work hardening often occurs as a step in three parts, as described in Figure 2.13 as gradients A, B and C. For the 120°C 1 hour specimen in Figure 4.7, the work hardening exponents are 0.08, 0.28 and 0.15 for the gradients labelled A, B and C respectively. For the 120°C 4 hour specimen in Figure 4.8, the work hardening exponents are 0.12, 0.22 and 0.15 for the gradients labelled A, B and C respectively. The n-values for at least one of these regions in both the 120°C graphs is in the expected range of 0.1 to 0.2. The n-value for C for both graphs is 0.15, for example, as summarized in Table 4.2. This value is in the expected range but is relatively low when compared to a predicted n value of about 0.2. As was described in Subsection 4.3.1, specimens with a low n-value have a lower capacity for formability. The cold rolling mill severely worked the CES and thus it has a lower capacity to undergo additional straining than if it had not been cold worked. The heat treatments at 120°C do not appear to have a significant effect on the as-CR specimens' mechanical properties. These properties are summarized in Table 4.2. From the lack of change to the mechanical properties, it may be inferred that the heat treatments at 120°C may not be sufficient to cause a considerable change to the microstructure and work hardening characteristics of the CES.

Figures 4.9 and 4.10 show the greyscale EBSD maps for the AA5182 CES heat treated at 120°C for 1 hour and 4 hours respectively.

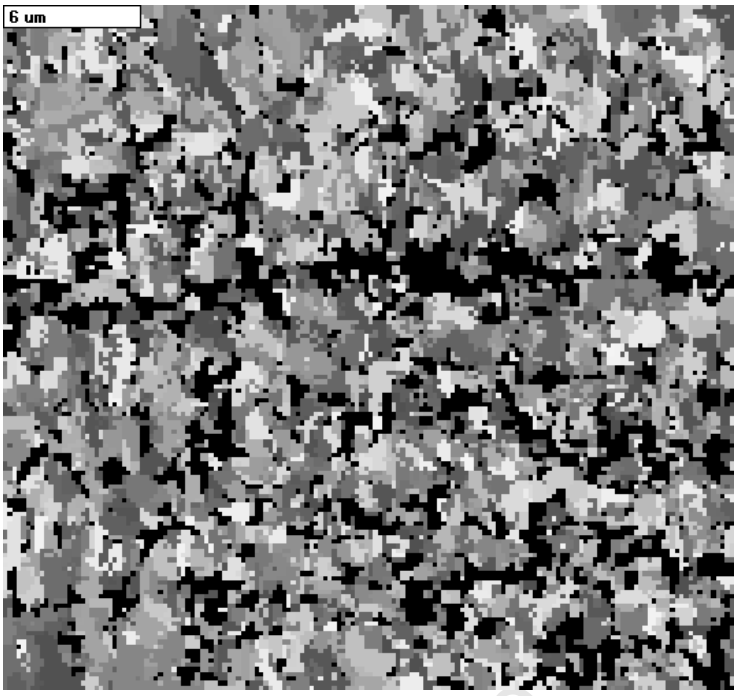

Figure 4.9: A representative EBSD map of a sample after a heat treatment at 120°C for 1 hour.

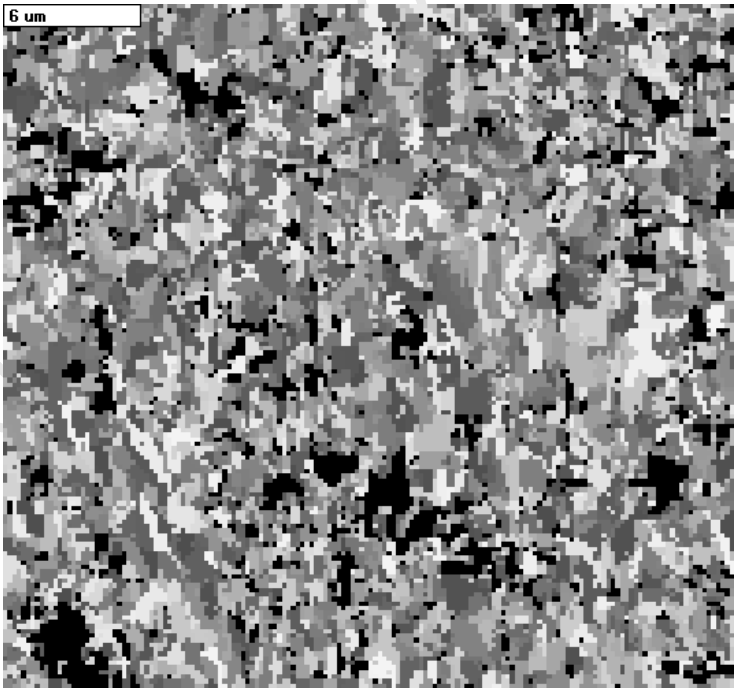

Figure 4.10: A representative EBSD map of a sample after a heat treatment at 120°C for 4 hours.

From 10 of these EBSD maps each, the average ECD values were calculated to be 0.70μm and 0.62μm, as shown in Table 4.2. These values are within 0.1μm of the as-CR average ECD of 0.62μm. This means that the average subgrain sizes for the 120°C 1 hour and 4 hour heat

treatment samples were 0.08μm greater and the same as that of the as-CR samples. This suggests that, although the 120°C 1 hour samples have a 0.08μm larger subgrain size than the as-CR samples, both heat treatments had only a small or no measurable effect on the sub-grain size as measured with the EBSD technique. These results are discussed further in Section 4.4. The mechanical and ECD results for the 120°C heat treatments are summarized in Table 4.2.

Table 4.2: Mechanical properties and ECD values for the 120°C specimens

Condition		σ_{yield}	σ_{uts}	**n values**			**average**
Temperature	**Time**	**(MPa)**	**(MPa)**	**a**	**b**	**c**	**ECD (μm)**
120°C	1 hour	376	443	0.07	0.22	0.14	0.70
		380	443	0.08	0.28	0.15	
120°C	4 hours	366	438	0.09	0.25	0.14	0.62
		366	437	0.12	0.22	0.15	

4.3.3 150°C Heat Treatments

The 0.2% yield stress values, shown in the bottom right hand corners of Figures 4.11 and 4.12, were 368MPa and 369MPa respectively. The average 0.2% yield stress values were calculated as 361MPa and 365MPa for the heat treatment for 1 hour and 4 hours respectively.

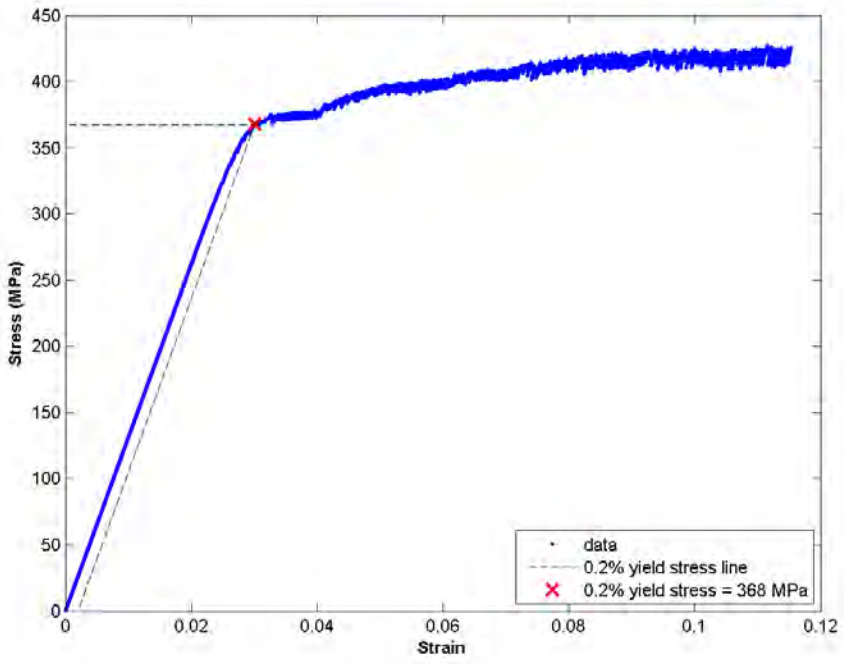

Figure 4.11: Stress-strain curve for AA5182 heat treated at 150°C for 1 hour.

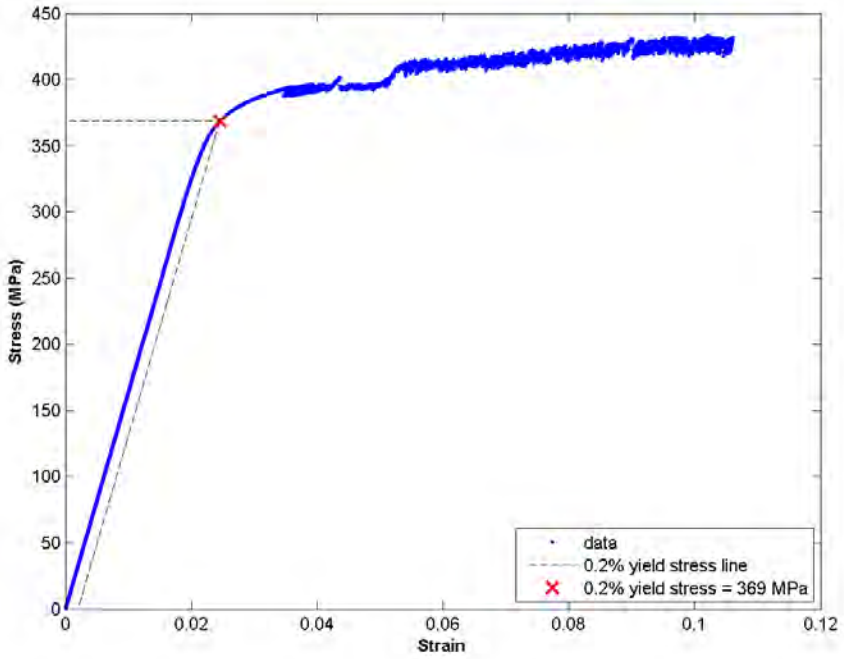

Figure 4.12: Stress-strain curve for AA5182 heat treated at 150°C for 4 hours.

The average 0.2% yield stress values were 12MPa and 8MPa less than that of the as-CR specimens at 373MPa. These average values are both considerably larger, 76MPa and 80MPa, than the 285MPa for the H34 condition shown in Table 2.4. These values suggest that the heat treatments at 150°C resulted in a slight decrease in the strength properties when compared to those of the as-CR condition, but these strength properties are still much higher than those of the H34, strain hardened and stabilized condition. The 150°C 4 hour heat treatment resulted in only an average 8MPa decrease from the average as-CR 0.2% yield stress value. This 150°C 4 hour treatment is the most similar to that used in the stabilization treatment at Hulamin and thus is investigated and referred to as the chosen stabilization heat treatment (CSHT).

The average UTS values for the 1 hour and 4 hour heat treatments are 425MPa and 429MPa respectively, which are considerably larger than the 340MPa value for the H34 condition shown in Table 2.4. These strength values are 2MPa smaller and 2MPa greater than the as-CR value of 427MPa, and thus the mechanical properties associated with these heat treatments are comparable to that of the as-CR specimens. Also, as was mentioned in Subsection 4.3.1, the as-CR specimens underwent room temperature age softening before mechanical testing, thus affecting the mechanical property values associated with the non-stabilized condition.

The true stress and true strain values were determined, as described in Subsection 2.4.2, for the 150°C heat treated specimens. The true stress-true strain values are shown in Figures 4.13a) and 4.14a). The logarithmic values of the true stress and true strain values are then plotted in Figures 4.13b) and 4.14b), in order to obtain the work hardening coefficient, as described in

Subsection 2.4.2.

Figures 4.13 and 4.14 show the true stress-true strain curves and the logarithmic true stress-true strain curves for the 150°C heat treatments for 1 hour and 4 hours respectively.

a) b)

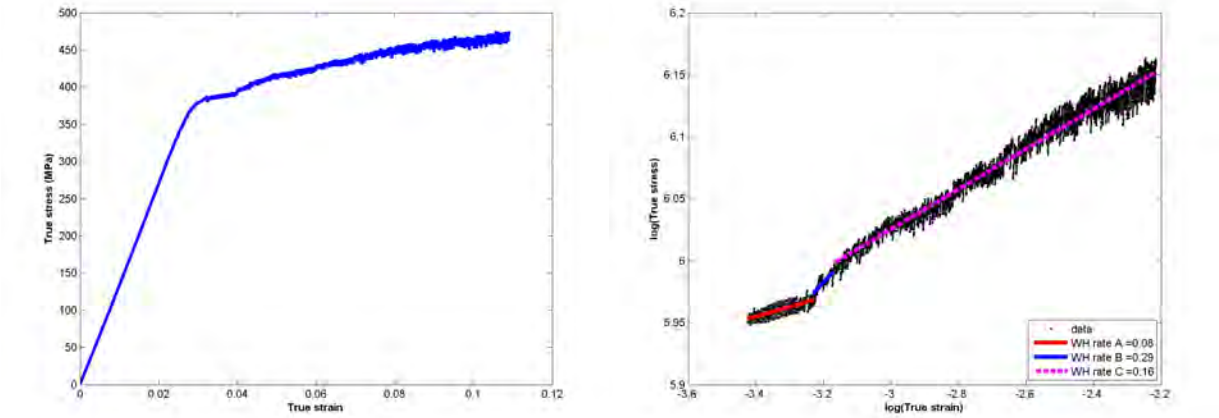

Figure 4.13: True stress-true strain curves showing work hardening for AA5182 heat treated at 150°C for 1 hour.

a) b)

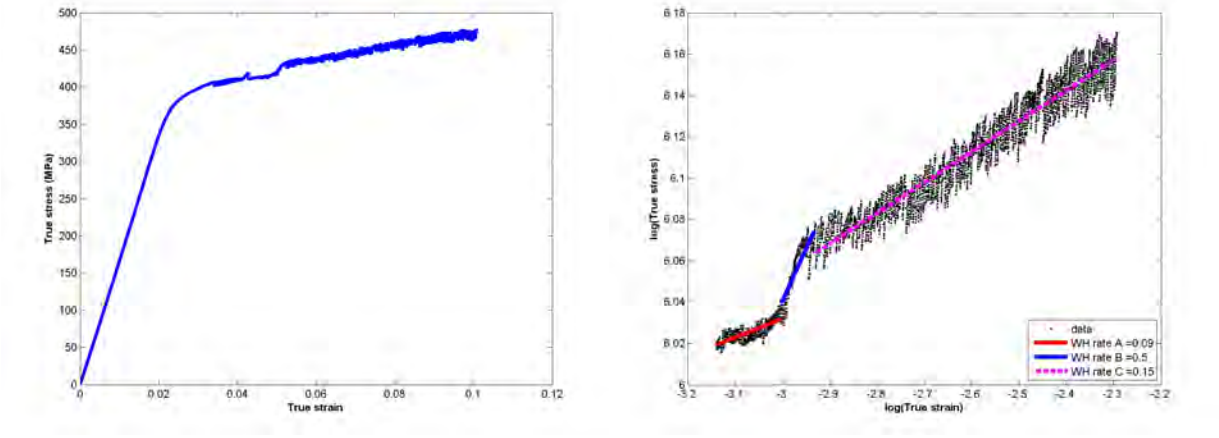

Figure 4.14: True stress-true strain curves showing work hardening for AA5182 heat treated at 150°C for 4 hours.

As was described in Subsection 4.3.1, the expected work hardening rate is between 0.1 and 0.2 for the AA5182 specimens. The work hardening for the 150°C heat treatment specimens in Figures 4.13 and 4.14, occurs with a step as three parts with gradients A, B and C. For the 150°C 1 hour specimen in Figure 4.13, the work hardening exponents are 0.06, 0.29 and 0.16 for the gradients labelled A, B and C respectively. For the 150°C 4 hour specimen in Figure 4.14, the work hardening exponents are 0.09, 0.5 and 0.15 for the gradients labelled A, B and C respectively. The n-values for at least one of these regions in both the 150°C graphs is in the expected range

of 0.1 to 0.2. The n-value for C is 0.16 and 0.15 for the two graphs, for example, as summarized in Table 4.3. These values are in the expected range but are relatively low when compared to a predicted n value of about 0.2. These values are the same or slightly larger than the as-CR and 120°C heat treated specimens. As was described in Subsection 4.3.1, specimens with a low n-value have a lower capacity for formability. The n-values for B are 0.29 and 0.5, however, which are on average greater than those for the as-CR and 120°C heat treatments of 0.04, 0.28 and 0.22. These mechanical properties are all summarized in Table 4.10. The 150°C heat treatment was identified as that heat treatment which most closely simulates the stabilization heat treatment at Hulamin. This 150°C heat treatment was thus investigated further and is referred to in this study as the chosen stabilization heat treatment (CSHT). Although the mechanical properties in the CSHT specimens may only differ to a small degree to those of the as-CR specimens, the CSHT may affect the long term properties of the CES if it is effective in stabilizing it.

Figures 4.15 and 4.16 show the greyscale EBSD maps for the AA5182 CES heat treated at 150°C for 1 hour and 4 hours respectively.

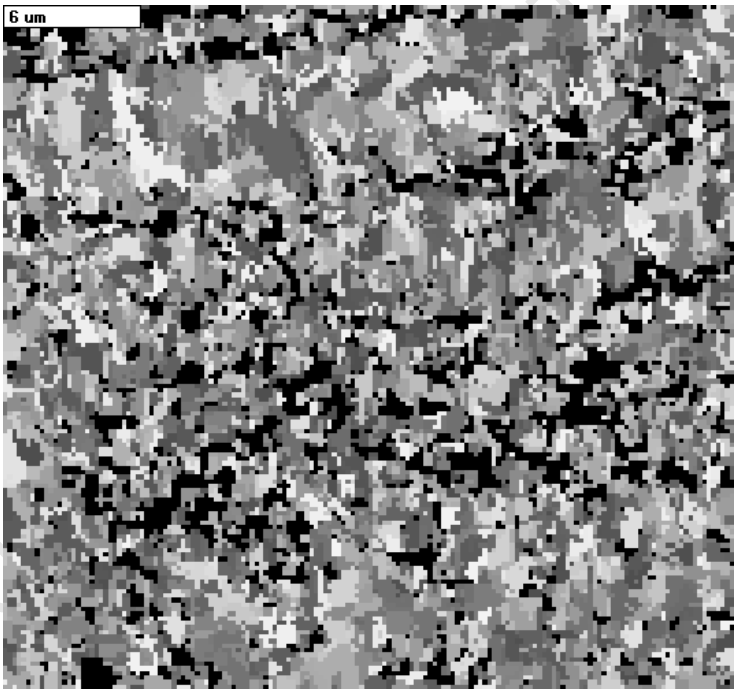

Figure 4.15: A representative EBSD map of a sample after a heat treatment at 150°C for 1 hour.

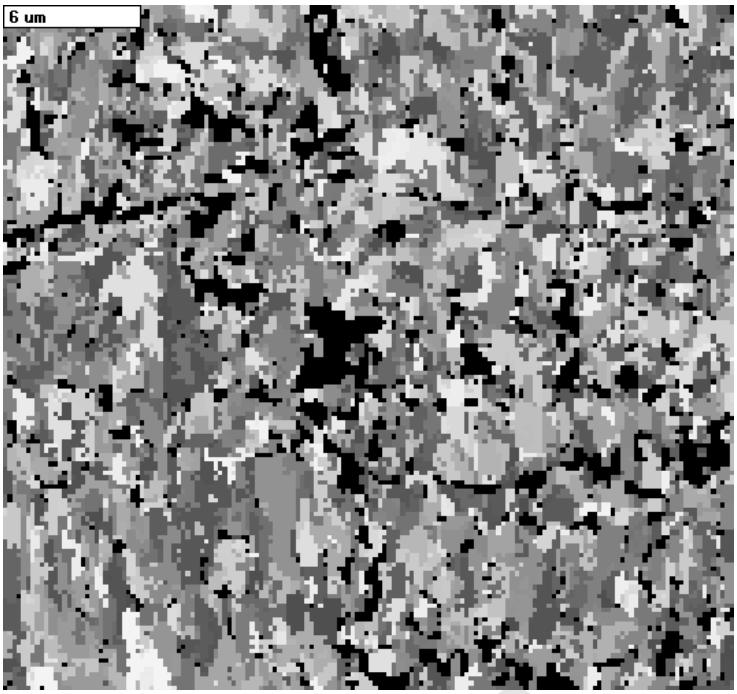

Figure 4.16: A representative EBSD map of a sample after a heat treatment at 150°C for 4 hours.

From 10 of these EBSD maps, the average ECD values were calculated to be 0.60μm and 0.66μm. These values are within 0.04μm of the as-CR average ECD of 0.62μm. This means that the average subgrain sizes for the 150°C 1 hour and 4 hour heat treatment samples were 0.02μm smaller and 0.04μm greater than that of the as-CR samples respectively. This suggests that both the 150°C heat treatments had only a small measurable effect on the sub-grain size as measured with the EBSD technique. These results are discussed further in Section 4.4. The mechanical properties and ECD results for the 150°C heat treatments are summarized in Table 4.3, with the blue coloured n values inserted for comparison purposes where no step was measured.

Table 4.3: Mechanical properties and ECD values for the 150°C specimens

Condition		σ_{yield}	σ_{uts}	**n values**			**average**
Temperature	**Time**	**(MPa)**	**(MPa)**	**a**	**b**	**c**	**ECD (μm)**
150°C	1 hour	354	431	0.17	0.17	0.17	0.60
		368	427	0.08	0.29	0.16	
150°C	4 hours	361	432	0.06	0.41	0.14	0.66
		369	427	0.19	0.50	0.15	

4.3.4 200°C Heat Treatments

The 0.2% yield stress values, shown in the bottom right hand corners of Figures 4.17 and 4.18, were 315MPa for the 200°C 1 hour and 310MPa for the 200°C 4 hour heat treated specimens. The average 0.2% yield stress values were both calculated as 316MPa for the heat treatment for 1 hour and 4 hours.

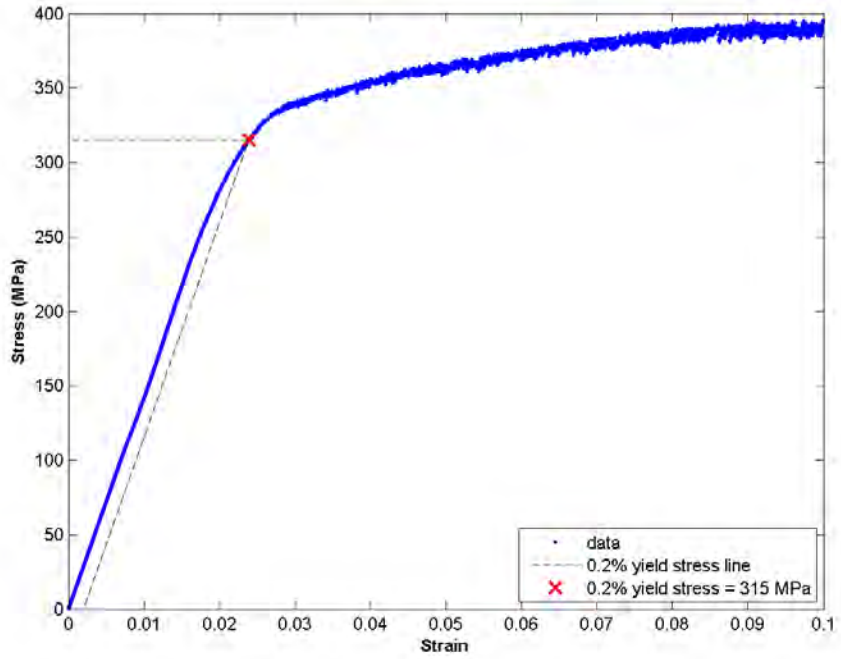

Figure 4.17: Stress-strain curve for AA5182 heat treated at 200°C for 1 hour.

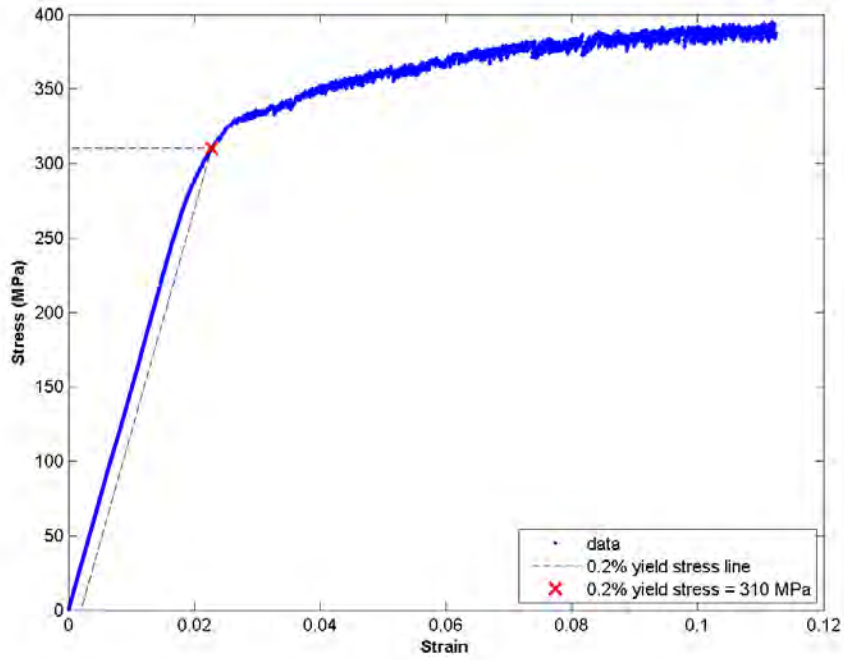

Figure 4.18: Stress-strain curve for AA5182 heat treated at 200°C for 4 hours.

The average 0.2% yield stress values were 57MPa less than that of the as-CR specimens at

373MPa. This decrease in strength of the as-CR specimens is larger than the decrease after 120°C and 150°C heat treatments. The strength values are also closer to the 285MPa value for the H34, strain hardened and stabilized condition, shown in Table 2.4. The values, however, are both still 31MPa larger than this H34 expected value. These values show that the heat treatments at 200°C resulted in a significant decrease in the strength properties when compared to those of the as-CR condition. This decrease in strength properties may result from the temperature of 200°C allowing significant recovery of the CES microstructure to occur, as described in 2.3.2.1. The decrease may also be due to rearrangement in the microstructure of the CES, such as the formation of the poorly defined dislocation cellular structures described in Subsection 2.5.6. This decrease may thus indicate that the 200°C heat treatment results in some stabilization of the CES.

The average UTS values for the 1 hour and 4 hour heat treatment are 395MPa and 397MPa respectively, which are considerably larger than the 340MPa value for the H34 condition shown in Table 2.4. These strength values, however, are 32MPa and 30MPa smaller than the as-CR value of 427MPa. This decrease in strength may be due to the softening of the CES due to recovery in its microstructure compared to that of the as-CR specimens. It may also be due to the rearrangement of the microstructure due to this 200°C heat treatment. Also, as was mentioned in Subsection 4.3.1, the as-CR specimens underwent room temperature age softening before mechanical testing, thus affecting the mechanical property values associated with the non-stabilized condition. The loss in strength properties due to the heat treatment at 200°C, therefore, may be even greater than expressed in this study.

The true stress and true strain values were determined, as described in Subsection 2.4.2, for the 200°C heat treated specimens. The true stress-true strain values are shown in Figures 4.19a) and 4.20a). The logarithmic values of the true stress and true strain values are then plotted in Figures 4.19b) and 4.20b), in order to obtain the work hardening coefficient, as described in Subsection 2.4.2.

Figures 4.19 and 4.20 show the true stress-true strain curves and the logarithmic true stress-true strain curves for the 200°C heat treatments for 1 hour and 4 hours respectively.

a) b)

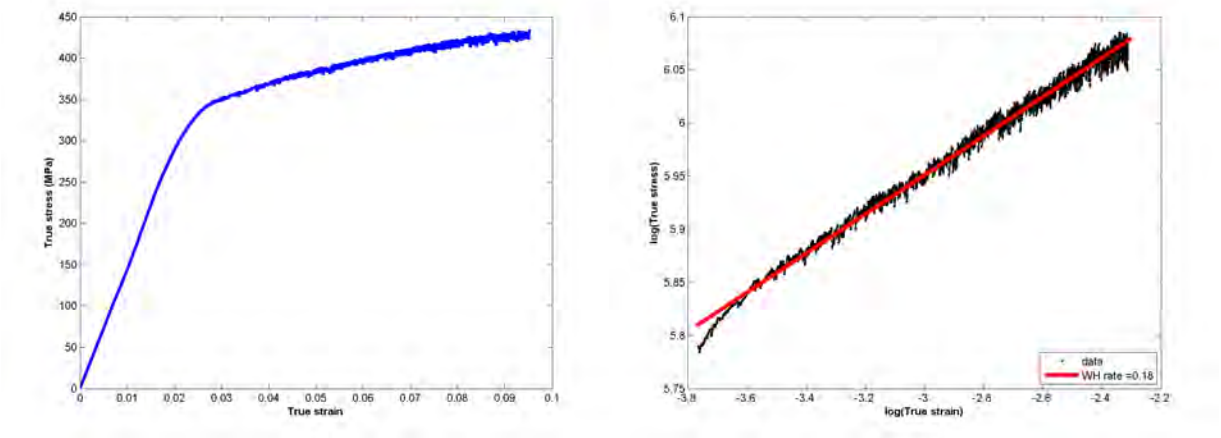

Figure 4.19: True stress-true strain curves showing work hardening for AA5182 heat treated at 200°C for 1 hour.

a) b)

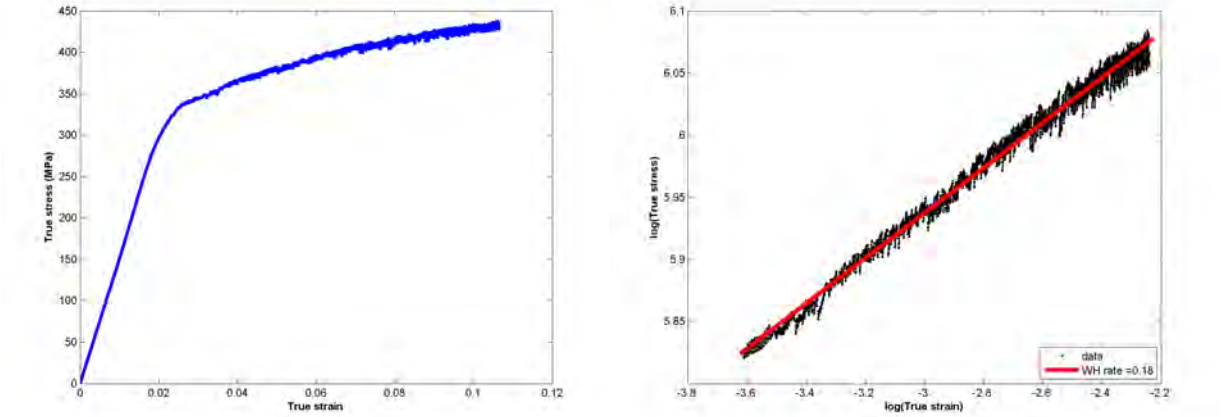

Figure 4.20: True stress-true strain curves showing work hardening for AA5182 heat treated at 200°C for 4 hours.

The work hardening for the 200°C heat treatment specimens in Figures 4.19 and 4.20, unlike the 120°C and 150°C heat treated and as-CR specimens, does not occur with a noticeable step. For both the 200°C 1 hour specimen in Figure 4.19 and the 200°C 4 hour specimen in Figure 4.20, the single work hardening exponent is 0.18. As was described in Subsection 4.3.1, the expected work hardening rate is between 0.1 and 0.2 for the AA5182 specimens. Specimens with a low n-value have a lower capacity for formability. These mechanical properties are all summarized in Table 4.10. The work hardening rate of 0.18 is greater than that of the corresponding values for the gradient C work hardening in the as-CR, 120°C and 150°C heat treated specimens. This suggests that the formability of the 200°C heat treated CES specimens is greater than that of the as-CR, 120°C and 150°C heat treated specimens. The average 0.2% yield stress of 316MPa

for the 200°C heat treated specimens is also relatively closer to that of the H34 condition value of 285MPa. Although these results may be due to recovery in the CES, they also suggest that the 200°C heat treatment may result in some stabilization of the AA5182 CES. The 150°C heat treatment was identified as that heat treatment which most closely simulates the stabilization heat treatment at Hulamin. The 150°C heat treated specimens were thus the ones investigated further in this study.

Figures 4.21 and 4.22 show the greyscale EBSD maps for the AA5182 CES heat treated at 200°C for 1 hour and 4 hours respectively.

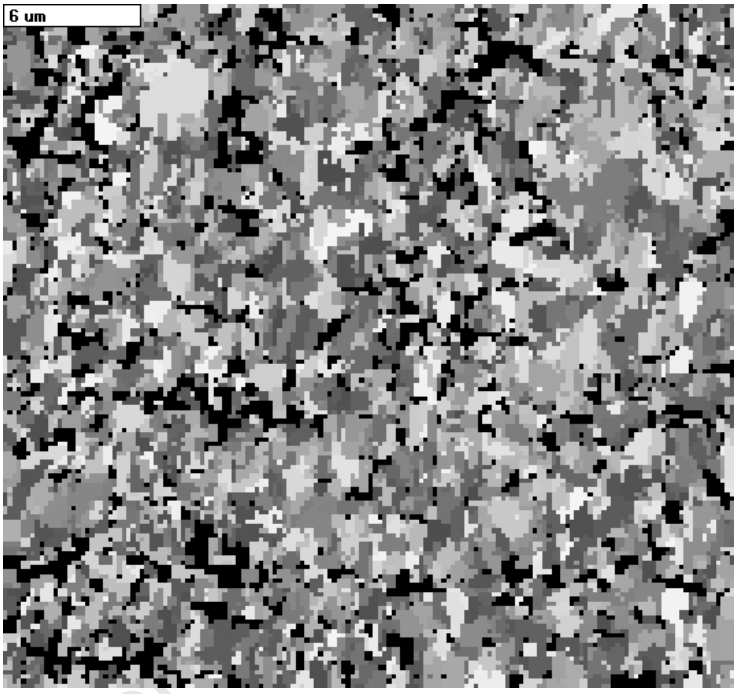

Figure 4.21: A representative EBSD map of a sample after a heat treatment at 200°C for 1 hour.

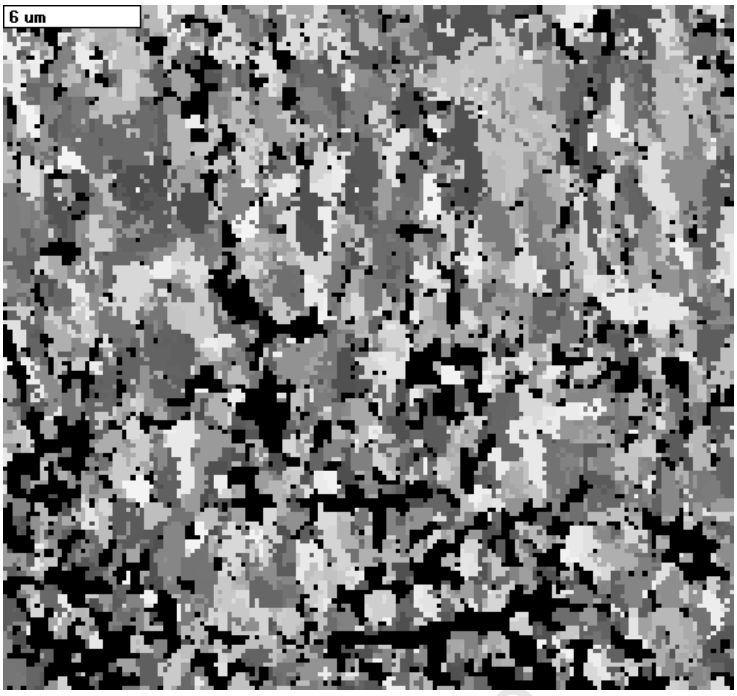

Figure 4.22: A representative EBSD map of a sample after a heat treatment at 200°C for 4 hours.

From 10 of these EBSD maps each, the average ECD values were calculated to be 0.66µm and 0.69µm, as shown in Table 4.4. These values are within 0.07µm of the as-CR average ECD of 0.62µm. This means that the average subgrain sizes for the 200°C 1 hour and 4 hour heat treatment samples were 0.04µm and 0.07µm greater than that of the as-CR samples respectively. This suggests that both the 200°C heat treatments had only a small measurable effect on the sub-grain size as measured with the EBSD technique. These results are discussed further in Section 4.4. Both the mechanical property and the ECD results for the 200°C heat treatments are summarized in Table 4.4, with the blue coloured n values inserted for comparison purposes where no step was measured.

Table 4.4: Mechanical properties and ECD values for the 200°C specimens

Condition		σ_{yield}	σ_{uts}	**n values**			**average**
Temperature	**Time**	**(MPa)**	**(MPa)**	**a**	**b**	**c**	**ECD (µm)**
200°C	1 hour	316	399	0.18	0.18	0.18	0.66
		315	395	0.18	0.18	0.18	
200°C	4 hours	322	410	0.18	0.18	0.17	0.69
		310	395	0.18	0.18	0.18	

4.3.5 The Simulated Coil Coating Procedure on the Specimens Heat Treated at 150°C for 4 hours

The AA5182 CES specimens heat treated at the chosen stabilization heat treatment (CSHT), 150°C for 4 hours, were further cold worked and heat treated in order to simulate the effects of coil coating, as shown in Figure 2.7. This simulated coil coating procedure (SCCP) involves first 10% cold work on the specimens and then a heat treatment at 220°C for either 4 minutes or 30 minutes. The SCCP is also carried out for 4 hours to study the effect of heat treatment at 220°C for this relatively long time. The CSHT is that which closely resembles the stabilization heat treatment used by Hulamin and thus was further investigated. The four sets of results are presented for the CSHT with 10%CW and then with a further heat treatment at 220°C for 4 minutes, 30 minutes and 4 hours.

The 0.2% yield stress values, shown in the bottom right hand corners of Figures 4.23, 4.24, 4.25 and 4.26, were 380MPa, 301MPa, 310MPa and 246MPa respectively. The average 0.2% yield stress values were calculated as 371MPa for the CSHT with 10%CW, 280MPa for the CSHT with SCCP for 4 minutes, 285MPa for the CSHT with SCCP for 30 minutes and 238MPa for the CSHT with SCCP for 4 hours.

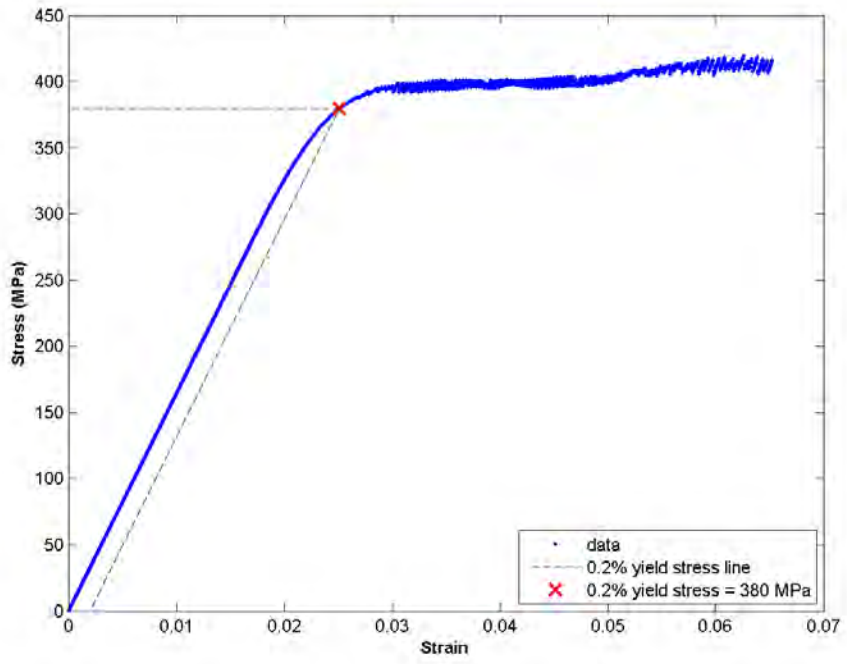

Figure 4.23: Stress-strain curve for the CSHT AA5182 with 10%CW.

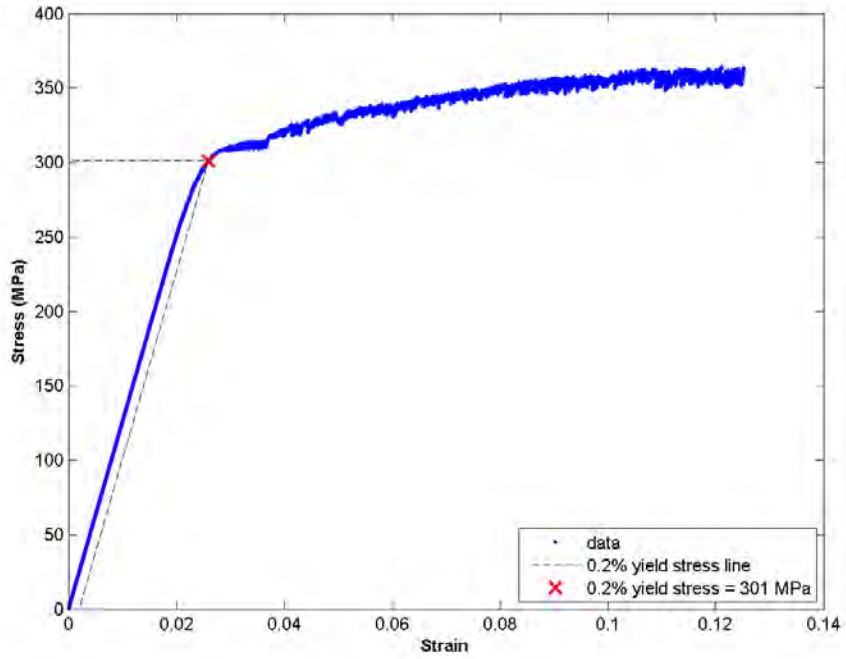

Figure 4.24: Stress-strain curve for the CSHT AA5182 with SCCP for 4 minutes.

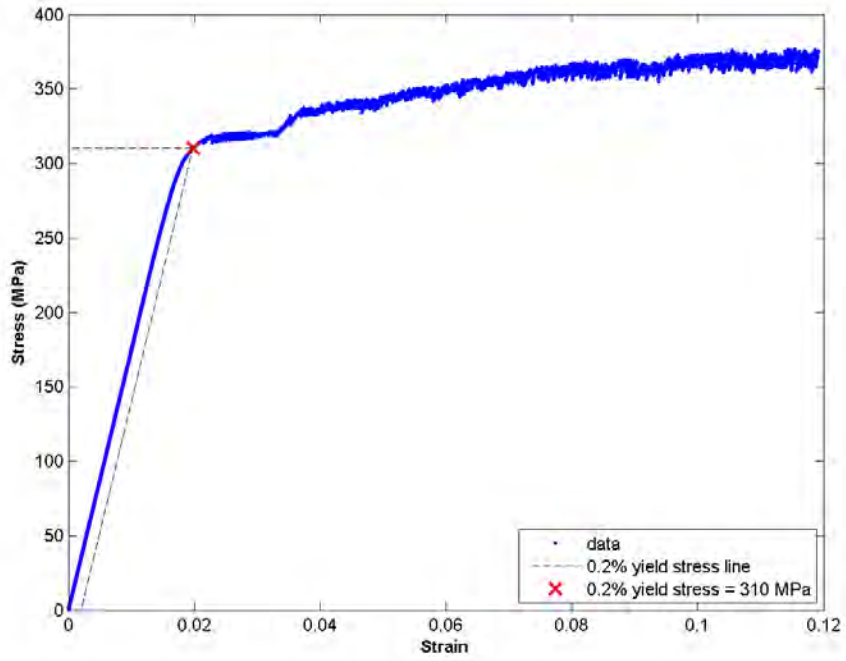

Figure 4.25: Stress-strain curve for the CSHT AA5182 with SCCP for 30 minutes.

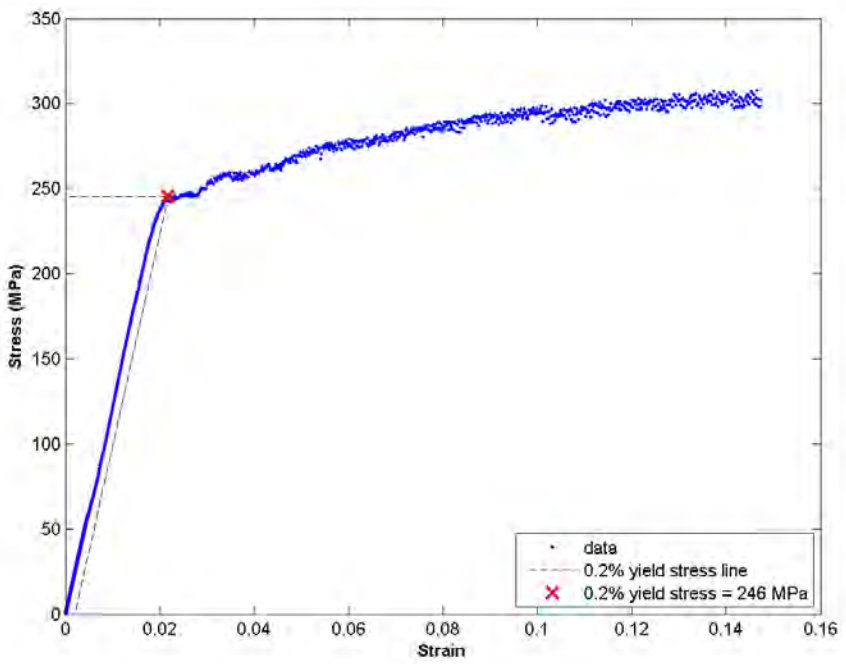

Figure 4.26: Stress-strain curve for the CSHT AA5182 with SCCP for 4 hours.

When compared to the average 0.2% yield stress value of 373MPa for the as-CR specimen, the CSHT with 10%CW specimen's value is only 2MPa lower. The increase in strength is 6MPa when compared to the average 0.2% yield stress value of 365MPa for the CSHT. This is expected as the softening or loss in strength of the CSHT specimens due to the heat treatment is counteracted by the strain hardening introduced by the 10%CW on the specimens. When the CSHT specimens are further heat treated at 220°C during the SCCP, their average 0.2% yield stress values decrease by 91MPa for the 4 minutes and 86MPa for the 30 minutes. While this decrease in strength is significant, the specimens strength is comparable to the 0.2% yield stress value of 285MPa for the strain-hardened and stabilized H34 condition shown in Table 2.4. The average 0.2% yield stress of 285MPa for the CSHT specimens after the SCCP for 30 minutes is actually the same as the expected H34 condition 0.2% yield stress. This SCCP heat treatment for 30 minutes simulates the coil coating at Hulamin, which is carried out for between 20 and 30 minutes above 200°C, as shown in Figure 2.6. This suggests that the CSHT is effective in stabilizing the microstructure of the CES as it retains its strength properties in a similar way to that of the H34 literature values. The reason that a stabilization heat treatment is used is to stabilize the strength properties of the alloy, in order to avoid any substantial recovery and hence, loss of strength properties, occurring in the alloy over time in service. For this reason, an average 0.2% yield stress value of 280MPa or 285MPa, as calculated in this study, is acceptable, as long as this value is stabilized and the strength properties are not lost over time. The average 0.2% yield stress value for the CSHT specimens with SCCP is 280MPa at 4 minutes and 285MPa at 30 minutes and this suggests that

the strength of the alloy does not decrease over this time if the CSHT is used.

When the CSHT specimens are heat treated for an extended time of 4 hours at the temperature of 220°C, the average strength does decrease significantly from 285MPa to 238MPa. These values are shown in Table 4.6. This may suggest that the CSHT is not effective at stabilizing the CES for extended times at temperature. However, it should be noted that the CES at Hulamin is not exposed to the elevated temperature of 220°C for such extended periods as 4 hours. After the CES has been rolled, it is coil coated and exposed to temperatures above 200°C for less than 30 minutes, as shown in Figure 2.6, the heat curve for coil coating at Hulamin. This temperature of 220°C is greater than a third of the melting temperature of AA5182, which is the industry estimate for the point of onset of recovery. When the CES is held at this temperature for a long time, it may thus recover even if the microstructure had previously been stabilized.

The average UTS values are 410MPa for the CSHT specimens with 10%CW, 348MPa for the CSHT specimens with SCCP for 4 minutes, 352MPa for the CSHT specimens with SCCP for 30 minutes and 304MPa for the CSHT specimens with SCCP for 4 hours. These values follow the trend seen in the average 0.2% yield stress values with the strength decreasing from as-CR value of 437MPa to the CSHT with 10%CW and then decreasing significantly further for the CSHT with SCCP. These values are similar for the 4 minute and 30 minute SCCP heat treatments but then decrease significantly for the SCCP heat treatment for 4 hours. The UTS value for the H34 condition is 340MPa, as shown in Table 2.4. This H34 value is 23MPa and 36MPa smaller than the CSHT with SCCP for 4 minutes and the CSHT with SCCP for 30 minutes respectively, but 36MPa greater than the CSHT with SCCP for 4 hours. The strength property values obtained in this study show that the AA5182 CES with the CSHT meet the strength requirements of the H34 condition, as shown in Table 2.4. These strength values also suggest that at an extended time, greater than that used at Hulamin for coil coating at temperatures above 200°C, the CSHT CES will lose strength. Since this temperature is above the CSHT of 150°C, it could reverse the previous microstructural arrangements or promote recovery in the previously CSHT specimens.

The true stress and true strain values were determined, as described in Subsection 2.4.2, for the CSHT SCCP heat treated specimens. The true stress-true strain values are shown in Figures 4.27a), 4.28a), 4.29a) and 4.30a). The logarithmic values of the true stress and true strain values are then plotted in Figures 4.27b), 4.28b), 4.29b) and 4.30b). From these logarithmic graphs, the work hardening coefficients are obtained, as described in Subsection 2.4.2.

Figures 4.27, 4.28, 4.29 and 4.30 show the true stress-true strain curves and the logarithmic true stress-true strain curves for the CSHT with 10%CW, the CSHT with SCCP for 4 minutes, the CSHT with SCCP for 30 minutes and the CSHT with SCCP for 4 hours respectively.

a) b)

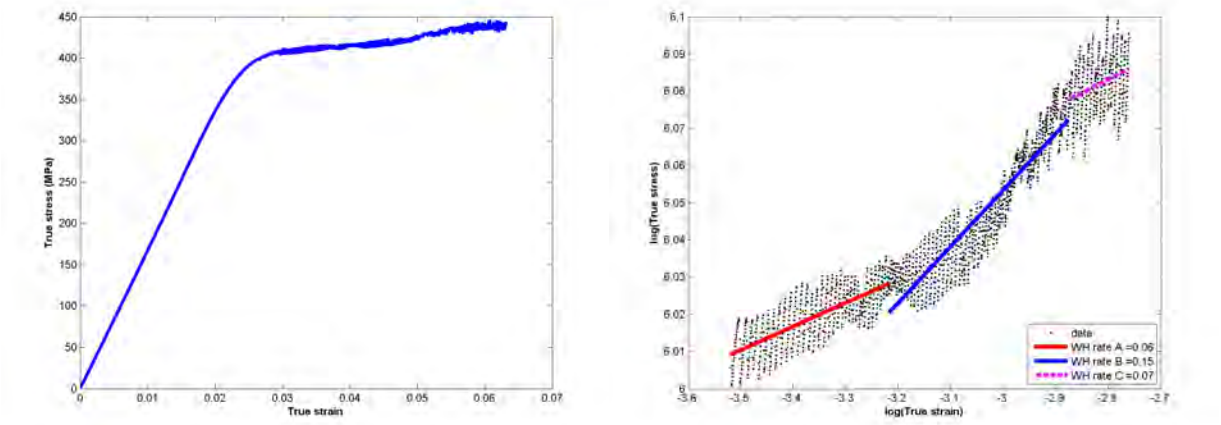

Figure 4.27: True stress-true strain curves showing work hardening for the CSHT AA5182 with 10% CW.

a) b)

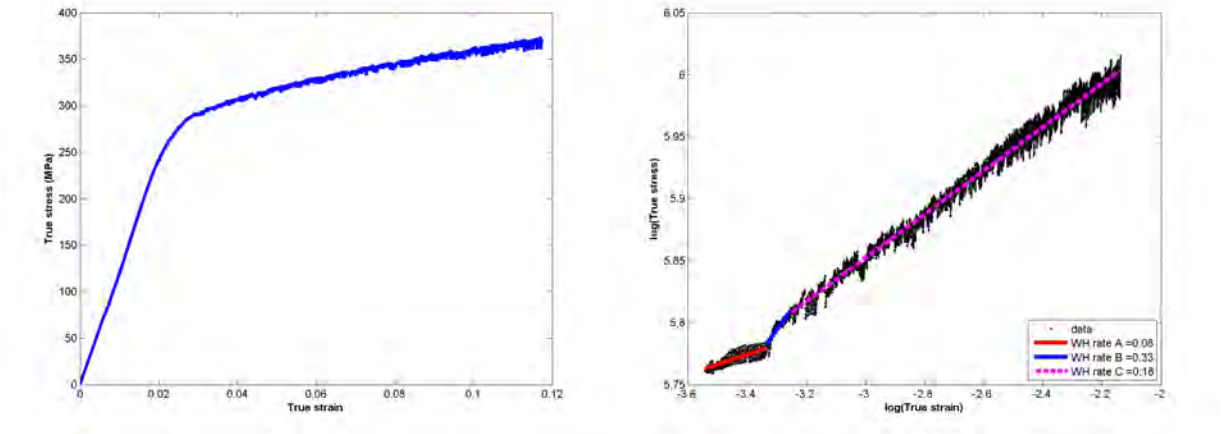

Figure 4.28: True stress-true strain curves showing work hardening for the CSHT AA5182 with SCCP for 4 minutes.

a) b)

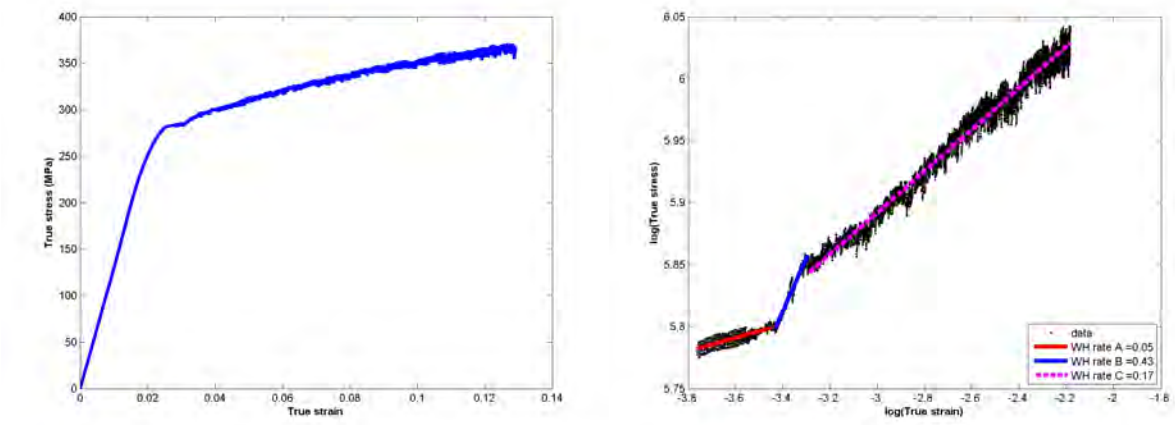

Figure 4.29: True stress-true strain curves showing work hardening for the CSHT AA5182 with SCCP for 30 minutes.

a) b)

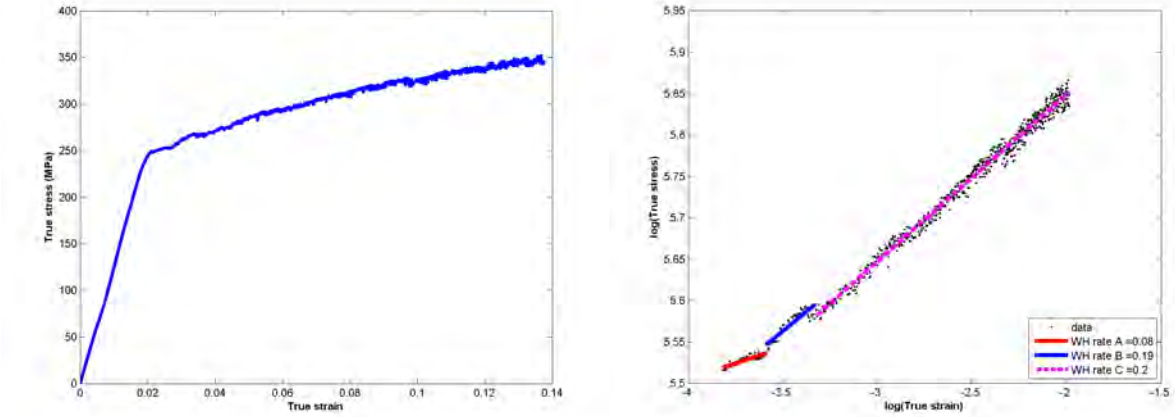

Figure 4.30: True stress-true strain curves showing work hardening for the CSHT AA5182 with SCCP for 4 hours.

As was described in Subsection 4.3.1, the expected work hardening rate is between 0.1 and 0.2 for the AA5182 specimens. The work hardening for the CSHT SCCP heat treated specimens in Figures 4.27, 4.28, 4.29 and 4.30, occurs with a step as three parts with gradients A, B and C. The work hardening coefficients, n-values, from these graphs are shown are displayed in Table 4.5.

Table 4.5: Work hardening n-values for the CSHT SCCP specimens

Condition		**n values**		
Temperature	**Time**	**a**	**b**	**c**
CSHT 10%CW	1 hour	0.06	0.15	0.07
CSHT, SCCP	4 mins	0.06	0.33	0.18
CSHT, SCCP	30 mins	0.05	0.43	0.17
CSHT, SCCP	4 hours	0.08	0.19	0.20

These values suggest that the formability of the CES increases from the CSHT with 10%CW to the CSHT with SCCP specimens. The cold rolling on the CSHT with 10%CW imparted work hardening and thus it has a lower capacity to undergo additional work hardening. This can be seen in the low B and C n-values of the CSHT 10%CW specimens compared to those of the CSHT SCCP specimens shown in Table 4.5. The CSHT 10%CW specimens have a lower formability than if they had been cold worked to a lesser extent. After the SCCP, the n-values for C, for instance, are closer to the expected 0.2 value and these relatively high n-values suggest that this CES has a greater capacity for formability.

The average 0.2% yield stress values for the CSHT with SCCP are within 5MPa of that of the H34 condition shown in Table 2.4. This suggests that the CES with the CSHT and the SCCP may have desirable strength properties before the work hardening afforded by later forming processes. The relatively high n-values suggest that the CSHT SCCP CES has a greater ability for the metal to harden during subsequent cold working, such as the beverage can formation process, than the as-CR CES does. These values are summarized in Table 4.6.

Figures 4.31, 4.32, 4.33 and 4.34 show the greyscale EBSD maps for the AA5182 CES CSHT with 10%CW, the CSHT with SCCP for 4 minutes, the CSHT with SCCP for 30 minutes and the CSHT with SCCP for 4 hours respectively.

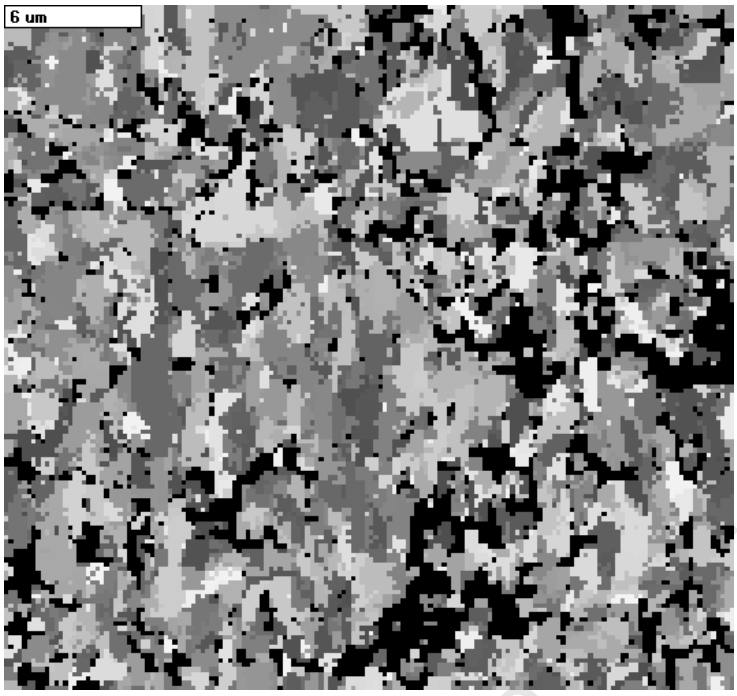

Figure 4.31: A representative EBSD map of a sample after a heat treatment at the CSHT with 10%CW.

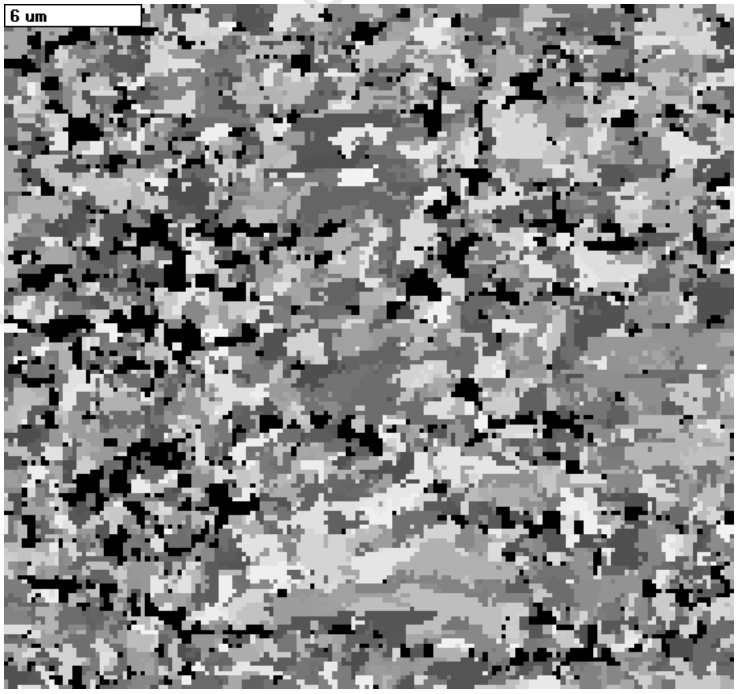

Figure 4.32: A representative EBSD map of a sample after a heat treatment at the CSHT with SCCP for 4 minutes.

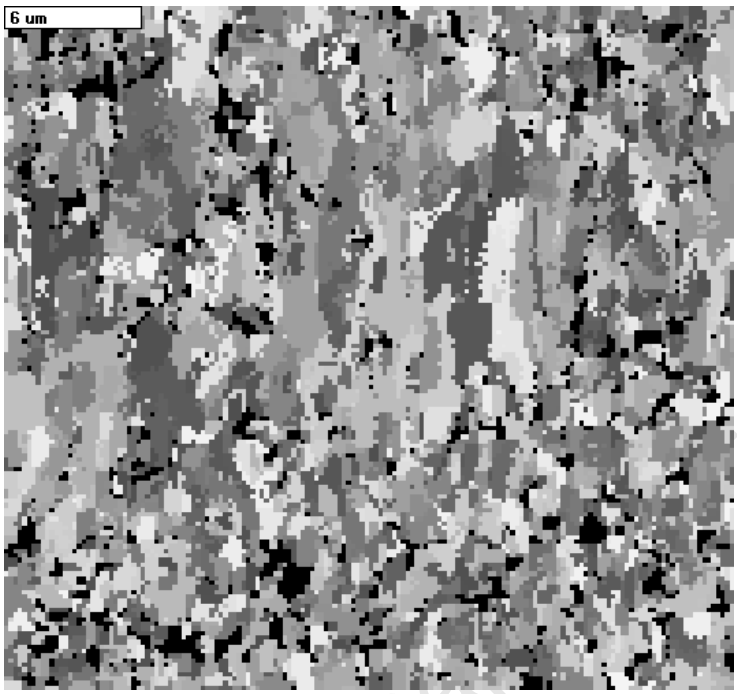

Figure 4.33: A representative EBSD map of a sample after a heat treatment at the CSHT with SCCP for 30 minutes.

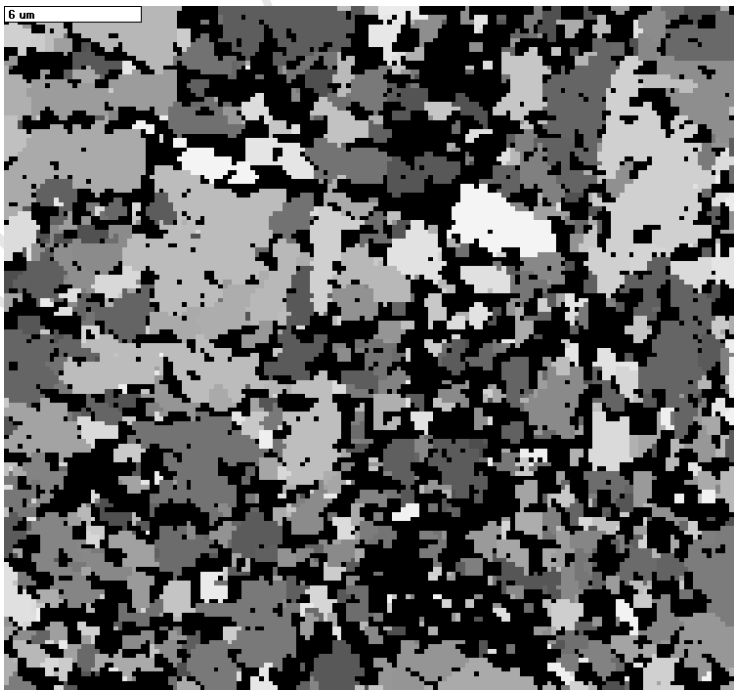

Figure 4.34: A representative EBSD map of a sample after a heat treatment at the CSHT with SCCP for 4 hours.

From 10 of these EBSD maps each, the average ECD values were calculated to be 0.74μm, 0.73μm, 0.72μm and 0.86μm respectively. These first 3 values are within 0.12μm of the as-CR average ECD of 0.62μm. These 3 values are all larger than the as-CR ECD by approximately 0.1μm, suggesting that some subgrain growth may have occurred after the CSHT with SCCP. The subgrain size does not appear to grow due to the SCCP up to 30 minutes, as the values show a maximum small measurable change of 0.02μm on the subgrain size. After 4 hours at 220°C, however, the average ECD subgrain size is 0.86μm, as measured with the EBSD technique. This value has a more significant difference of 0.24μm from the as-CR value when compared to the CSHT with SCCP for shorter times. This suggests that some recovery is occurring when the CES is exposed to elevated temperatures above 200°C for extended periods of 4 hours. This correlates with the significant decrease in strength properties in the CSHT SCCP specimens treated for 4 hours when compared to specimens heat treated for shorter times.

The 0.2% yield stress and UTS values show a large variation between the two tensile specimens used to obtain each average mechanical property. This variation of about 40MPa in some cases, is much larger than that of about 10MPa for the CSHT specimens. This variation may be reduced by obtaining an average from more specimens than investigated in this study. These results are discussed further in Section 4.4.

The mechanical property and ECD results for the CSHT with 10%CW, the CSHT with SCCP for 4 minutes, the CSHT with SCCP for 30 minutes and the CSHT with SCCP for 4 hours are summarized in Table 4.6. The blue coloured n values were inserted for comparison purposes where no step was measured.

Table 4.6: Mechanical properties and ECD values for the CSHT specimens with the SCCP

Condition		σ_{yield}	σ_{uts}	**n values**			**average**
Temperature	**Time**	**(MPa)**	**(MPa)**	**a**	**b**	**c**	**ECD (μm)**
CSHT 10%CW		362	402	0.10	0.17	0.17	0.74
		380	420	0.06	0.15	0.07	
CSHT, SCCP	4 mins	258	333	0.17	0.17	0.17	0.73
		301	364	0.08	0.33	0.18	
CSHT, SCCP	30 mins	260	327	0.05	0.21	0.17	0.72
		310	377	0.05	0.43	0.17	
CSHT, SCCP	4 hours	232	300	0.08	0.21	0.19	0.86
		246	308	0.08	0.19	0.20	

4.3.6 The Simulated Coil Coating Procedure on the As-CR Specimens

In order to compare the effect of the CSHT on the AA5182 CES specimens subjected to the SCCP, the same SCCP was carried out on as-CR specimens that had not been heat treated. This was carried out in order to investigate the effectiveness of the CSHT in stabilizing the CES. The 0.2% yield stress values, shown in the bottom right hand corners of Figures 4.35, 4.36, 4.37 and 4.38 were 394MPa, 263MPa, 248MPa and 246MPa respectively. The average 0.2% yield stress

values were calculated as 382MPa, 280MPa, 271MPa and 243MPa for as-CR with 10%CW, the as-CR with SCCP for 4 minutes, the as-CR with SCCP for 30 minutes and the as-CR with SCCP for 4 hours respectively.

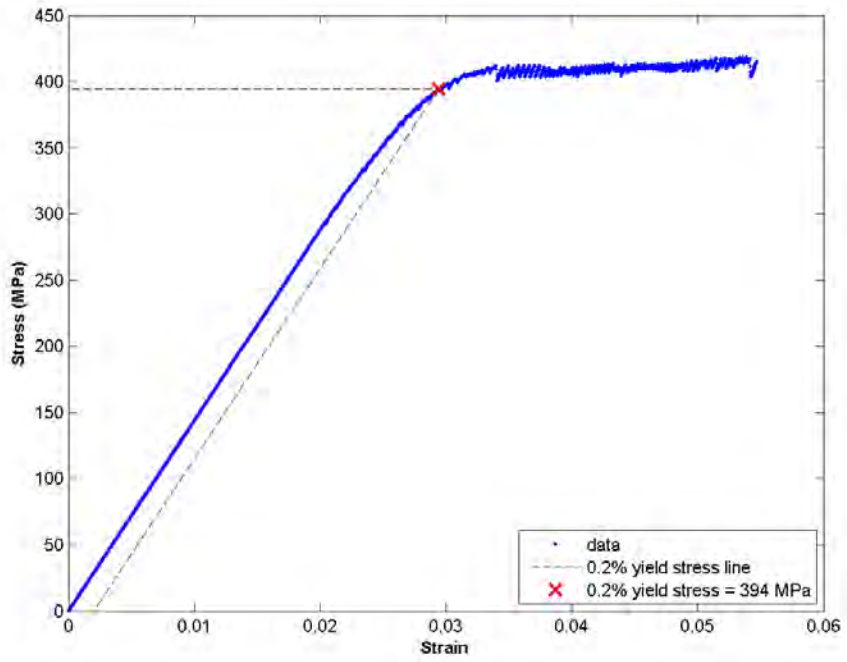

Figure 4.35: Stress-strain curve for the as-CR AA5182 with 10% CW.

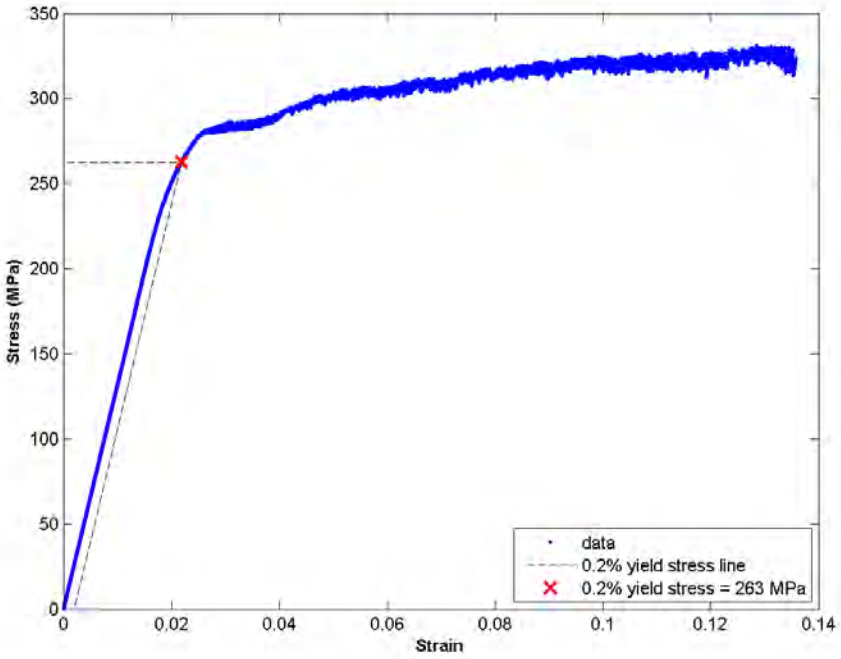

Figure 4.36: Stress-strain curve for the as-CR AA5182 with SCCP for 4 minutes.

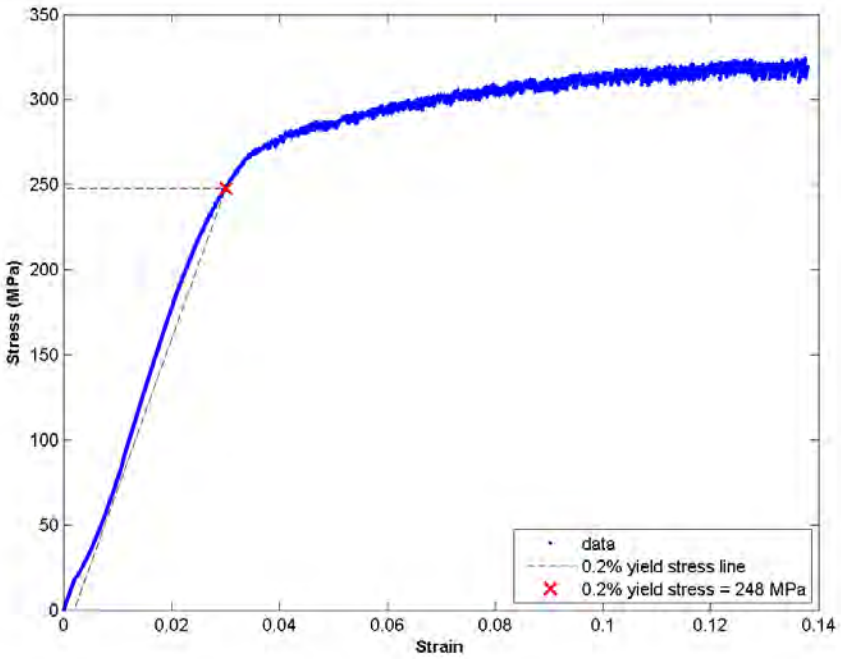

Figure 4.37: Stress-strain curve for the as-CR AA5182 with SCCP for 30 minutes.

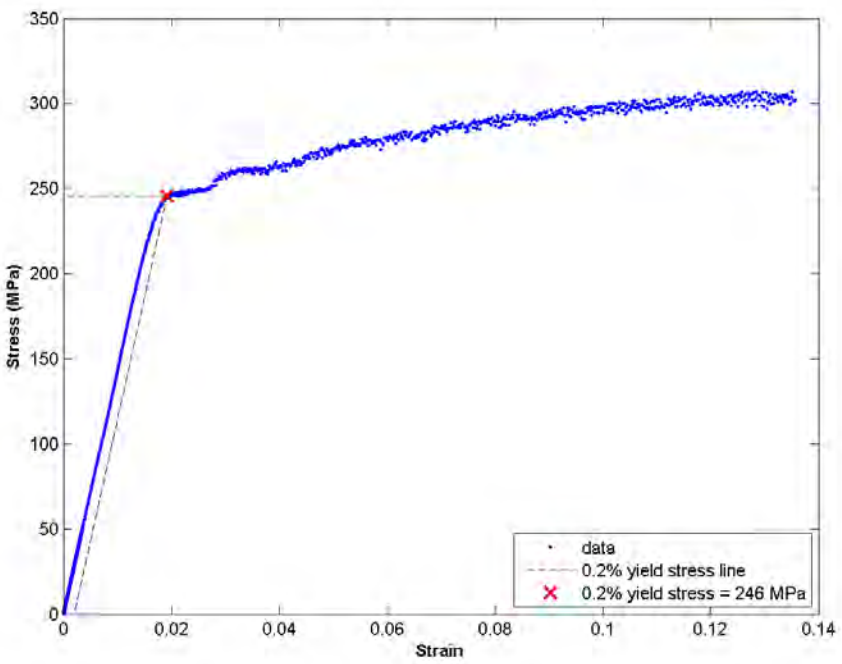

Figure 4.38: Stress-strain curve for the as-CR AA5182 with SCCP for 4 hours.

When compared to the average 0.2% yield stress value of 373MPa for the as-CR specimen, the as-CR with 10%CW specimen's value is only 9MPa higher. The increase in strength is likely due to the strain-hardening of the CES during the 10% cold rolling. When the as-CR specimens are further heat treated at 220°C during the SCCP, their average 0.2% yield stress values decrease by 102MPa and 111MPa respectively. While this decrease in strength is similar to the decrease in strength for the CSHT specimens, the CSHT SCCP specimens tested at 30 minutes did not lose strength compared to the CSHT SCCP at 4 minutes, whereas the as-CR SCCP specimens tested at 30 minutes had an average 0.2% yield stress value 9MPa lower than the as-CR SCCP tested at 4 minutes. These results suggest that there may be a trend in significant softening due to recovery continuing in the as-CR specimens which had not undergone a stabilization heat treatment. The reason that a stabilization heat treatment is used is to stabilize the strength properties of the alloy and thus avoid any substantial recovery occurring in the alloy over time. Although after the SCCP for 4 minutes, both the as-CR and CSHT specimens had similar average 0.2% yield stress values of 280MPa, after the SCCP was carried out for 30 minutes, the as-CR average 0.2% yield stress value was 9MPa lower, whereas the CSHT average 0.2% yield stress value actually increased by 5MPa. The CSHT may thus be successfully stabilizing the AA5182 microstructure and thus the strength properties may be more robust, with a value of approximately 280MPa over time, compared to as-CR AA5182 CES, which did not have this stabilization.

When the as-CR specimens are heat treated for an extended time of 4 hours at the temperature of 220°C, the average strength does decrease significantly from 271MPa to 243MPa. These values

are shown in Table 4.8. CES at Hulamin is not exposed to such elevated temperatures of 220°C for such extended periods as 4 hours. After the CES has been rolled, it is coil coated and exposed to temperatures above 200°C for less than 30 minutes, as shown in Figure 2.6, the heat curve for coil coating at Hulamin. This temperature of 220°C is greater than a third of the melting temperature of AA5182, which is the industry estimate for the point of onset of recovery. When the CES is held at this temperature for a long time, it may thus recover even if the microstructure had previously been stabilized. This suggests that whether or not the CES has had the CSHT, a further treatment of 220°C for 4 hours will still soften the alloy. This softening may be due to recovery of the AA5182 microstructure.

The average UTS values are 403MPa, 347MPa, 341MPa and 304MPa for the as-CR with 10%CW, the as-CR with SCCP for 4 minutes, the as-CR with SCCP for 30 minutes and the as-CR with SCCP for 4 hours respectively. These values follow the trend seen in the average 0.2% yield stress values with the strength decreasing from the as-CR with 10%CW, to the as-CR with SCCP for 4 minutes and even further decreasing for the as-CR with SCCP for 30 minutes. The as-CR specimens with SCCP for 4 hours show a significant decrease of 37MPa in average UTS, which decreases from 341MPa to 304MPa from the SCCP of 30 minutes to that of 4 hours.

The true stress and true strain values were determined, as described in Subsection 2.4.2, for the CSHT SCCP heat treated specimens. The true stress-true strain values are shown in Figures 4.39a), 4.40a), 4.41a) and 4.42a). The logarithmic values of the true stress and true strain values are then plotted in Figures 4.39b), 4.40b), 4.41b) and 4.42b). From these logarithmic graphs, the work hardening coefficients are obtained, as described in Subsection 2.4.2.

Figures 4.39, 4.40, 4.41 and 4.42 show the true stress-true strain curves and the logarithmic true stress-true strain curves for the as-CR with 10%CW, the as-CR with SCCP for 4 minutes, the as-CR with SCCP for 30 minutes and the as-CR with SCCP for 4 hours respectively.

a) b)

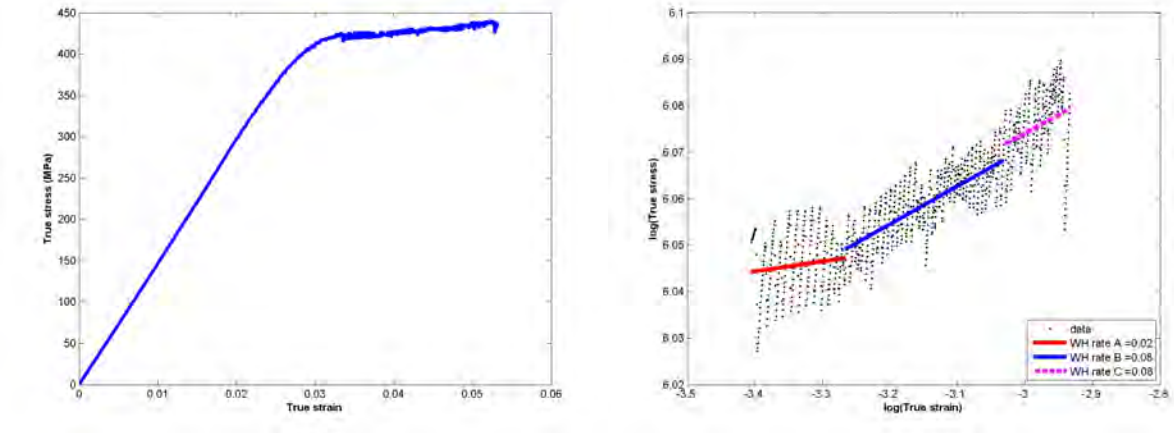

Figure 4.39: True stress-true strain curves showing work hardening for the as-CR AA5182 with 10% CW.

a) b)

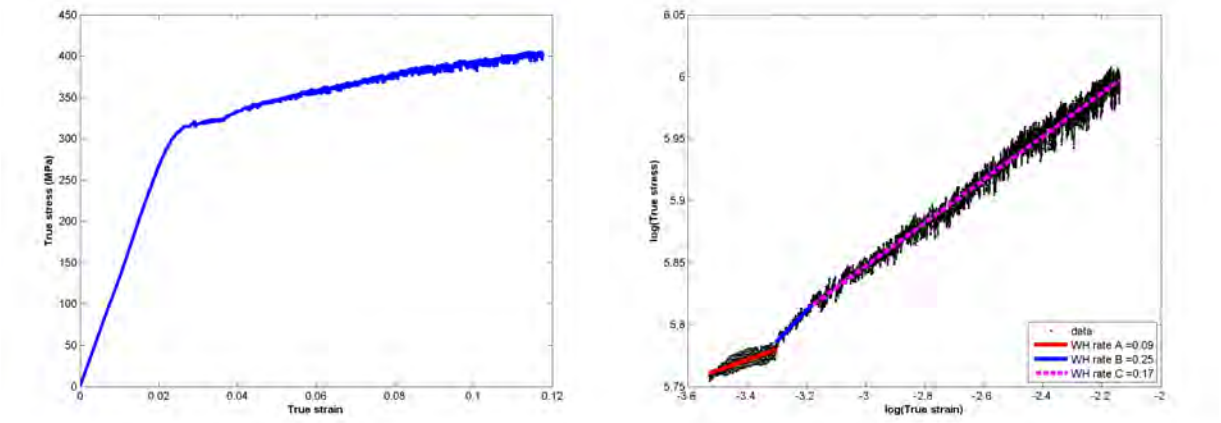

Figure 4.40: True stress-true strain curves for the as-CR AA5182 with SCCP for 4 minutes.

a) b)

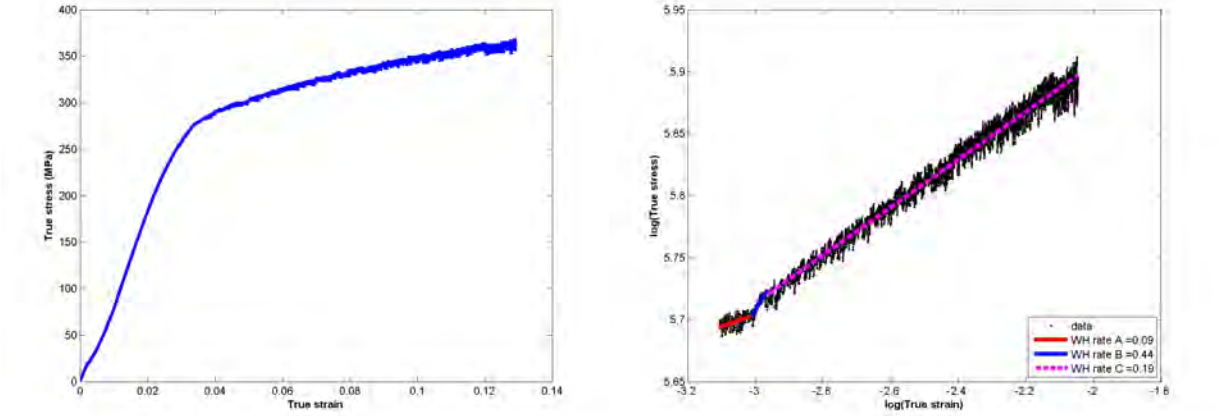

Figure 4.41: True stress-true strain curves for the as-CR AA5182 with SCCP for 30 minutes.

a) b)

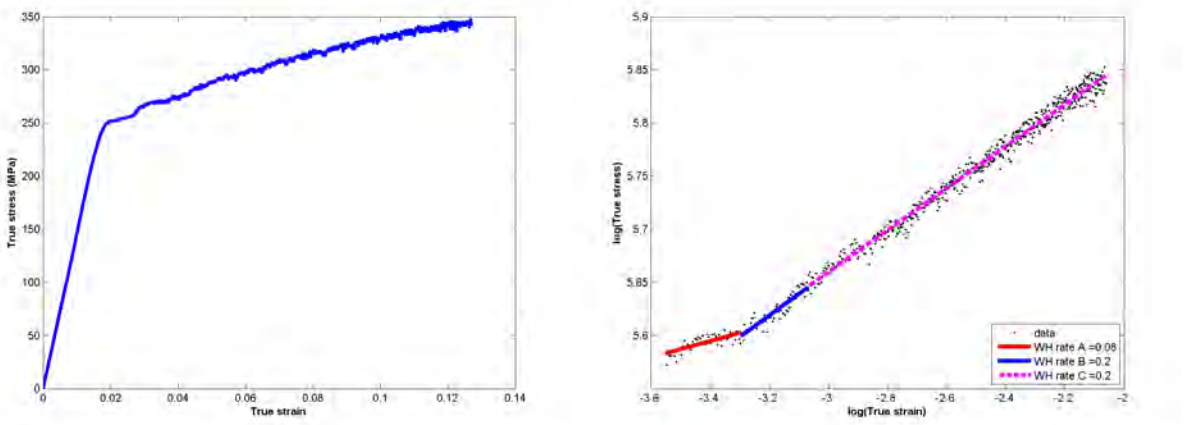

Figure 4.42: True stress-true strain curves for the as-CR AA5182 with SCCP for 4 hours.

As was described in Subsection 4.3.1, the expected work hardening rate is between 0.1 and 0.2 for the AA5182 specimens. The work hardening for the as-CR SCCP heat treated specimens in Figures 4.39, 4.40, 4.41 and 4.42, occurs with a step as three parts with gradients A, B and C. The work hardening coefficients, n-values, from these graphs are shown are displayed in Table 4.7.

Table 4.7: Work hardening n-values for the as-CR SCCP specimens

Condition		**n values**		
Temperature	**Time**	**a**	**b**	**c**
as-CR 10%CW	1 hour	0.02	0.08	0.08
as-CR, SCCP	4 mins	0.09	0.25	0.17
as-CR, SCCP	30 mins	0.09	0.44	0.19
as-CR, SCCP	4 hours	0.08	0.20	0.20

These values suggest that the formability of the CES increases from the as-CR with 10%CW to the as-CR with SCCP specimens. The cold rolling on the as-CR specimens with 10%CW imparted work hardening and thus it has a lower capacity to undergo additional work hardening. This can be seen in the lower B and C n-values of the as-CR 10%CW specimens compared to those of the as-CR SCCP specimens shown in Table 4.7. The as-CR 10%CW specimens have a lower formability than if they had been cold worked to a lesser extent. This formability is much less than the expected 0.1 to 0.2 work hardening range. After the SCCP, the n-values for C, for instance, are increased greatly and are closer to the expected 0.2 value. These relatively high n-values suggest that this CES has a greater capacity for formability.

The average 0.2% yield stress values for the as-CR with SCCP specimens are within 5MPa of that of the H34 condition shown in Table 2.4. The relatively high n-values suggest that the as-CR SCCP CES has a greater ability for the metal to harden during subsequent cold working, such as the beverage can formation process, than the as-CR CES does. These values are summarized

in Table 4.8.

Figures 4.43, 4.44, 4.45 and 4.46 show the greyscale EBSD maps for the AA5182 CES as-CR with 10%CW, the as-CR with SCCP for 4 minutes, the as-CR with SCCP for 30 minutes and the as-CR with SCCP for 4 hours respectively.

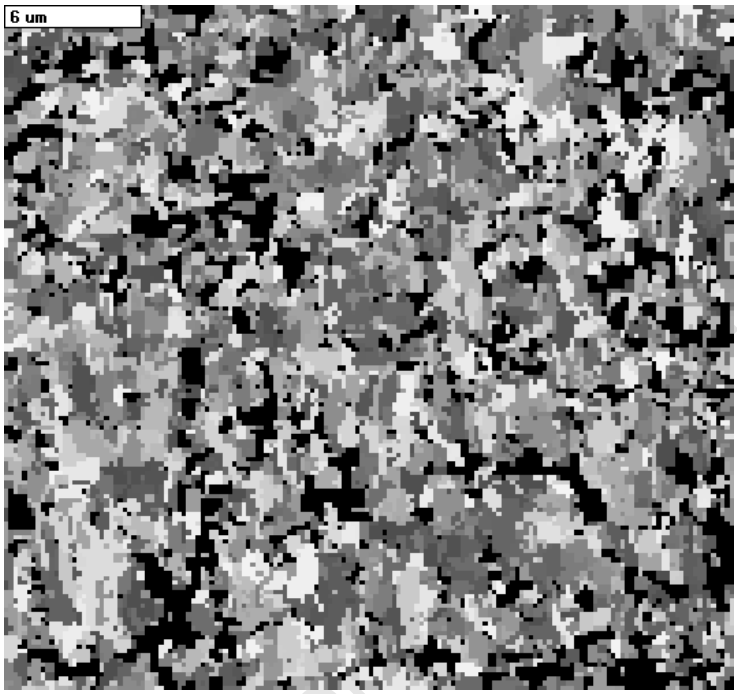

Figure 4.43: A representative EBSD map of an as-CR sample with 10%CW.

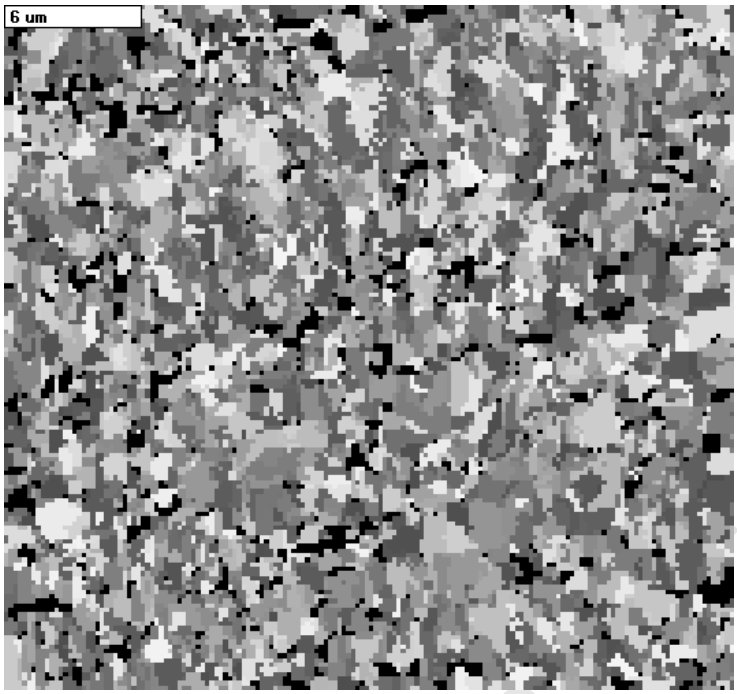

Figure 4.44: A representative EBSD map of an as-CR sample after a heat treatment at the SCCP for 4 minutes.

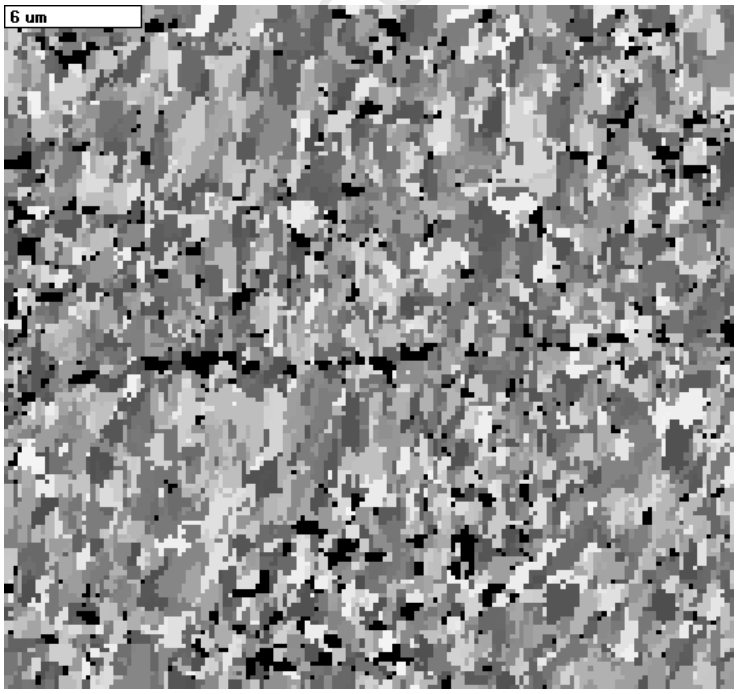

Figure 4.45: A representative EBSD map of an as-CR sample after a heat treatment at the SCCP for 30 minutes.

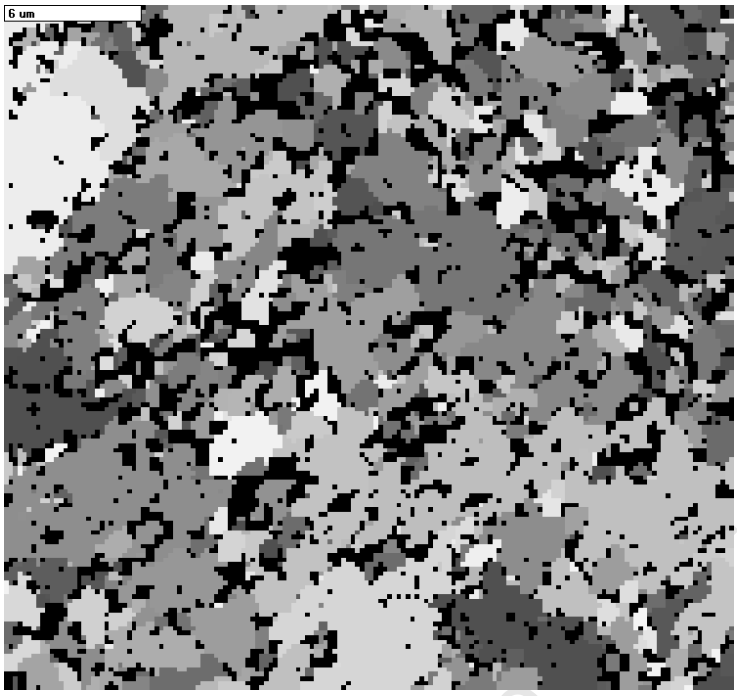

Figure 4.46: A representative EBSD map of an as-CR sample after a heat treatment at the SCCP for 4 hours.

From 10 of these high-indexed EBSD maps, the average ECD values were calculated to be 0.66μm, 0.68μm, 0.64μm and 1.03μm respectively. The first 3 values are within 0.06μm of the as-CR average ECD of 0.62μm. These 3 values are all larger than the as-CR ECD by at approximately 0.02μm, suggesting that some small amount of subgrain growth may have occurred after the as-CR with SCCP. The EBSD technique is discussed further in Section 4.4. The subgrain size does not appear to increase or decrease substantially due to the SCCP of up to 30 minutes, as the values show a relatively small measurable change of 0.02μm to the subgrain size. After 4 hours at 220°C, however, the average ECD subgrain size is 1.03μm as measured with the EBSD technique. This value has a more significant difference of 0.41μm, from the as-CR value, when compared to the as-CR SCCP for shorter times. This can be seen in the relatively larger, less elongated subgrains in Figure 4.46 compared to those in Figure 4.45. If the areas with less unindexed points are visually inspected, the typical subgrain ECD sizes appear to be 3μm or greater. This suggests that some recovery is occurring when the CES is exposed to elevated temperatures above 200°C for extended periods of 4 hours. This recovery stage may be subgrain growth, as shown in Figure 2.24e). This EBSD data correlates with the significant decrease in strength properties in the as-CR SCCP specimens treated for 4 hours, when compared to specimens heat treated for shorter times.

The 0.2% yield stress and UTS values are quite similar for the two as-CR SCCP 4 hours specimens tested. For the other as-CR specimens, these values show a large variation between the two tensile specimens used to obtain each average mechanical property. This variation of about 40MPa in some cases, is much larger than that of about 9MPa for the as-CR specimens.

This variation may be reduced by obtaining an average from more specimens than investigated in this study. These results are discussed further in Section 4.4.

The mechanical property and ECD results for the as-CR with 10%CW, the as-CR with SCCP for 4 minutes, the as-CR with SCCP for 30 minutes and the as-CR with SCCP for 4 hours are summarized in Table 4.8. The blue coloured n values were inserted for comparison purposes where no step was measured.

Table 4.8: Mechanical properties and ECD values for the as-CR specimens with the SCCP

Condition		σ_{yield}	σ_{uts}	**n values**			**average**
Temperature	**Time**	**(MPa)**	**(MPa)**	**a**	**b**	**c**	**ECD (μm)**
as-CR 10%CW		394	419	0.02	0.08	0.08	0.66
		370	387	0.25	0.25	0.25	
as-CR, SCCP	4 mins	263	331	0.09	0.24	0.17	0.68
		298	363	0.09	0.25	0.17	
as-CR, SCCP	30 mins	248	325	0.09	0.44	0.19	0.64
		294	357	0.15	0.38	0.19	
as-CR, SCCP	4 hours	241	301	0.06	0.15	0.20	1.03
		246	307	0.08	0.20	0.20	

4.4 Discussion and Summary of Mechanical Property and EBSD Results

4.4.1 Strength Property Discussion

The 0.2% yield stress and UTS values summarized in Table 4.9 are averaged from the two specimens tested for each condition. The literature values for the 0.2% yield stress and UTS are given for the H18 and H34 conditions described in Table 2.4. These AA5182 CES conditions are the strain hardened, fully hard condition and the strain hardened and stabilized, half hard condition respectively. The average mechanical values are then displayed in Table 4.9 for the as-CR specimens, followed by the heat treated specimens. The relative differences between the average 0.2% yield stress and average UTS values is also given in Table 4.9, as these values indicate the work hardening property in the specimens.

Table 4.9: Average mechanical properties of the AA5182 specimens

Condition		σ_{yield}	σ_{uts}	σ_{uts} - σ_{yield}
Temperature	**Time**	**(MPa)**	**(MPa)**	**(MPa)**
H18 condition [3, 8]		375	400	25
H34 condition [3, 8]		285	340	55
as-CR		373	437	64
120°C	1 hour	378	443	65
120°C	4 hours	366	437	71
150°C	1 hour	361	429	68
150°C	4 hours	365	433	68
200°C	1 hour	316	397	81
200°C	4 hours	316	402	86
CSHT 10%CW		371	410	39
CSHT, SCCP	4 mins	280	348	68
CSHT, SCCP	30 mins	285	352	67
CSHT, SCCP	4 hours	238	304	66
as-CR 10%CW		382	403	21
as-CR, SCCP	4 mins	280	347	67
as-CR, SCCP	30 mins	271	341	70
as-CR, SCCP	4 hours	243	304	61

The as-CR AA5182 CES specimens from Hulamin are strain hardened, fully hard and their 0.2% yield strength values are expected to be very similar to the literature H18 AA5182 values. The as-CR CES specimens from Hulamin show a very similar average 0.2% yield stress to that of the H18 literature value, with a difference of 2MPa. This suggests that the received CES specimens do have the required strength properties expected in the aluminium industry. Some of the variation observed in the mechanical properties in Table 4.9 could be reduced by carrying out more repeats of the experiments. This is especially true for the specimens treated with the SCCP. For this study, the mechanical properties were determined from two tensile test specimens for each condition due to time and material constraints. The average UTS value for these as-CR specimens is 37MPa higher than the expected H18 value. The ultimate strength properties of these as-CR specimens from Hulamin was thus found to be superior to those of the expected H18 condition.

The as-CR specimens were heat treated in order to simulate the stabilization process at Hulamin. Based on information from Hulamin, the design matrix was constructed as described in Table 3.1. The temperatures used to simulate the stabilization were 120°C, 150°C and 200°C and the times were 1 hour and 4 hours. The average 0.2% yield stress and average UTS values for this design matrix are also summarized in Table 4.9.

When the as-CR specimens were heat treated at 120°C for both 1 hour and 4 hours, the mechanical properties did not vary substantially from those of the as-CR specimens. The mechanical properties for the 120°C 1 hour specimens appear to increase from the as-CR by 5MPa

and 6MPa. As was discussed in Subsection 4.3.1, the as-CR specimens were not stored at sub-zero temperatures and were tested approximately 6 months after the other specimens in this study. This may explain why the as-CR specimens' strength properties are less than that of the 120°C 1 hour specimens. The relatively small variation in strength properties will likely be reduced if further repeat experiments are performed. These AA5182 specimens were not stabilized after the 120°C heat treatment for 1 hour.

When the as-CR specimens were heat treated at 150°C for 1 hour, the mechanical properties decreased by 12MPa and 8MPa. When the as-CR specimens are heat treated at 150°C for 4 hours, the mechanical properties decreased by 8MPa and 4MPa. These differences would likely be greater if the as-CR specimens had been stored at sub-zero temperatures and were tested at the same time as the other specimens in this study. The fact that these mechanical properties are all lower than that of the as-CR specimens suggests that some microstructural rearrangement in the AA5182 may have occurred. This effect may be due to recovery of the microstructure, as described in Figure 2.5, or the rearrangement of dislocations into structures, such as the poorly defined cell-like structures described in Subsection 2.5.6. The mechanical property values for these 150°C specimens are all significantly greater than those of the H34, strain hardened and stabilized condition. The H34 mechanical property values are expected to be similar to those of the 150°C specimens which resulted in stabilization of the CES microstructure. The heat treatment of 150°C for 4 hours was further investigated, as it was identified as the heat treatment most closely simulating the stabilization process used at Hulamin. This heat treatment was designated as the chosen stabilization heat treatment and labelled 'CSHT' accordingly.

When the as-CR specimens were heat treated at 200°C for both 1 hour and 4 hours, the average 0.2% yield stress decreased by 57MPa. The average UTS values decreased by 40MPa and 35MPa for the 1 hour and 4 hour heat treatments respectively. A decrease in 0.2% yield stress of 57MPa is significantly large and results in an average 0.2% yield stress similar to that of the H34 condition. The average 0.2% yield stress for the 200°C heat treatments are 31MPa greater than that of the H34 condition. These values are thus closer to those of the H34 condition than those of the H18 condition in Table 4.9. This would suggest that the heat treatment of 200°C results in a microstructural change similar to that in the H34 specimens and may result in the stabilization of the AA5182. This change may be due to recovery of the microstructure, as described in Figure 2.5, or the rearrangement of dislocations into structures, such as the poorly defined cell-like structures described in Subsection 2.5.6. In this study, the CSHT was investigated further, although heat treatments in the range of 150°C to 200°C may result in varying degrees of stabilization of the AA5182 CES.

When the AA5182 specimens were subjected to the simulated coil coating procedure (SCCP), they were first cold worked to a reduction of 10% of their thickness (10%CW). These cold worked specimens were then heat treated at 220°C for either 4 minutes or 30 minutes to simulate the effects of coil coating shown in Figure 2.6. To investigate the effect of an extended time at this elevated temperature, the SCCP was also performed for 4 hours. This extended time is not used

at Hulamin, as only a period of up to 30 minutes is used above 200°C. After 10%CW, both the CSHT and as-CR specimens increased in their average 0.2% yield stress values due to strain hardening.

When the AA5182 specimens were cold worked to 10% in the SCCP, their average 0.2% yield stress values increased as shown from 373MPa to 382MPa for the as-CR and as-CR with 10%CW, and from 365MPa to 371MPa for the CSHT and CSHT with 10%CW specimens. These 10%CW specimens have increased strain hardening induced by the cold work and this explains their higher average 0.2% yield stress values. Their UTS values are lower after the 10%CW by 34MPa and 23MPa for the as-CR and the CSHT respectively. If further repeat experiments are performed and these average UTS values are obtained from a larger number of results, they may become relatively more similar on average.

After being heat treated at 220°C for 4 minutes, the specimens' average 0.2% yield stress values decrease by 102MPa and 91MPa for the as-CR and CSHT specimens respectively. This large decrease in strength can be explained by the fact that the temperature of 220°C is high enough for substantial recovery to occur in the CES, as shown in Figure 2.5. When the CSHT specimens are subjected to this 220°C temperature for a longer period of 30 minutes, the average 0.2% yield stress value does not decrease but actually increases by 5MPa compared to the 220°C for 4 minutes heat treatment. In the as-CR specimens, the 220°C temperature for a longer period of 30 minutes results in a decrease in the average 0.2% yield stress value by 9MPa from the 220°C for 4 minutes heat treatment value. These results suggest that the SCCP decreases the strength in both the CSHT and the as-CR specimens but the CSHT specimens retain their strength properties over time whereas the as-CR specimens have their strength properties decrease over this same length of time. These observations are also seen in the average UTS values which follow a similar trend for the CSHT and as-CR specimens to that seen in the average 0.2% yield stress values.

If the CSHT has resulted in CES which retains its strength properties, then the alloy has been stabilized. When both the as-CR and CSHT specimens are heat treated at 220°C for 4 hours, however, their average 0.2% yield points decrease by 30MPa and 35MPa. When the CES is held at this temperature for a long time, it likely recovers even if the microstructure had previously been stabilized. This suggests that whether or not the CES has had the CSHT, a further treatment of 220°C for 4 hours will still decrease the strength of the alloy. This softening would be as a result of recovery steps in the AA5182 microstructure, such as subgrain growth shown schematically in Figure 2.24e). The CSHT of 150°C is below the SCCP temperature of 220°C and thus a heat treatment at 220°C will affect any previous rearrangement of the microstructure, such as the cell formation shown in Figure 2.24b). As described in Subsection 4.3.6, 220°C is greater than a third of the melting temperature of AA5182, which is the industry estimate for the point of onset of recovery. When the CES is held at this temperature for a long time, it may thus recover even if the microstructure had previously been stabilized. The microstructure observed in the CES after heat treatments is discussed further in Section 4.5.

4.4.2 Work Hardening Discussion

The work hardening exponents, n-values, are summarized in Table 4.10 for all the conditions tested in this study. As explained in Subsection 2.4.2, the work hardening exponent measures the ability of a material to harden during cold work. A n-value of zero represents a perfectly plastic material and a n-value of one represents a perfectly elastic material. In principle, however, a n-value of 1 need not mean elastic behaviour. A greater n-value shows a higher formability with a greater ability for deformation to become uniform in the material. CES with a high n-value has a greater capacity to be formed during the subsequent can forming processes than CES with a lower n-value. All the specimens in this study are heavily cold worked when they are received from Hulamin, as they have undergone cold rolling with a large reduction in original thickness. Although the expected n-values for metals are in the range of 0.1 to 0.5, the expected n-values for this aluminium CES are thus between 0.1 and 0.2, as shown in Figure 2.5.

Table 4.10: Mechanical properties of the AA5182 specimens

Condition		σ_{yield}	σ_{uts}	n values		
Temperature	**Time**	**(MPa)**	**(MPa)**	**a**	**b**	**c**
as-CR		368	437	0.19	0.04	0.15
		377	437	0.05	0.30	0.15
120°C	1 hour	376	443	0.07	0.22	0.14
		380	443	0.08	0.28	0.15
120°C	4 hours	366	438	0.09	0.25	0.14
		366	437	0.12	0.22	0.15
150°C	1 hour	354	431	0.17	0.17	0.17
		368	427	0.08	0.29	0.16
150°C	4 hours	361	432	0.06	0.41	0.14
		369	427	0.09	0.50	0.15
200°C	1 hour	316	399	0.18	0.18	0.18
		315	395	0.18	0.18	0.18
200°C	4 hours	322	410	0.17	0.17	0.17
		310	395	0.18	0.18	0.18
CSHT 10%CW		362	402	0.10	0.17	0.17
		380	420	0.06	0.15	0.07
CSHT, SCCP	4 mins	258	333	0.17	0.17	0.17
		301	364	0.08	0.33	0.18
CSHT, SCCP	30 mins	260	327	0.05	0.21	0.17
		310	377	0.05	0.43	0.17
CSHT, SCCP	4 hours	232	300	0.08	0.21	0.19
		246	308	0.08	0.19	0.20
as-CR 10%CW		394	419	0.02	0.08	0.08
		370	387	0.25	0.25	0.25
as-CR, SCCP	4 mins	263	331	0.09	0.24	0.17
		298	363	0.09	0.25	0.17
as-CR, SCCP	30 mins	248	325	0.09	0.44	0.19
		294	357	0.15	0.38	0.19
as-CR, SCCP	4 hours	241	301	0.06	0.15	0.20
		246	307	0.08	0.20	0.20

The n-values for these CES specimens generally occur as a step with 3 gradients, labelled a, b and c. These gradients are discussed fully in Section 4.3. The exception in this study were the 200°C heat treated specimens, which had no measurable step in the plastic regions of their stress-strain curves after the yield point, as shown in Figures 4.19 and 4.20. The n-values for these 200°C specimens are expressed as only the c values. The lack of the step observed at other temperatures, together with the strength values' similarity to the H34 values, as described in Subsection 4.4.1, suggests that the 200°C heat treatments may result in some rearrangement of the CES microstructure and stabilization of the CES. A comparison of the c n-values in Table 4.10 can be made to indicate the work hardening and formability of the specimens tested. These

values are very similar for the 120°C heat treatment and the as-CR specimens. This correlates with the discussion in Subsection 4.4.1 about the 120°C temperature being too low to sufficiently affect the CES's microstructure. The n-values for the 150°C specimens are slightly higher than the as-CR on average and those for the 200°C are higher still. This suggests that the formability of both the 150°C and 200°C specimens is increased compared to the as-CR specimens, with the 200°C having the greater formability. An increased formability is desirable in the CES from Hulamin, as it will be required when it is further fabricated in subsequent can forming processes. During these can forming processes, a maximum possible uniform reduction of the CES is desired with a reduction in irregularities or tearing. The average n-values for both the as-CR and CSHT specimens are decreased after 10%CW. The further cold work increases the entangled dislocation density and this reduces the ability of dislocations to move past these obstacles by cross-slip. The ability of dislocations in a material to pass around these obstacles to their motion is referred to as 'cross-slip'. The entangled dislocations impede the movement of dislocations through the material. After the SCCP in both the as-CR and CSHT specimens, the average n-values increase once more to between 0.17 and 0.20. This suggests that the CES in these conditions has good formability, though its strength properties may be undesirable, especially in the case of the SCCP 4 hour treatments.

4.4.3 Subgrain Size Discussion

The average subgrain sizes for specimens tested in this study are expressed as ECD values in Table 4.11.

Table 4.11: Average subgrain sizes of AA5182 samples

Condition		**ECD (μm)**
Temperature	**Time**	
as-CR		0.62
120°C	1 hour	0.70
120°C	4 hours	0.62
150°C	1 hour	0.60
150°C	4 hours	0.66
200°C	1 hour	0.66
200°C	4 hours	0.69
CSHT 10%CW		0.74
CSHT, SCCP	4 mins	0.73
CSHT, SCCP	30 mins	0.72
CSHT, SCCP	4 hours	0.86
as-CR 10%CW		0.66
as-CR, SCCP	4 mins	0.68
as-CR, SCCP	30 mins	0.64
as-CR, SCCP	4 hours	1.03

There are minor differences in the subgrain sizes shown in Table 4.11 for the specimens in this study. The average subgrain sizes for all the CSHT specimens are greater than those of the as-CR, with the SCCP 4 hour specimens having the greatest of these subgrain sizes. This increase in subgrain size is consistent with recovery occurring in the alloy or some rearrangement occurring in its microstructure. This is also evident in the as-CR specimens which have similar ECD values for the SCCP up to 30 minutes but then the ECD value is significantly higher for the SCCP after 4 hours. This increase is from 0.64 to 1.03.

The light microscopy investigation in Section 4.2 showed the average elongated grain sizes in the CES to be 150μm in the RD and 16μm in the TD direction. The ECD values in Table 4.11 are all in the range of 0.60 to 1.03μm. This suggests that there is no substantial increase or decrease in subgrain size as measured by the EBSD technique. The exceptions are the specimens with the SCCP for 4 hours. The changes in strength properties observed in the CES after different heat treatments may thus be due to effects other than the effect of changes in subgrain size. Some of these effects are described in Section 2.5. The effect of Mg solute precipitates and Al_6(Fe, Mn) dispersoids as barriers to dislocation movement during strain hardening is one such effect. AA5182 is an aluminium alloy supersaturated with Mg and therefore excess Mg solute atoms may precipitate out during heat treatments, such as the CSHT. More precipitation may occur with an increase in time at the heat treatment temperature. These precipitates are Al_3Mg_2 and may form on the grain boundaries where high dislocation density occurs, as shown in Figure 4.49. A decrease in the Mg concentration, as well as any effects of microvoid formation at these precipitates, may result in the decrease in the average UTS values as it may cause the early fracture during tensile testing of these specimens. A decrease in Mg concentration may also result in a decrease in the serrated yielding described in Subsection 2.4.1. In Section 4.5, the TEM micrographs show the effect of these precipitates and dispersoids in pinning dislocations, thereby strengthening the CES microstructure and perhaps preventing the loss in strength of the CES by recovery. Besides regions of high strain energy due to work hardening of the CES during cold rolling, the CES may also form cell-like structures, as described in Section 2.5, which has an influence on the strength of the material also. These structures prevent cross-slip, which is a major deformation mechanism in this AA5182 alloy. Though no shear bands were observed in the regions investigated under the light microscope in Section 4.2, dense dislocation walls are present in the CES and affect the strength properties, as described further in Section 4.5. The results from the mechanical properties may thus be explained by microstructural rearrangements in the CES, and these rearrangements are not evident in the ECD data. The EBSD technique may measure substructures, such as dense dislocation forests, as subgrains and thus give an unclear representation of the microstructure in the AA5182. The microstructure of the AA5182 CES specimens is further investigated using TEM in Section 4.5.

4.5 AA5182 CES Microstructure

4.5.1 TEM Micrographs

Transmission electron microscopy was used to study the microstructure of the AA5182 CES in detail. During the stages of dislocation recovery in alloys such as AA5182, microstructures similar to those described in Subsection 2.5.6 form. During recovery, the microstructure will evolve with time at temperature, from that of tangled dislocations to cell-like structures, with some free dislocations, to cell structures with fewer free dislocations within them, to subgrains. The next stage is where subgrains then grow in size for longer times. These structures associated with recovery are annotated and presented schematically in Figure 4.47.

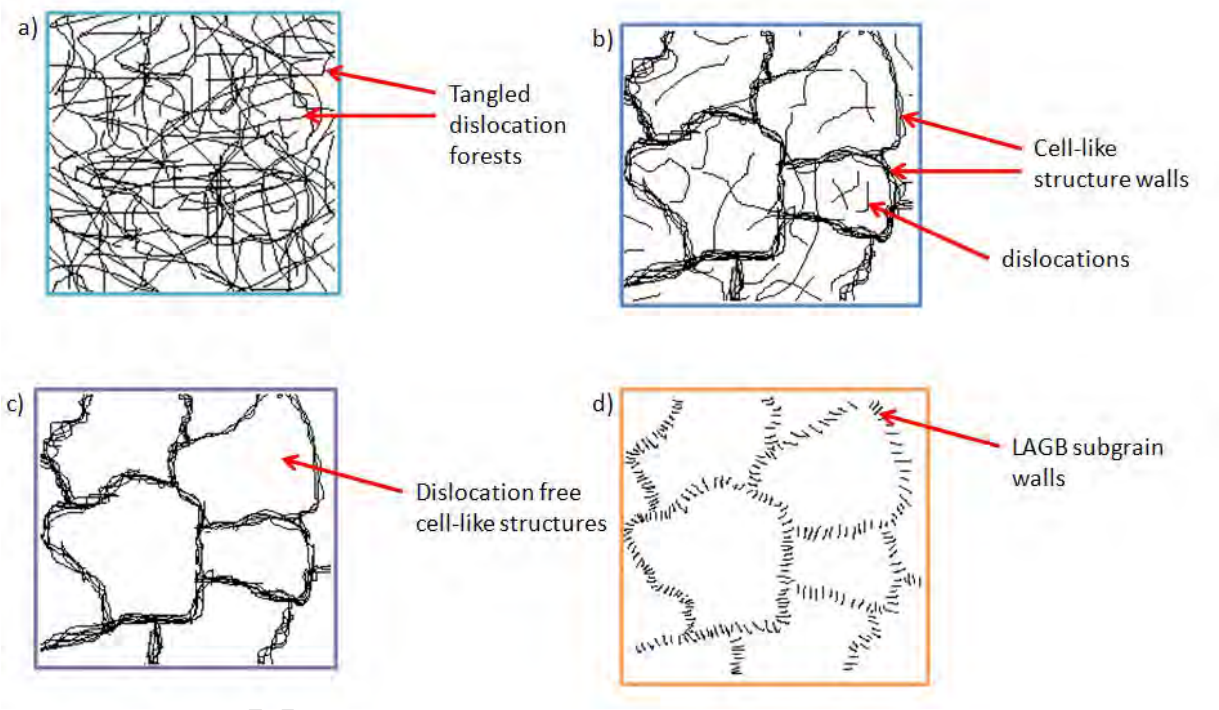

Figure 4.47: Schematic representation of dislocation recovery stages in AA5182 showing: a) tangled dislocations b) the formation of cell structures c) the annihilation of the free dislocations within cell structures and d) the formation of subgrains.

[10]

During recovery, when many dislocations become entangled, they arrange themselves into structures called dense dislocation walls (DDWs) [34], [35]. When these DDWs occur as pairs, they are referred to as microbands (MBs). Microbands (MBs) and dense dislocation walls (DDWs) are both geometrically necessary boundaries (GNBs) and form in order to reduce the internal stress in the microstructure, as discussed in Section 2.5. The MBs are similar to shear bands but do not cut across grain boundaries, and rather appear in just individual grains. Although there is dispute about which plane the GNBs correspond to, previous studies found that slip

occurs primarily along the <111> plane in the FCC aluminium alloy [35]. The GNBs are thus aligned with this <111> plane as shown in the near parallel DDWs represented in Figure 4.48 and the corresponding elongated cell block structures seen in EBSD maps in Section 4.3. Cell blocks are the volumes enclosed by DDWs and MBs in the AA5182 microstructure, as displayed schematically in Figure 4.48. In Al-Mg alloys such as AA5182, the overall arrangement of poorly defined cells within the cell blocks is random, but the arrangement of cell blocks in relation to their neighbours is more regular. This regular arrangement of cell blocks is known as a Taylor Lattice (TL) [35]. The plastic deformation of Al-Mg alloys is approximated by models such as the Taylor-type models described in Subsection 2.5.7. Figure 4.48 illustrates schematically, on a lower magnification than Figure 4.47, the microstructure which evolves within grains in stabilized AA5182 during recovery. The features in this schematic will be identified within the TEM micrographs in this section. The schematic representations in Figure 4.47 and Figure 4.48 will be used to discuss the microstructural evolution occuring during recovery in the coil coating procedure for both CSHT and as-CR samples.

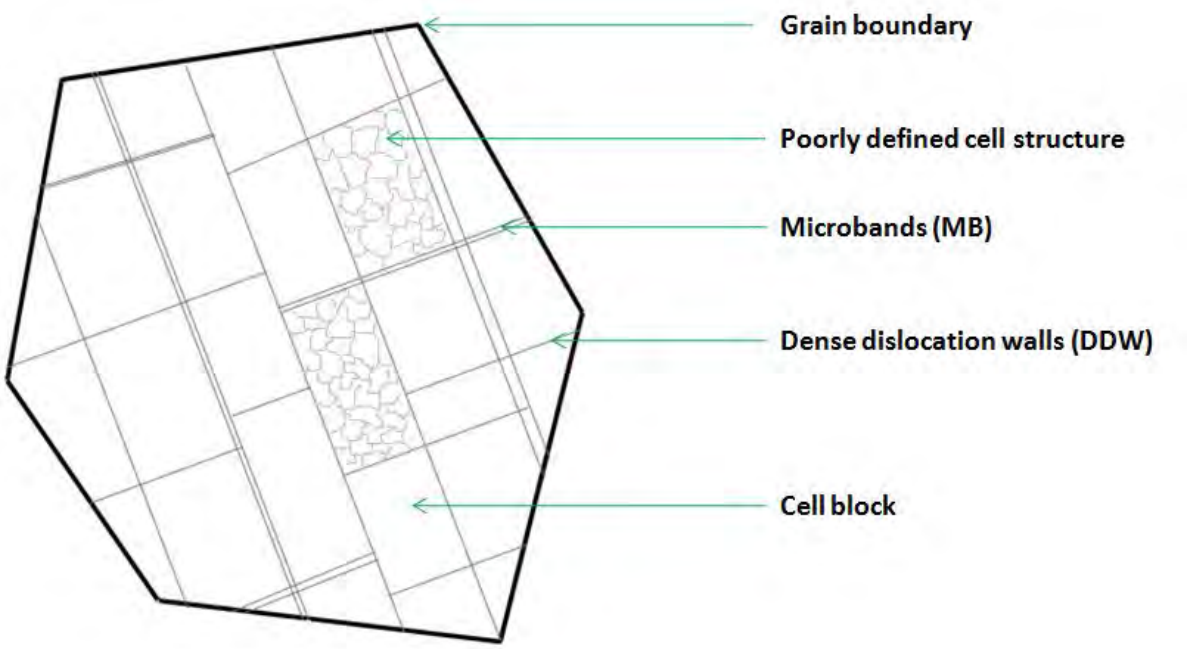

Figure 4.48: Schematic of cell structures observed in TEM micrographs of AA5182 specimens.

Representative TEM micrographs were taken from carefully prepared samples from CSHT specimens and as-CR specimens. Representative CSHT sample micrographs are first discussed with reference to the microstructural features identified in the micrographs. The as-CR sample micrographs are then discussed and compared to those of the CSHT samples. The CSHT samples with 10%CW are then discussed, followed by the CSHT samples with SCCP for 4 minutes and 30 minutes. Finally, the CSHT samples with SCCP for 4 hours are discussed, together with the as-CR samples with SCCP for 4 hours, for comparison purposes. The micrographs discussed in

this section are representative of the microstructure in the CES samples, with further micrographs displayed in Appendix C.

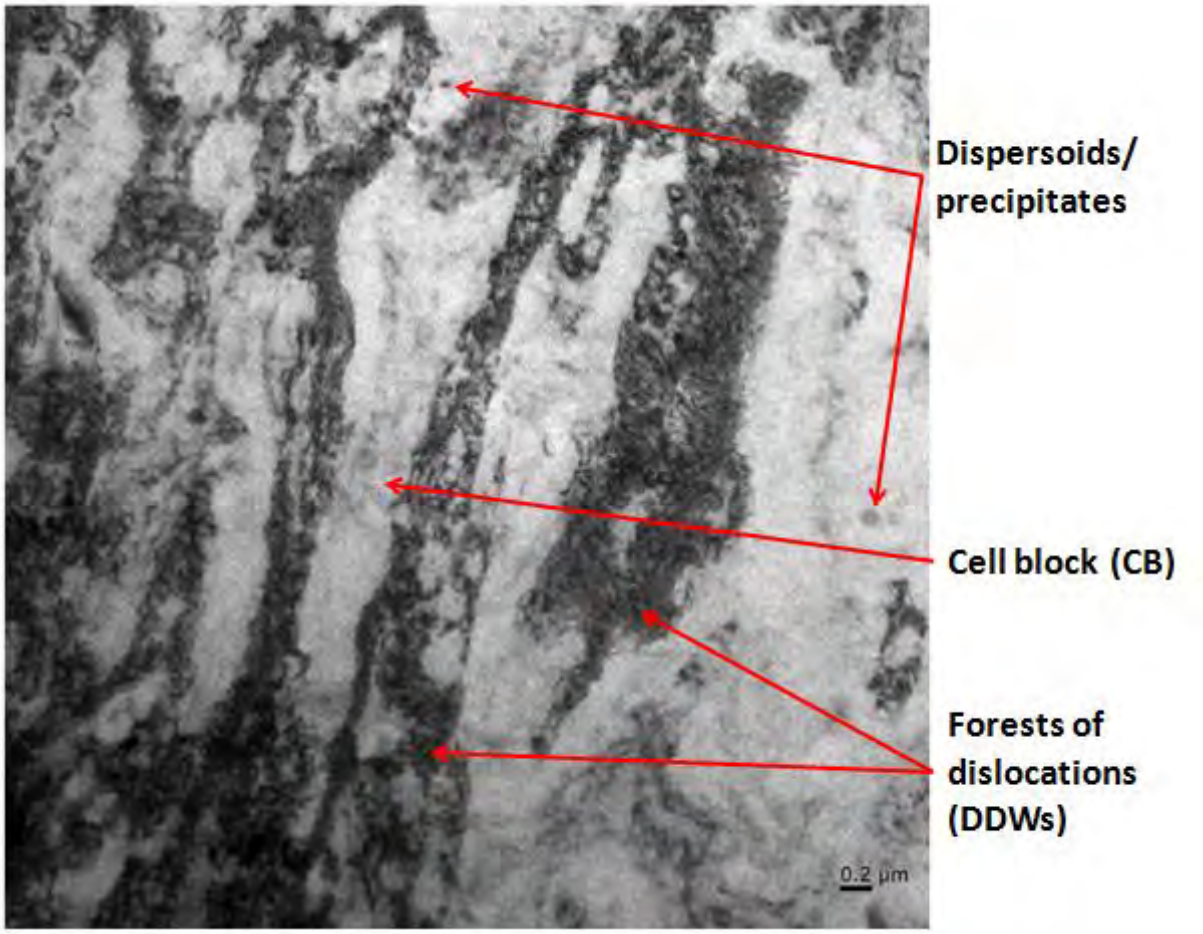

Figure 4.49: A representative TEM micrograph of a CSHT sample showing cell block structures.

A representative micrograph of CSHT samples is displayed in Figures 4.49. This micrograph is annotated to show the observed features in the CES microstructures. The CSHT samples show regions of high dislocation density called 'forests of dislocations'. The shape of these entangled dislocations is dependent on the small precipitates which pin their motion, as described in Section 2.5. The precipitates observed are, on average, 0.2µm in diameter and are thus referred to as 'dispersoids'. As described in Section 2.5, these dispersoids are either Al_6Fe or Al_6Mn and are together referred to as Al_6(Fe, Mn) dispersoids. The CSHT samples showed dislocation forests throughout their microstructure and the presence of cell blocks formed by DDWs, as described in Figure 4.48. These cell blocks run near parallel to eachother, as described in Figure 4.48. From selected area measurements between the DDWs, the average cell block sizes were determined to be 1.6µm in the elongated direction and 0.5µm across the perpendicular to the elongated direction. The arrangement of the cell blocks in relation to their neighbours is regular and forms the Taylor lattice (TL) structure. There is also evidence of free dislocations within the cell blocks

as described in Figure 4.47 a) and b), however these dislocations are not as clearly displayed in the TEM micrographs as the DDWs are. In the EBSD technique described in Subsection 2.6.2, structures of approximately 0.7μm in diameter were identified within elongated structures of approximately 20μm in length. These structures are not subgrains and grains but are cells and cell blocks respectively. The average subgrain sizes represented as ECD values in Table 4.11 thus measure cell sizes and information for rearrangements in the microstructure other than subgrain formation. The high dislocation density within the cell block structure as well as the width of the DDWs themselves, resulted in the poor indexing in the EBSD maps in Section 4.3.

In order to compare the effect of the CSHT on the as-CR specimens, as-CR samples were prepared and investigated with the TEM. A representative TEM micrograph for the as-CR samples is shown in Figure 4.50.

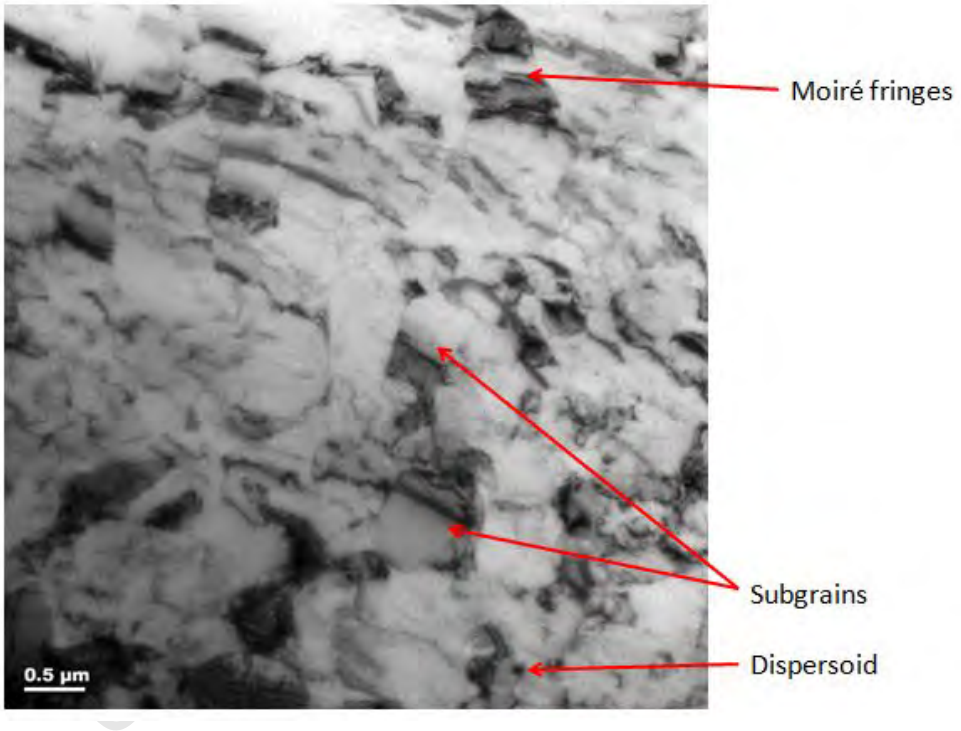

Figure 4.50: A representative TEM micrograph of an as-CR sample.

The TEM micrograph for the as-CR samples differs greatly from that of the CSHT samples. Although the as-CR samples do show the presence of dispersoids of, on average, 0.2μm in diameter, the incidence of these dispersoids in the TEM images is lower than in the CSHT samples. The TEM images indicate that there is also a lower dislocation density in the as-CR samples than in the CSHT samples. Although there are still some visible dislocations pinned by dispersoids in the as-CR samples, these are far fewer in the TEM micrographs than those in the CSHT samples. The major difference in the as-CR samples is the presence of distinct subgrains emphasized by the presence of Moiré fringes, which, as discussed in Subsection 2.6.3, are evidence of subgrain walls. The formation of these subgrains means that the as-CR samples have undergone recovery

to an extent indicated in the schematic shown in Figure 4.47 d). As was mentioned in Section 4.3 and discussed in Section 4.4, the as-CR samples were investigated as a control and were tested last in this study. The as-CR specimens thus recovered over the time they were stored at room temperature, to the stage in dislocation recovery where cell structures form subgrains, as shown in Figure 4.47.

A representative TEM micrograph for the CSHT with 10%CW samples is shown in Figure 4.51. The effect of the 10% cold work on the AA5182 microstructure, shown in Figure 4.51, is compared to that of the CSHT samples without subsequent cold work.

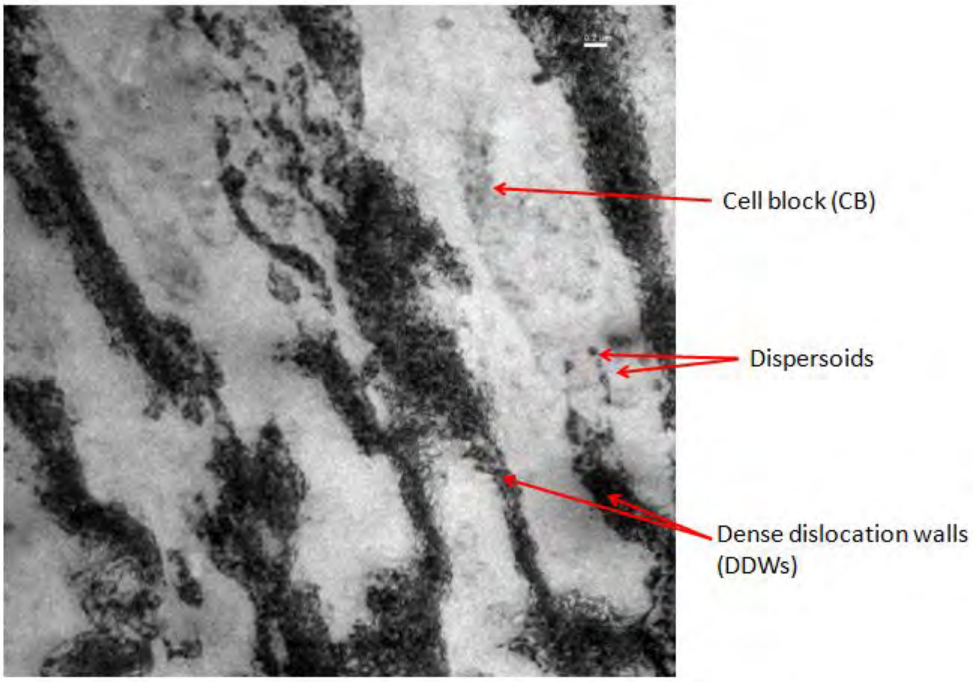

Figure 4.51: A representative TEM micrograph of a CSHT sample with 10%CW.

In Figure 4.51, there are dislocation forests which form DDWs in the CSHT with 10%CW samples. These DDWs run near parallel to eachother, forming cell blocks between themselves in a similar way to those shown in Figure 4.49 for the CSHT samples. After 10%CW on the CSHT samples, the samples still have dispersoids of approximately 0.2μm in diameter. The arrangement of the cell blocks with respect to their neighbours is not random and forms a Taylor Lattice (TL). The microstructure in Figure 4.51 is similar to that of the CSHT, but from selected area measurements between the DDWs, the average cell block sizes were determined to be 2.4μm in the elongated direction and 0.8μm across the perpendicular to the elongated direction. The CSHT samples were between the recovery stages a) and b) shown in Figure 4.47, whereas the CSHT with 10%CW has more narrowly defined cell block walls and is in stage b) shown in Figure 4.47. The 10% cold work resulted in the further entanglement of dislocations around dispersoids and existing dislocation forests in the CSHT samples. The average length and width of the cell blocks which the DDWs encompass was thus greater after the 10%CW had been performed on

the CSHT samples. There was no evidence of any subgrain formation in the TEM micrographs for the CSHT 10%CW samples.

A representative TEM micrograph for the CSHT with SCCP for 4 minutes samples is shown in Figure 4.52. The effect of the heat treatment at 220°C (SCCP) for 4 minutes is investigated and compared to that of the CSHT with 10% cold work.

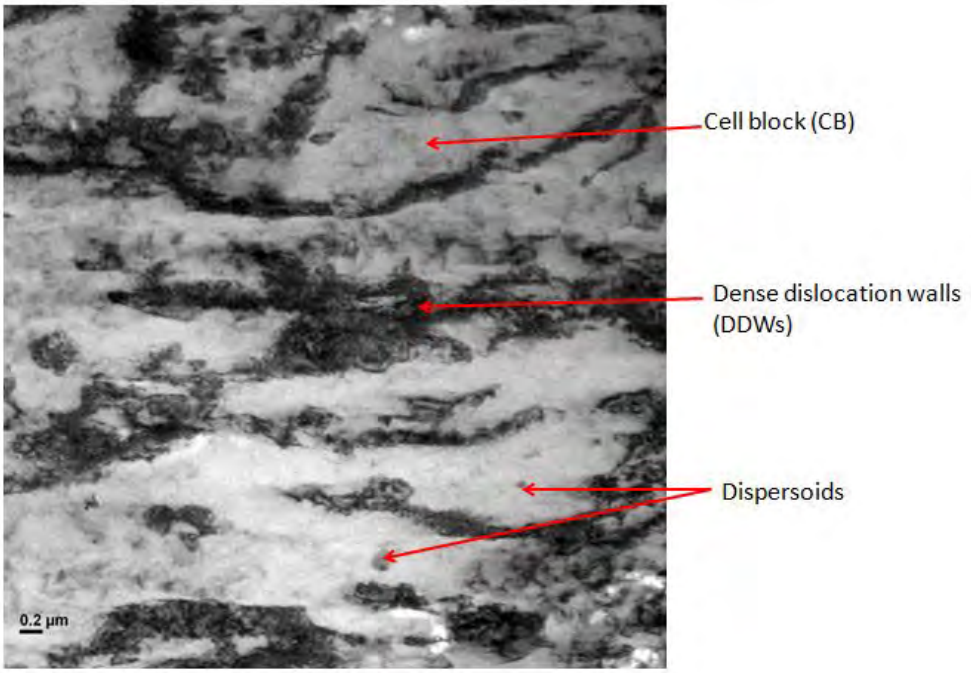

Figure 4.52: A representative TEM micrograph of CSHT samples with SCCP for 4 minutes.

The TEM micrograph in Figure 4.52 shows that the SCCP for 4 minutes results in a microstructure with a lower dislocation density than the CSHT 10%CW samples. The DDWs are less dense than those in the CSHT 10%CW samples. There are also less free dislocations within the cell blocks (CBs) and hence, within the cells. Selected area measurements between the DDWs, showed the average cell block sizes were 2.6µm in the elongated direction and 1.0µm across the perpendicular to the elongated direction. Although the average sizes of these CBs are similar to those of the CSHT 10%CW samples, the DDWs do not fully connect to form neat CBs. Due to the stacking fault energy in the samples, some of the dislocations within the cell blocks have been annihilated during the recovery process when they change their cross-slip planes. These CBs do still form a regular, near parallel Taylor lattice arrangement with their neighbours. Dispersoids of approximately 0.2µm in diameter are present in the TEM micrographs. The microstructure does vary more than the CSHT samples, depending on the regions of the samples investigated. This variation is due to the microstructural changes occuring during dislocation recovery being less well defined than the stages shown in the schematic in Figure 4.47. The TEM micrographs are at varying stages in the dislocation recovery process between the steps b) and c) shown in Figure 4.47.

A representative TEM micrograph for the CSHT with SCCP for 30 minutes samples is shown in Figure 4.53. The effect of the heat treatment at 220°C (SCCP) for a longer time of 30 minutes is investigated and compared to that of the CSHT with SCCP for 4 minutes.

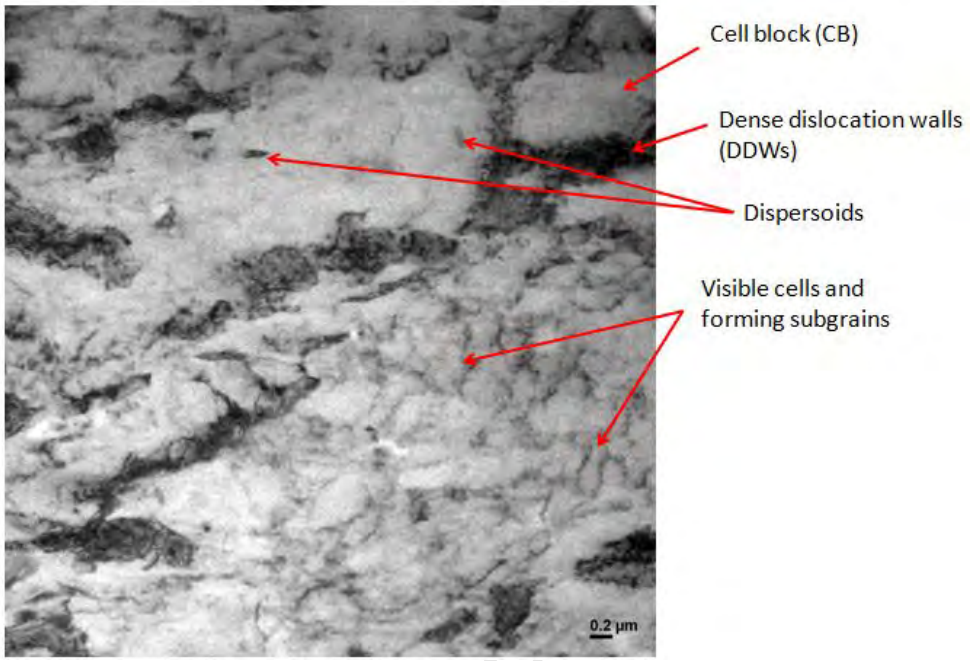

Figure 4.53: A representative TEM micrograph of CSHT samples with SCCP for 30 minutes.

As shown in the TEM micrograph in Figure 4.53, the SCCP for 30 minutes results in a microstructure similar to some regions in the CSHT SCCP for 4 minutes samples, but with what appear to be lower dislocation density DDWs. These DDWs appear in the TEM micrographs to be narrower than those in the the CSHT samples. The cell blocks in Figure 4.53 have DDWs which are discontinuous along their lengths and show less of a regular relationship to their neighbours. These CBs do not obey the Taylor lattice criteria and are not arranged in the regular Taylor lattice seen in the CSHT samples. Dispersoids of approximately 0.2µm in diameter are still present in the CES after this heat treatment and there are entangled dislocations pinned around these dispersoids. Within the cell blocks, there are now visible cells and some subgrain structures. These samples are at a stage of dislocation recovery between c) and d) in Figure 4.47, where dislocation free cells can be seen and some subgrain boundaries have begun to form. After this extended time at the SCCP temperature, the microstructure has only recovered to a stage before the formation of subgrains.

A representative TEM micrograph for the CSHT with SCCP for 4 hours samples are shown in Figure 4.54. The effect of the heat treatment at 220°C (SCCP) for a greatly extended time of 4 hours is investigated and compared to that of the CSHT with SCCP for 30 minutes.

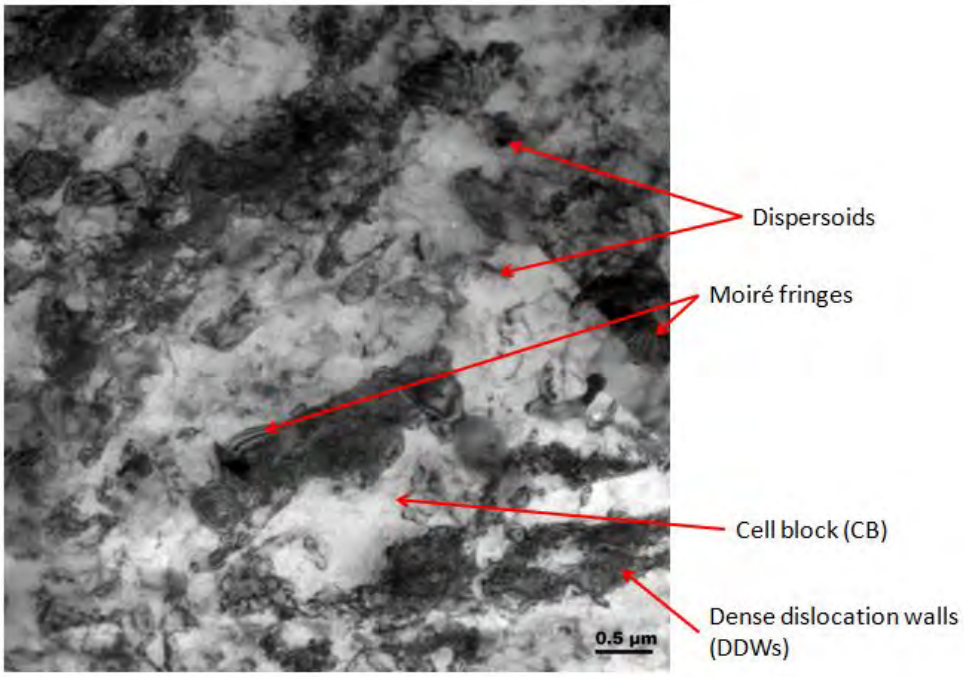

Figure 4.54: A representative TEM micrograph of CSHT samples with SCCP for 4 hours.

As shown in the TEM micrograph in Figure 4.54, the SCCP for 4 hours results in a microstructure which differs from that of the previous CSHT samples. The microstructure now shows Moiré fringes which, as described in Subsection 2.6.3, appear when there is the formation of subgrain low angle grain boundaries (LAGBs). The formation of subgrains is seen in the CSHT samples after they have been treated at 220°C for 4 hours. This extended period of time at high temperature is not used in practice, with the SCCP used at Hulamin only running for less than 30 minutes, as shown in Figure 2.6. This resulting microstructure, however, does further the understanding of recovery in the AA5182 CSHT samples, as it is similar to that shown in Figure 4.47 d). The observations also evaluate the effectiveness of the stabilization heat treatment at minimizing dislocation recovery in AA5182 CES. Although the CSHT samples do begin to form subgrains after the SCCP for 4 hours, their microstructures still show some DDWs and CBs, unlike the as-CR specimens which form subgrains only, as shown in Figure 4.55. The mechanical properties of the CSHT and as-CR samples are similar after the SCCP heat treatment for 4 hours, with average yield stress values of 238MPa and 243MPa respectively. Subgrains evolve from the cell block arrangement of CSHT samples if this extended coil coating time at the SCCP is used, as explained from c) to d) in Figure 4.47. Dispersoids of approximately 0.2µm in diameter are still present in the CSHT samples after this heat treatment and there are entangled dislocations pinned around these dispersoids.

A representative TEM micrograph for the as-CR with SCCP for 4 hours samples are shown in Figure 4.55. The effect of the CSHT is investigated by comparing the microstructures of these

as-CR with SCCP for 4 hours samples and the CSHT with SCCP for 4 hours samples.

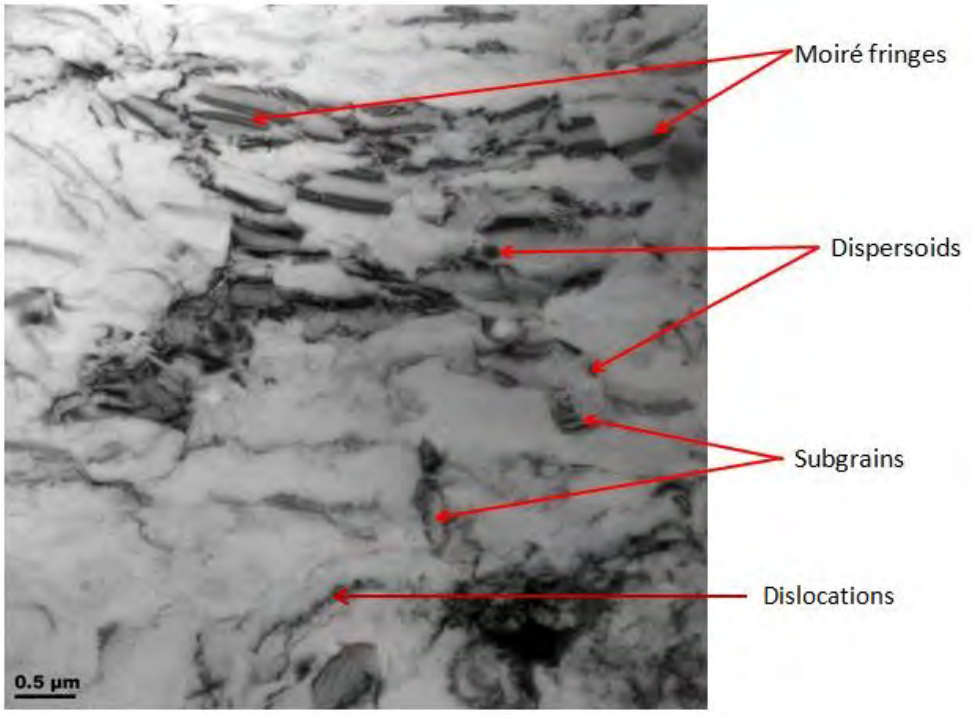

Figure 4.55: A representative TEM micrograph of as-CR samples with SCCP for 4 hours.

As shown in the TEM micrograph in Figure 4.55, the SCCP for 4 hours on the as-CR samples results in a microstructure which shows Moiré fringes and distinct subgrains. The amount of recovery that has occured is similar to that of the dislocation recovery stage d) shown in Figure 4.47. Although there are some sparsely distributed dislocations present in Figure 4.55, no DDWs are seen and the Taylor lattice of cell blocks is not present. The microstructure is similar to that of the recovered structure seen in Figure 4.50for the as-CR samples. The microstructure does display some dispersoids of approximately 0.2µm in diameter, as seen in Figure 4.55.

4.5.2 Summary of the AA5182 Microstructures Investigated

In Subsection 4.5.1, the as-CR samples were shown to have fewer dislocations, and thus a lower dislocation density on average, than the CSHT samples. The as-CR samples also displayed none of the cell block (CB) structures and the Taylor lattice (TL) arrangements seen in CSHT samples. The deformation mechanism in these as-CR samples is by subgrain formation and not the formation of cell structures [10] [26]. The as-CR samples were tested last in this study, and were stored at room temperature for a year. When the as-CR samples were investigated, it was found that their microstructures had undergone dislocation recovery and subgrain formation. The

as-CR microstructure is shown in Figure 4.56 a). When the as-CR samples were heat treated at the simulated coil coating procedure (SCCP) temperature for the extended period of 4 hours, the microstructure was found to display Moiré fringes and distinct subgrains. This microstructure is shown in Figure 4.56 b). Unlike the CSHT samples, the as-CR samples in both conditions did not show dense dislocation walls (DDWs), cell blocks (CBs) or the Taylor lattice (TL) arrangement in their microstructures. Dispersoids of approximately 0.2μm in diameter were present in the as-CR CES microstructure. These dispersoids pin the motion of the few dislocations present but are unable to pin them for a sufficient time for the dislocation density to increase. Dislocation forests thus do not form in the as-CR samples in the manner that they do in the CSHT samples.

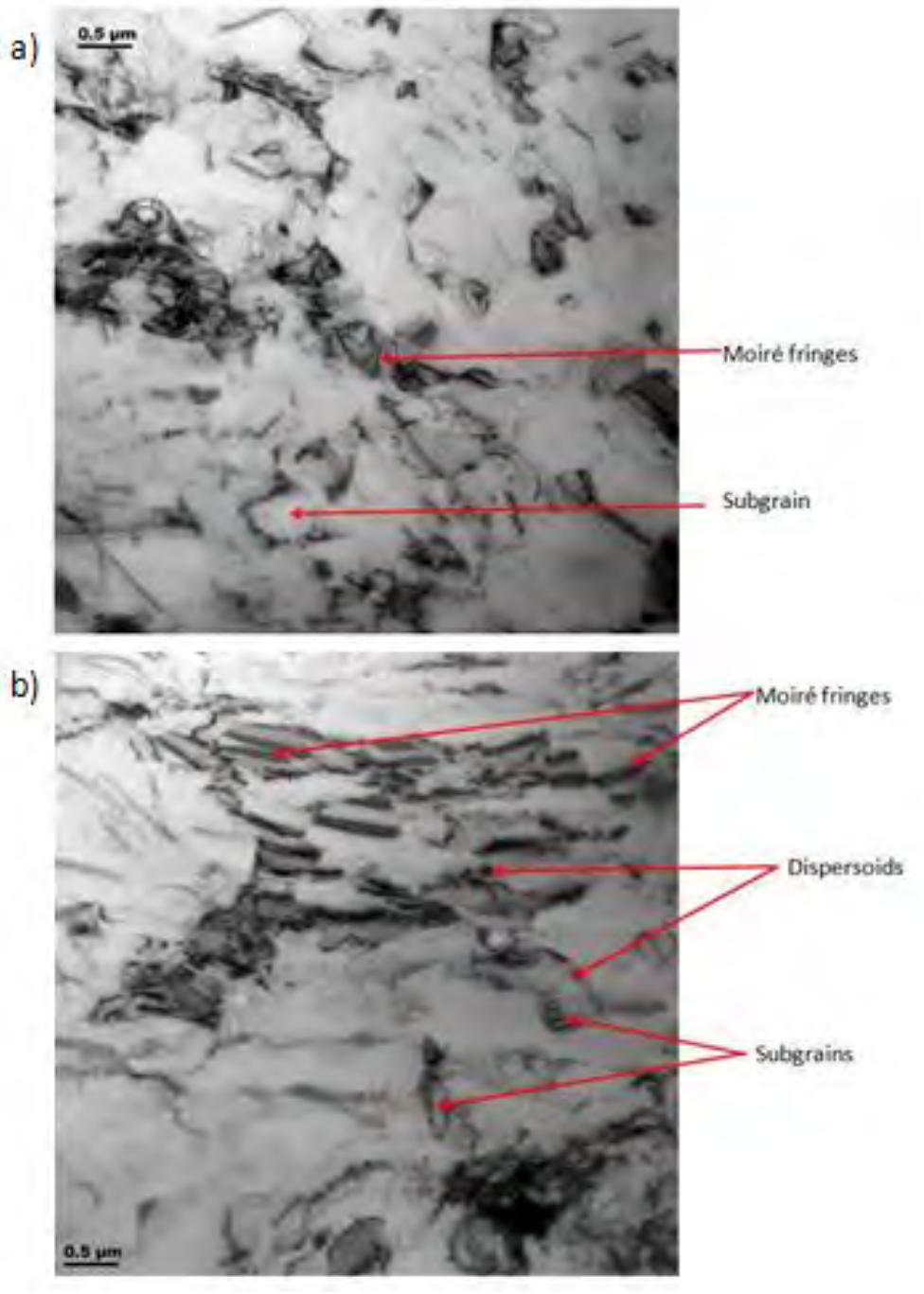

Figure 4.56: Summary of TEM micrographs for the a) as-CR samples and the b) as-CR samples with SCCP for 4 hours.

In Subsection 4.5.1, the CSHT samples were shown to display regions of high dislocation density, unlike the as-CR samples. These dislocation forests formed dense dislocation walls (DDWs). At the magnification investigated, no DDW pair microbands were observed. The CSHT samples showed a similar microstructure to the CSHT samples after 10%CW and thus the TEM micrographs are summarized from the CSHT 10%CW samples onwards in Figure 4.57.

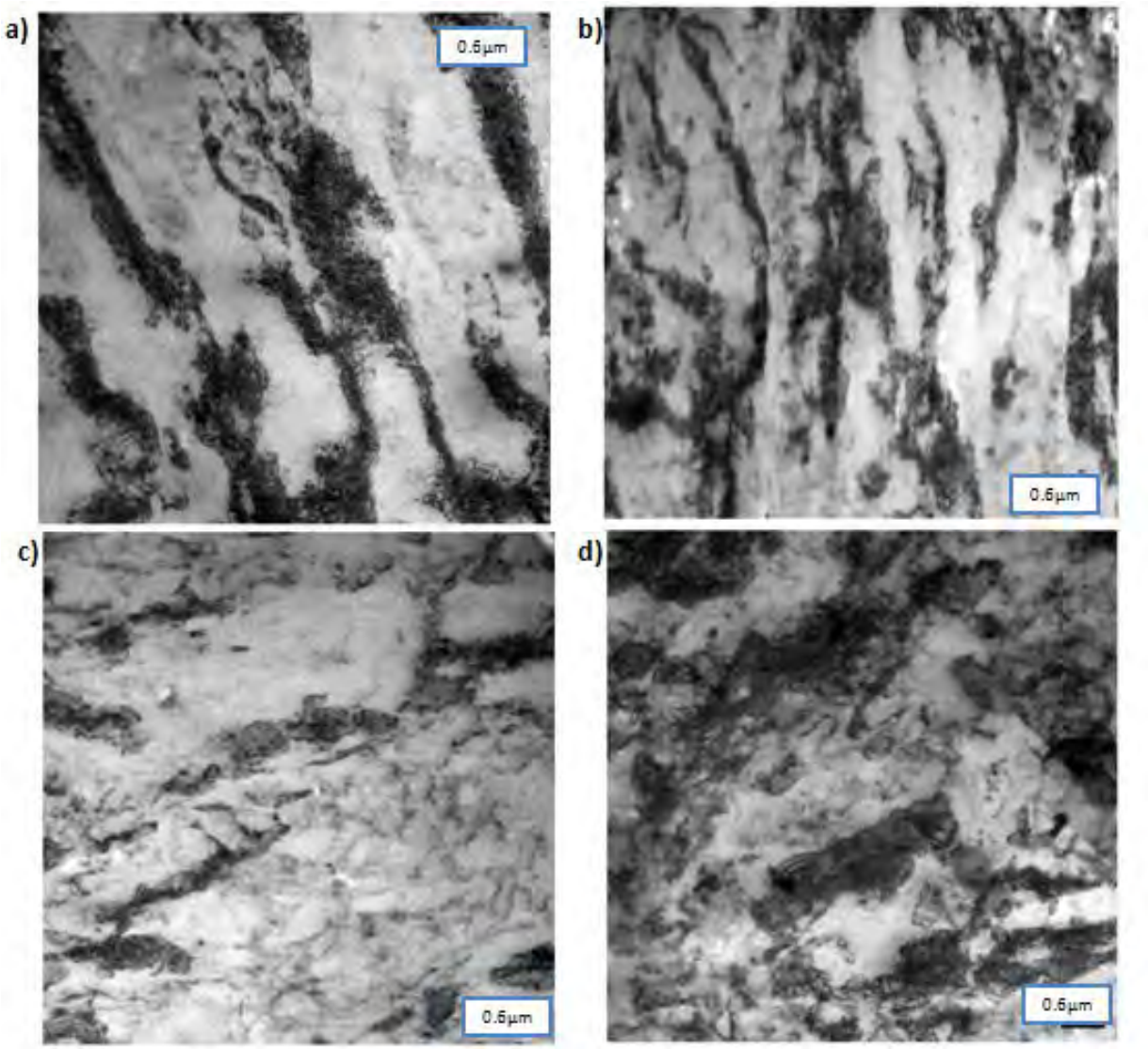

Figure 4.57: Summary of TEM micrographs for the CSHT samples showing the dislocation recovery stage progression from cell formation to subgrain formation over time at the SCCP.

In Figure 4.57, the CSHT 10%CW sample shows a regular Taylor lattice arrangement of cell blocks. These cell blocks are surrounded by many tangled dislocations forming the DDWs. The DDWs form the cell block (CB) structures in the all the CSHT samples.

The SCCP caused the dislocation density to decrease as the SCCP time increased. In Figure 4.57 b), the DDWs have fewer dislocations than in a), as some dislocations were annihilated during the heat treatment. The cell blocks are still present and form a Taylor lattice arrangement.

In Figure 4.57 c), the DDWs are poorly defined and discontinuous. There are also dislocation free cells and some subgrain formation visible in the TEM micrographs. The SCCP for 30 minutes simulates the maximum coil coating used at Hulamin. These specimens with the previous CSHT retain some of their CB and DDW structures, unlike the as-CR specimens with the same heat treatment, which can be seen to recover further and form distinct subgrains. This indicates that

the CSHT is thus effective at retarding recovery and dislocation mobility, which consequently results in retained mechanical properties in the CES. This can be seen in the relatively higher average yield stress of the CSHT samples than the as-CR samples after the SCCP for 30 minutes, 285MPa and 271MPa respectively. The desired industry yield strength for stabilized AA5182 CES, as described as H34 in Table 4.9, is 285MPa, which is the same as the average yield stress determined experimentally for the CSHT SCCP 30 minutes samples.

In order to investigate the effectiveness of the CSHT in retaining the CES microstructural features at elevated temperatures for an extended period, the samples were heat treated at the SCCP temperature for 4 hours, which exceeds the typical time used at temperature during coil coating at Hulamin. After the SCCP 4 hour treatment, the CSHT samples did show Moiré fringes and the appearance of subgrains, as shown in Figure 4.57 d). This explains why the average yield strength of CSHT and as-CR samples is similar after the SCCP 4 hour heat treatment, 238MPa and 243MPa, as shown in Table 4.9. The SCCP heat treatment for 4 hours is long enough for the previously CSHT samples to recover to the stage of subgrain formation which as-CR samples recover to, as described from c) to d) in Figure 4.47. The amount of recovery by subgrain formation, however, is less in the CSHT treated at the SCCP temperature for 4 hours than it is for the as-CR specimens with the same heat treatment. This can be seen in the relative greater amount of distinct subgrains and the fewer DDWs in the as-CR samples, as seen in Figure 4.55 b), compared to those in the CSHT samples in Figure 4.54 d). The CSHT is thus more effective in limiting the amount of recovery in AA5182 CES than if the samples did not undergo a stabilization heat treatment.

Throughout the recovery stages in the CSHT samples, the micrographs show the presence of dispersoids of approximately 0.2μm in diameter. For the CSHT samples, these dispersoids pin the dislocations for a significant enough time for other dislocations to also become entangled around the dispersoids. During recovery in these CSHT samples, a regularly aligned cell block arrangement is thus formed when the glide dislocations are trapped [36]. These cell blocks form a Taylor lattice arrangement in the CSHT sample TEM micrographs a) and b) shown in Figure 4.57.

Chapter 5

Conclusions

The effectiveness of using a low temperature stabilization heat treatment after final cold rolling of AA5182, in order to minimize recovery, has been investigated. The AA5182 can end stock (CES) material was heat treated at various temperatures and times, based on those used at Hulamin. The stabilization heat treatment and the coil coating procedure were simulated and their effects on the mechanical properties and microstructure of the CES were investigated. The success of the stabilization heat treatment was evaluated by looking at recovery during a simulated coil coating procedure that was applied to samples in two different conditions: the as-cold rolled condition and after a stabilization heat treatment at 150°C for 4 hours.

The microstructures of these specimens were investigated using the EBSD technique and TEM. These microstructures were described and discussed with emphasis on the effect of stabilization heat treatment on the microstructural evolution in the CES.

5.1 The Mechanical Properties of AA5182 CES

The as-cold rolled (as-CR) specimens and heat treated specimens were mechanically tested using tensile tests. These mechanical properties were compared using average yield stress, UTS and work hardening coefficient measurements. The mechanical properties of the AA5182 CES in this study demonstrate that:

- The as-CR AA5182 CES specimens had average yield strengths comparable to those of the H18 literature values. The AA5182 CES produced at Hulamin has the mechanical properties expected in the aluminium industry.
- The heat treatments at 120°C for 1 hour and 4 hours did not stabilize the CES. The average strength properties were similar to the as-CR condition and not the industry standard H34 condition for stabilized AA5182.
- The heat treatments at 150°C did stabilize the AA5182 CES. After the coil coating procedure used at Hulamin is simulated using a 220°C heat treatment for 30 minutes, the

average yield strengths of the samples were found to be the same as the industry standard H34 stabilized condition.

- The heat treatments at 200°C for 1 hour and 4 hours also resulted in stabilization of the CES. This heat treatment, however, involves more energy costs to raise the temperature than the 150°C heat treatment, and thus is less economically viable and was not investigated further in this research.

5.2 The Microstructure of AA5182 CES

5.2.1 EBSD Subgrain Analysis

The subgrain sizes of the CES determined using the EBSD technique did not substantially change with the heat treatments used in this study. The overall subgrain sizes measured varied between 0.60μm and 1.03μm in diameter.

- The TEM investigation showed that the structures measured as subgrains were complex arrangements of dislocations at various stages of recovery.
- The subgrain sizes did correlate with the cell structure sizes seen in the TEM micrographs.
- Poor indexing in the EBSD maps is attributed to the high dislocation density within the cells and to the thickness of the dense dislocation walls (DDWs).
- The EBSD technique, at the resolution used for this investigation, was not successful at attaining reliable subgrain size measurements.

5.2.2 TEM Analysis of Dislocation Structures

Dislocation structures were identified in the TEM micrographs. These dislocation structures were made up of: dense dislocation walls (DDWs), cell blocks (CBs), Taylor lattice (TL) arrangements, cell structures and subgrains. The evolution of these features during the simulated coil coating procedure (SCCP) was used to interpret the progress of recovery in each case.

- After SCCP the AA5182 in the as-CR condition undergoes dislocation recovery by subgrain formation.
- In the AA5182 alloy heat treated at 150°C for 4 hours, however, the microstructure is stabilized. This can be seen by the limited evolution of the dislocation structures during SCCP, where DDWs and cell structures are still present after 4 hours at 220°C.
- In the stabilized samples, subgrain refinement occurs by the formation of cell blocks surrounded by dense dislocation walls.

5.2.3 Effect of Dispersoids

Al_6(Mn, Fe) and Al_3Mg dispersoids of approximately 0.2μm in diameter hinder the dislocation annihilation in cold worked AA5182, thereby increasing the dislocation density in the alloy. The TEM investigation revealed the presence of a number of dispersoids evenly distributed throughout the microstructure. Notwithstanding the fact that the dispersoids hinder dislocation motion locally, their size and distribution indicates that they are not solely responsible for the stabilization of the microstructure and the hindering of the recovery process.

In the stabilized AA5182, the dislocation density is retained after the simulated coil coating procedure of 220°C for 30 minutes, resulting in greater strength properties in the AA5182 than in the as-CR AA5182 after the same SCCP procedure. This can be seen in both the TEM micrographs and the resulting mechanical properties. If the AA5182 is heat treated at 220°C for the extended period of 4 hours, it undergoes dislocation recovery to the stage of subgrain formation, regardless of whether or not the alloy was previously stabilized. However, the stabilized microstructures did contain a number of DDWs at this point, indicating that the stabilization treatment is successful.

Chapter 6

Recommendations For Future Work

6.1 The Anisotropy Effect

This study only investigated tensile specimens cut from CES with the rolling direction (RD) representing the tensile pulling direction, as shown in Figure 2.8. This was performed in order to simplify the study so that comparisons could be made between specimens after different heat treatments. The yield strength of severely cold worked samples (greater than 90% cold worked), however, may decrease to a greater or lesser extent in the RD than in transverse direction (TD) or the 45 degree angle to the rolling direction. The serration intensity may also be greater or lesser in the RD than in the TD or 45 degree direction. The effect of the orientation of the tensile specimens, in terms of where they are cut from the CES, may be substantial, especially when the CES is later drawn into cans. It is recommended that the anisotropy effect is studied and the anisotropy coefficient (r) is determined in a similar way to how the n-value was determined in this study. The r value is measured in the 3 directions of RD, TD, and at 45 degrees to the rolling direction. A high anisotropy coefficient (r value) of the CES is required so that the beverage can ends may be drawn in a stamping die. If all the mechanical properties are the same in all three of these directions, the CES is perfectly isotropic and r = 1. If the CES stretches more than it thins, r > 1, and the CES will easily flow without excessive thinning in a drawing die. If the CES thins more than it stretches, r < 1, this leads to tearing of the drawn CES. To test this, at least three rectangular specimens should be cut from the CES in each of the three directions. A strain gauge should then be attached to the specimens in the two directions of the rectangle; the long and short side directions. The r-value can then be calculated. The r values also account for the earring phenomenon when the CES is drawn into a beverage can shape.

6.2 Extended Design Matrix

The samples heat treated at 150°C for 4 hours had a significantly different microstructural evolution to as-CR control samples. The initial heat treatment at 200°C showed an interesting decrease in its mechanical properties compared to that of the as-CR specimens. The investigated

design matrix could thus be extended to temperatures between the CSHT of 150°C and this 200°C temperature. These temperatures may also result in some stabilization of the CES by the microstructural formation of the cell-like structures.

6.3 Refined Rolling Process

The 10% cold work specimens show a wide scatter in their mechanical test data. This may be due to non-uniformity in the thickness and straightness of the specimens after cold rolling. The rolling process could be refined to ensure uniform rolling thickness during this deformation in the simulated coil coating procedure step.

6.4 The Effect of Time on the CSHT

In this study, the effect of the CSHT appears to be in stabilizing the CES so that the strength properties do not decrease over time. This effect was compared to that of the as-CR specimens with no stabilization heat treatment, which appeared to decrease in strength over time. It is recommended that the study be extended to determine if this stabilization effect continues in the CSHT specimens over a longer time than 30 minutes. It could also be determined whether or not the as-CR specimens continue to lose strength properties over these longer periods of time.

6.5 Time Sensitive Specimen Testing

The AA5182 CES specimens in this study were not all tested at the same time or on the same day. Some of these specimens may have recovered over time and thus have lower strength properties than expected. This is perhaps most evident in the as-CR specimens as they were tested last in this study. The texture of severely cold worked samples shows an ageing effect when investigated over long periods of time at room temperature. The deformation texture components were found to decrease in intensity while the softening texture components were found to increase in intensity [27] [1] . For these reasons, a similar design matrix is recommended to be used to test the AA5182 specimens, but with the effect of the loss of strength properties over time being taken into consideration.

6.6 Further Microstructural Investigation in AA5182

Lattice arrangements such as stacking faults and twinning, described in Subsection 2.5.5, occur more commonly in BCC and HCP structures than in FCC structures. Under specific conditions, however, these deformation mechanisms, especially the deformation twinning, may still occur in the AA5182 CES. It is recommended that these types of lattice arrangements and other developed texture be investigated to determine if they have an effect on the microstructure of the AA5182 alloy or not. To this effect, in-situ TEM deformation experiments could be performed at elevated

temperatures simulating the heat treatments used in this study. The microstructure could also be investigated at lower and higher magnifications than used in this experiment, in order to further analyze structures such as microbands and cells respectively. The further study of the formation of inversion domain boundaries (IDBs) such cell structures is also recommended, with respect to their effect on stabilizing the AA5182 CES. This study could incorporate the use of x-ray diffraction to compliment the microscopy results and easily measure the dislocation structures which give rise to dislocation wall broadening. An alternate interpretation of the EBSD data may also be investigated with regards to the size distribution of dispersoids and dislocations within the spatial resolution limits.

6.7 Computer Modeling

It is recommended that computer modeling be used to more closely approximate the deformation modes in the AA5182 CES than the Taylor-type models described in Subsection 2.6. Once the deformation modes and texture formation, such as the cell-like formations, are understood for AA5182, the stabilization effect can be more thoroughly understood.

6.8 Acoustic Emission

During tensile testing of AA5182 CES investigated in this study, a 'pinging' sound emanated from the tensile specimens soon after they had been strained past their yield points. This sound is audible to the human ear. It is recommended that acoustic emission be used to attempt to correlate the intensity of this noise with the microstructural texture evolution in the alloy at varying strain rates and thermal treatments. The two types of serrations and the work-hardening coefficients could also be correlated with this data. The use of HRTEM to compare this data to the microstructure observed could be used as well.

6.9 Serrated Yielding and Surface Roughening

Serrated yielding may have an effect on the surface roughening of the CES. It is thus recommended that experiments, such as cupping tests, be carried out to investigate the surface roughness which may occur in the CES after it has been drawn into the can end shape. This would increase the understanding of texture effects, such as the effect of the precipitation of Mg solute atoms, on the surface roughness of the drawn CES.

Bibliography

[1] F. King, *Aluminium and Its Alloys.* Ellis Horwood Limited, 1987. 5, 6, 8, 120

[2] K. Van Horn, "Aluminium." American Society for Metals, 1967, vol. 1, p. 283. 5, 14

[3] S. Malan and A. Paterson, *Introduction to Aluminium.* Aluminium Federation of South Africa, 1987, no. 70. 5, 6, 8, 9, 12, 13, 96

[4] J. G. Kaufman, *Introduction to Aluminium Alloys and Tempers.* ASM International (OH), 2000. 7, 9

[5] Aluminium Company of Canada, *Heat Treating Aluminium.* Alcan Technical Books, 1950. 7, 12

[6] A. Cottrell, *An Introduction to Metallurgy.* London: Edward Arnold (Publisher) Ltd., 1975. 7

[7] C. Keyser, *Materials of Engineering.* Prentice-Hall Inc., 1956. 8

[8] G. Brady, *Materials Handbook*, 14th ed. McGraw-Hill Book Company, Inc., 1997. 9, 96

[9] G. Dieter, *Mechanical Metallurgy.* McGraw-Hill Book Company, Inc., 1961. 10, 12, 16, 18, 21, 22, 28

[10] F. J. Humphreys and M. Hatherly, *Recrystallization and related phenomena.* New York: Pergamon, 1995. 11, 22, 29, 30, 103, 111

[11] J. E. Hatch, *Aluminium: Properties and Physical Metallurgy.* American Society for Metals, 1984. 12, 17, 33, 60

[12] M. van Lancker, *Metallurgy of Aluminium Alloys.* Chapman and Hall, 1967. 12

[13] A. Cottrell, *An Introduction to Metallurgy.* Edward Arnold (Publishers) Ltd., 1975. 14

[14] W. Wen, "The effect of precipitation of Mg2Al3 and of MnAl6 on texture evolution during isothermal annealing and subsequently on formability of CC AA5182 Al alloy," *Materials Science and Engineering A*, vol. 380, no. 1-2, pp. 191–207, Aug. 2004. 15, 25

[15] W. Wen and J. Morris, "An investigation of serrated yielding in 5000 series aluminum alloys," *Materials Science and Engineering: A*, vol. 354, no. 1-2, pp. 279–285, Aug. 2003. 15, 16

[16] W. Wen, Y. Zhao, and J. Morris, "The effect of Mg precipitation on the mechanical properties of 5xxx aluminum alloys," *Materials Science and Engineering: A*, vol. 392, no. 1-2, pp. 136–144, Feb. 2005. 15, 16, 17

[17] C. Roberts, "Grain Growth and the Zener Pinning Phenomenon: A Computational and Experimental Investigation," Ph.D. dissertation, Carnegie Mellon University, 2008. 22

[18] E. H. Edwards, J. Washburn, and E. R. Parker, "Fundamental Studies Related to the Origin and Nature of Creep of Metals: Some Observations on the Work Hardening of Metals," University of California, Tech. Rep., 1953. 22

[19] M. Verdier, M. Janecek, and Y. Bre, "Microstructural evolution during recovery in Al 2 . 5 % Mg alloys," vol. 248, pp. 187–197, 1998. 24

[20] L. Z. He, X. H. Li, X. T. Liu, X. J. Wang, H. T. Zhang, and J. Z. Cui, "Effects of homogenization on microstructures and properties of a new type AlMgMnZrTiEr alloy," *Spectroscopy*, vol. 527, pp. 7510–7518, 2010. 24, 25, 26, 38, 39

[21] O. Engler, M. Crumbach, and S. Li, "Alloy-dependent rolling texture simulation of aluminium alloys with a grain-interaction model," *Acta Materialia*, vol. 53, no. 8, pp. 2241–2257, May 2005. 27, 28, 33

[22] A. Duckham and R. Knutsen, "Asymmetric flow during plane strain compression testing of aluminum alloys," *Materials Science and Engineering: A*, vol. 256, no. 1-2, pp. 220–226, Nov. 1998. 27

[23] R. Pond and L. Garcia-Garcia, *Institute of Physics Conference Series*, 61st ed., 1981. 28

[24] R. D. Doherty, "Recrystallization and texture," *Progress in Materials Science*, vol. 42, pp. 39–58, 1997. 29

[25] R. D. Boyer, "Shear-Induced Homogeneous Deformation Twinning in FCC Aluminum and Copper via Atomistic Simulation by Shear-Induced Homogeneous Deformation Twinning in FCC Aluminum and Copper via Atomistic Simulation," 2003. 29

[26] I. Polmear, *Light Alloys: From Traditional Alloys to Nanocrystals*. Elsevier, 2006. 29, 111

[27] S. G. Chowdhury, "Development of texture during cold rolling in AA5182 alloy," *Analysis*, vol. 52, pp. 99–105, 2005. 30, 31, 32, 120

[28] P. V. Houtte, S. Li, M. Seefeldt, and L. Delannay, *Deformation texture prediction : from the Taylor model to the advanced Lamel model*, 2005, vol. 21. 32, 33

[29] M. Berveiller, H. Bouaouine, N. Fakri, and P. Lipinski, "Texture Transition, Micro Shear Bands and Heterogeneous Plastic Strain in F.C.C. and B.C.C. Metals in Rolling," *Textures and Microstructures*, vol. 8, no. C, pp. 351–379, 1988. 33

[30] M. Koizumi, S. Kohara, and H. Inagaki, "Rolling Textures in Al-Mg alloys," *Z. Metallkd*, vol. 91, pp. 88–96, 2000. 33

[31] M. Slámová, V. Očenášek, and G. Vander Voort, "Polarized light microscopy: utilization in the investigation of the recrystallization of aluminum alloys," *Materials Characterization*, vol. 52, no. 3, pp. 165–177, Jun. 2004. 33, 34

[32] G. F. Vander Voort and W. Van Geertruyden, "Specimen Preparation for Electron Backscattered Diffraction," *La Metallurgia Italiana*, vol. 11, 2009. 36

[33] Z. Horita, D. J. Smith, M. Furukawa, M. Nemoto, R. Z. Valiev, and T. G. Langdon, "An investigation of grain boundaries in submicrometer-grained Al-Mg solid solution alloys using high-resolution electron microscopy," *Journal of materials research*, vol. 11, no. 8, pp. 1880–1890, 1996. 40

[34] B. Bay, N. Hansen, D. A. Hughes, and D. Kuhlmann-Wilsdorf, "Overview no. 96 evolution of f.c.c. deformation structures in polyslip," *Acta Metallurgica et Materialia*, vol. 40, no. 2, pp. 205–219, 1992. 103

[35] D. A. Hughes and A. Godfrey, "Dislocation Structures Formed During Hot and Cold Working," 2000. 103, 104

[36] P. J. Apps, M. Berta, and P. B. Prangnell, "The effect of dispersoids on the grain refinement mechanisms during deformation of aluminium alloys to ultra-high strains," *Acta Materialia*, vol. 53, no. 2, pp. 499–511, 2005. 115

Chapter 7

Appendices

Appendix A Average Subgrain ECD Values

Table 7.1: As-cold rolled CES specimens

Sample	**% indexed**	**Vmap value (μm)**
1	61.4	0.63
2	64.6	0.64
3	58.1	0.65
4	55.3	0.65
5	30.2	stopped halfway
6	66.5	0.59
7	64	0.65
8	61.8	0.63
9	69.2	0.59*
10	70.1	0.6
11	65.7	0.59
Average		**0.62**

Table 7.2: 120°C for 1 hour and for 4 hours

Sample	**% indexed**	**Vmap value (μm)**
1hr_1	53.3	0.82
2	60.8	0.76
3	57.9	0.7*
4	58.1	0.67
5	53.6	0.69
6	54.5	0.7
8	58.9	0.7
9	58	0.72
10	56.7	0.62
11	65.4	0.62
Average		**0.702**
4hrs_1	57.1	0.64
2	75.6	0.64
3	68.1	0.59*
4	52.3	0.57
5	58.6	0.6
6	53.8	0.61
7	58	0.63
8	58.4	0.6
9	52.7	0.66
10	67.2	0.64
Average		**0.62**

Table 7.3: 150°C for 1 hour and for 4 hours

Sample	**% indexed**	**Vmap value (μm)**
1hr_1	70.1	0.6
2	68.8	0.61
3	61.4	0.59
4	61.8	0.58
5	62.1	0.6*
6	66.5	0.59
7	57.9	0.6
8	63.2	0.6
9	68.3	0.61
10	68.7	0.62
Average		**0.6**
4hrs_1	60.5	0.61
2	64	0.64
3	66.8	0.64*
4	59.1	0.62
5	60.4	0.69
6	63.6	0.68
7	58.6	0.69
8	54.2	0.69
9	58.7	0.7
10	57.3	0.68
Average		**0.66**

Table 7.4: 200°C for 1 hour and for 4 hours

Sample	% indexed	Vmap value (μm)
1hr_1	68.4	0.65
2	65.4	0.63
3	69.7	0.64
4	70	0.66
5	69.1	0.66
6	73.2	0.66
7	74.1	0.68
8	69.2	0.67
9	68.5	0.69
10	64.1	0.67*
Average		**0.66**
4hrs_1	70.2	0.62
2	61.6	0.65
3	67.3	0.66
4	58.8	0.67
5	66.2	0.71
6	59.9	0.7
7	64.1	0.71
8	60.3	0.71
9	59.8	0.71*
10	56.9	0.75
Average		**0.69**

Table 7.5: CSHT then 10%CW

Sample	% indexed	Vmap value (μm)
1	50.3	0.78
2	54.3	0.78
3	63.1	0.76*
4	50.2	0.76
5	52.7	0.73
6	53.8	0.74
7	53.3	0.72
8	55	0.74
10	50.7	0.69
11	53.9	0.7
Average		**0.74**

Table 7.6: CSHT then SCCP for 4 minutes

Sample	% indexed	Vmap value (μm)
1	57	0.88
3	53.7	0.78
6	59.2	0.79
8	52.6	0.77
9	55.2	0.78
12	63.4	0.64
13	68.3	0.66*
23	63.7	0.67
24	59.2	0.66
25	60.1	0.69
Average		**0.73**

Table 7.7: CSHT then SCCP for 30 minutes

Sample	% indexed	Vmap value (μm)
3.5 spot-1	59.3	0.65
3.5 spot-2	72.4	0.73
3.5 spot-3	72	0.71*
3.5 spot-4	61.7	0.69
3.5 spot-5	61.2	0.71
3.5 spot-6	64.7	0.72
3.5 spot-7	60.9	0.73
3.5 spot-8	63.5	0.75
3.5 spot-9	65.2	0.77
3.5 spot-10	64.4	0.78
Average		**0.72**

Table 7.8: CSHT SCCP for 4 hours

Sample	% indexed	Vmap value (μm)
1	52	1.02
2	50	0.9
3	51	0.91
4	55	0.84
5	54	0.82*
6	57	0.81
7	56	0.82
8	56	0.84
9	55	0.81
10	54	0.83
Average		**0.86**

Table 7.9: As-CR then 10%CW

Sample	% indexed	Vmap value (μm)
as-cold rolled 10%CW_1	63.47	0.62
2	61.1	0.65*
3	60.3	0.66
4	57.6	0.70
5	63.8	0.69
6	53.0	0.70
7	53.5	0.65
8	50.7	0.66
9	55.9	0.65
10	59.0	0.66
Average		**0.66**

Table 7.10: As-CR SCCP for 4 minutes

Sample	% indexed	Vmap value (μm)
1	66.1	0.67
2	63	0.70
3	67.2	0.72
4	75.5	0.68
5	77.4	0.66
6	73.2	0.65*
7	64.6	0.66
8	74.1	0.65
9	67.2	0.72
10	65.6	0.66
Average		**0.68**

Table 7.11: As-CR SCCP for 30 minutes

Sample	**% indexed**	**Vmap value (μm)**
1	70.7	0.64
2	68.1	0.70
3	71.2	0.64
4	70.7	0.63
5	75.7	0.64*
6	78.4	0.65
7	75.9	0.63
8	68.0	0.61
9	71.2	0.64
10	74	0.65
Average		**0.64**

Table 7.12: As-CR SCCP for 4 hours

Sample	**% indexed**	**Vmap value (μm)**
1	55	1.02
2	56	1.06
3	60	1.04
4	53	1.09*
5	57	1.01
6	52	0.98
7	55	0.99
8	58	1.04
9	55	1.06
10	59	1.01
Average		**1.03**

Appendix B Summary Bar Chart

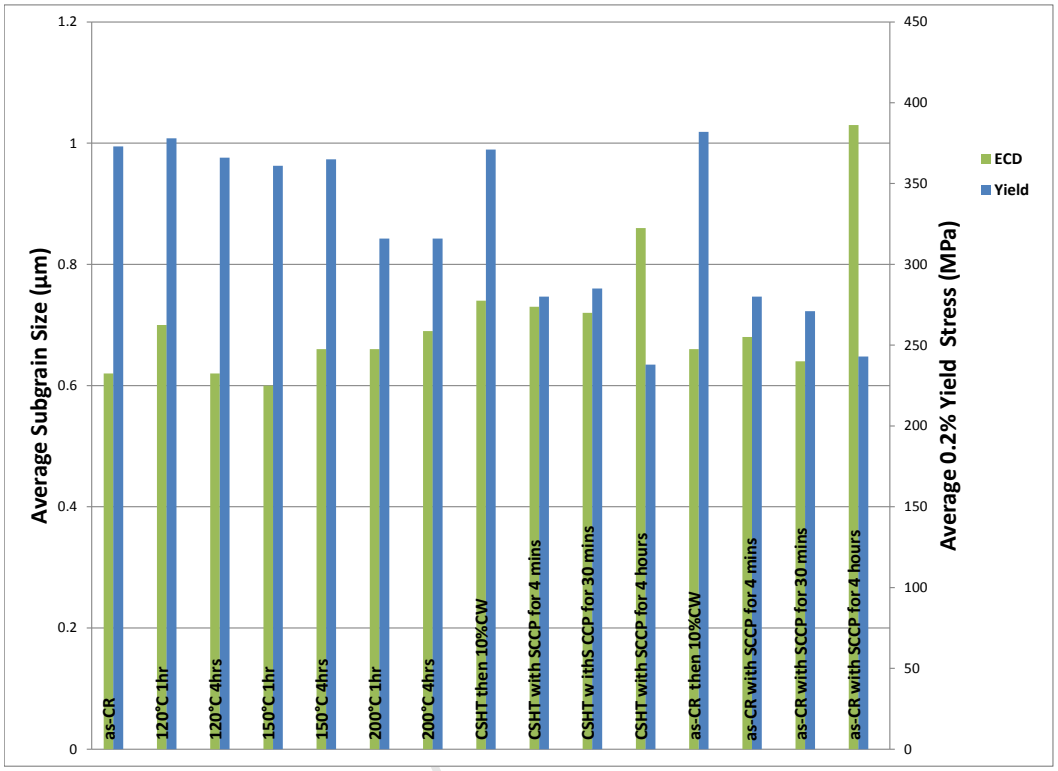

Figure 7.1: Summary bar chart of average subgrain sizes and average mechanical properties for all AA5182 specimens in this study.

Appendix C TEM Micrographs

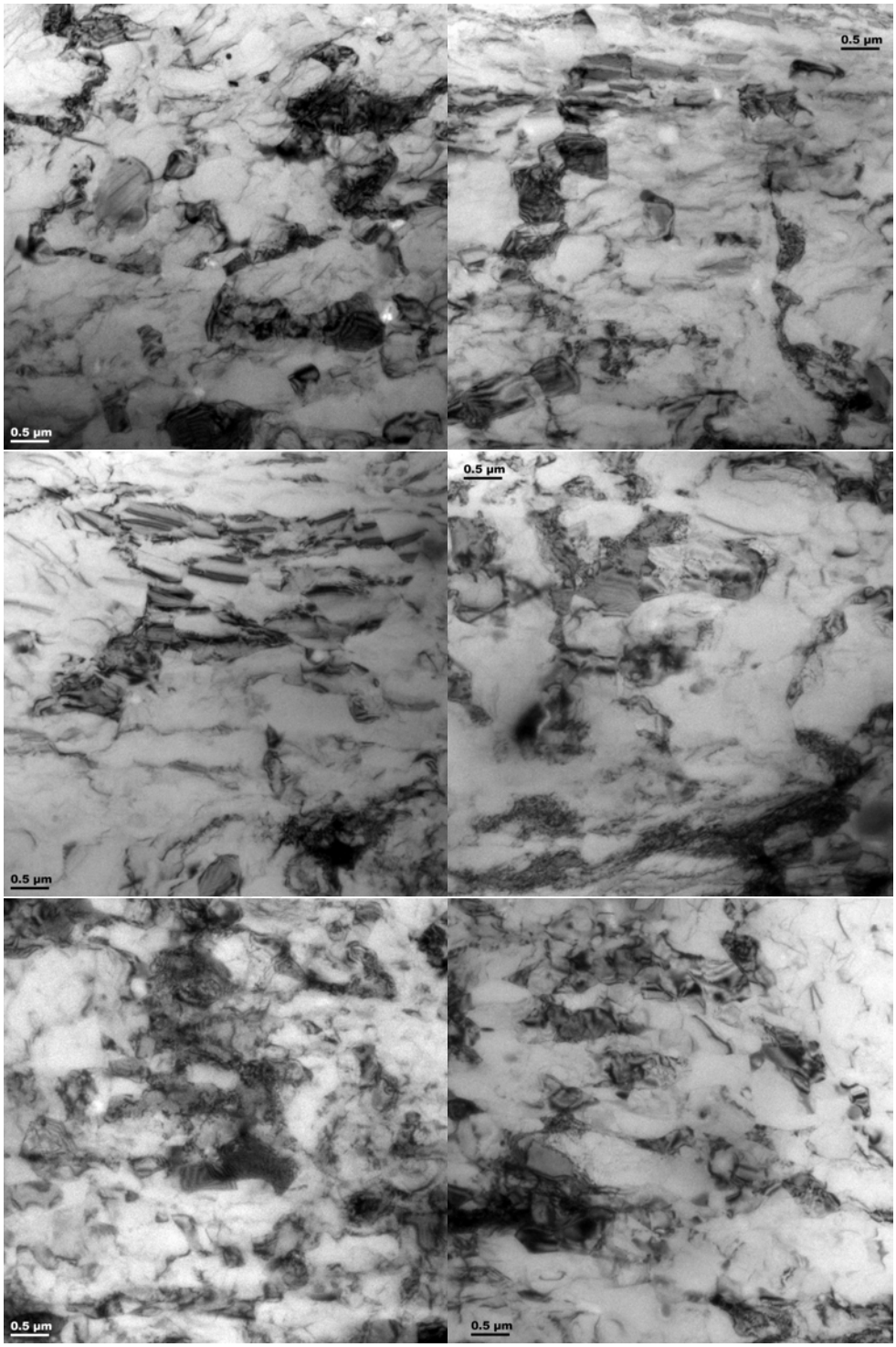

Figure 7.2: TEM micrographs of as-CR samples.

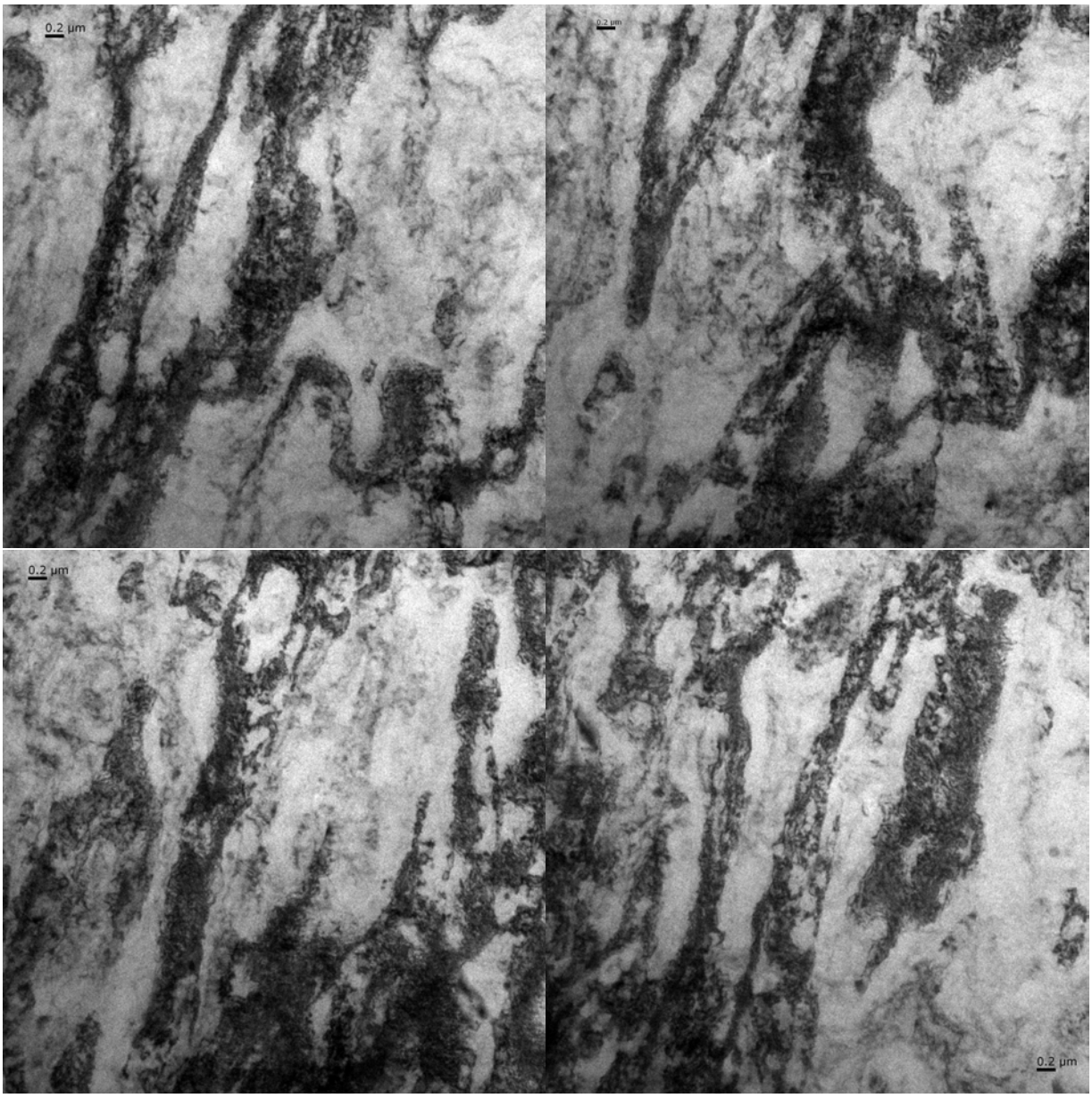

Figure 7.3: TEM micrographs of the CSHT samples.

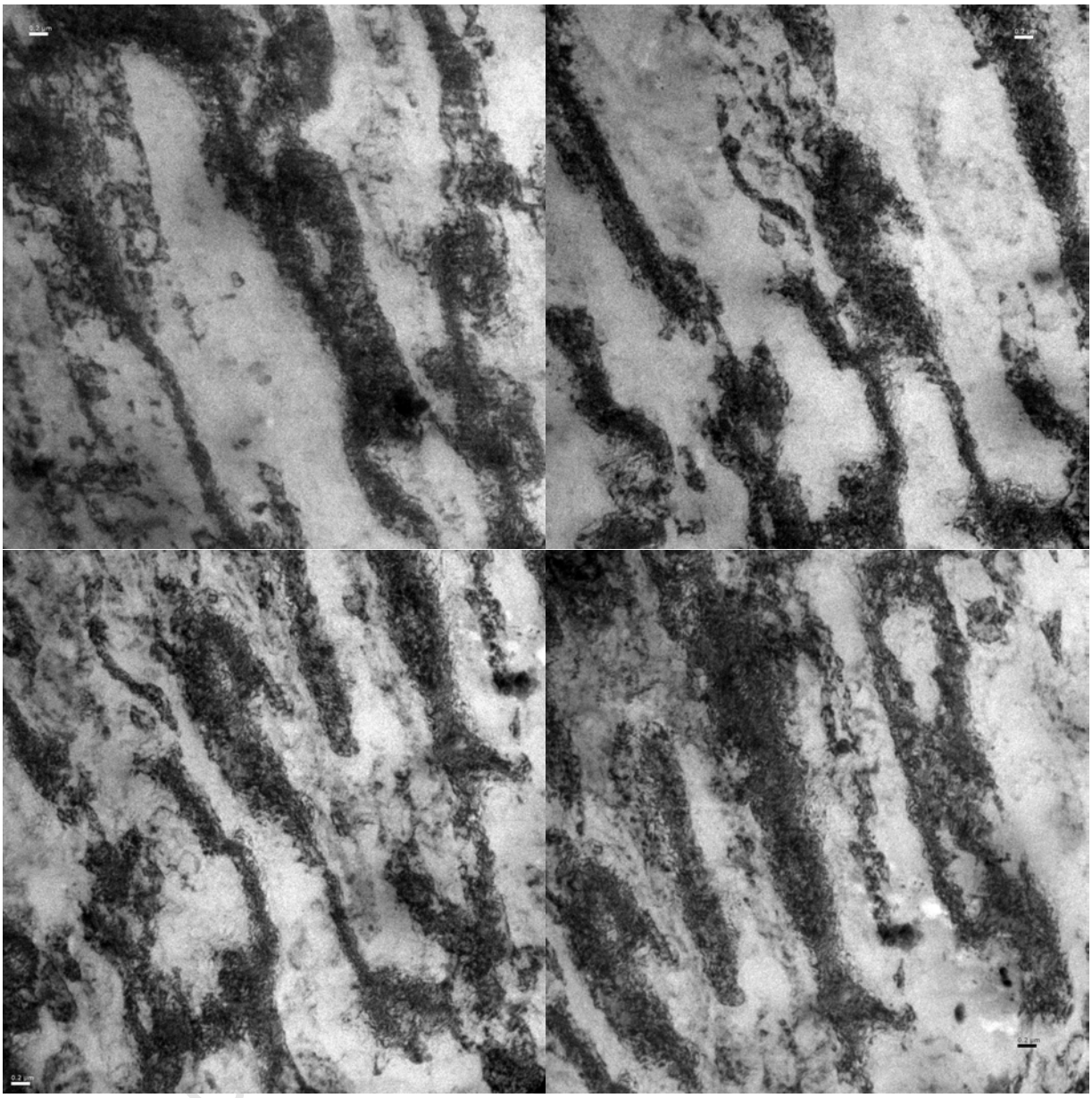

Figure 7.4: TEM micrographs of CSHT samples with 10% CW.

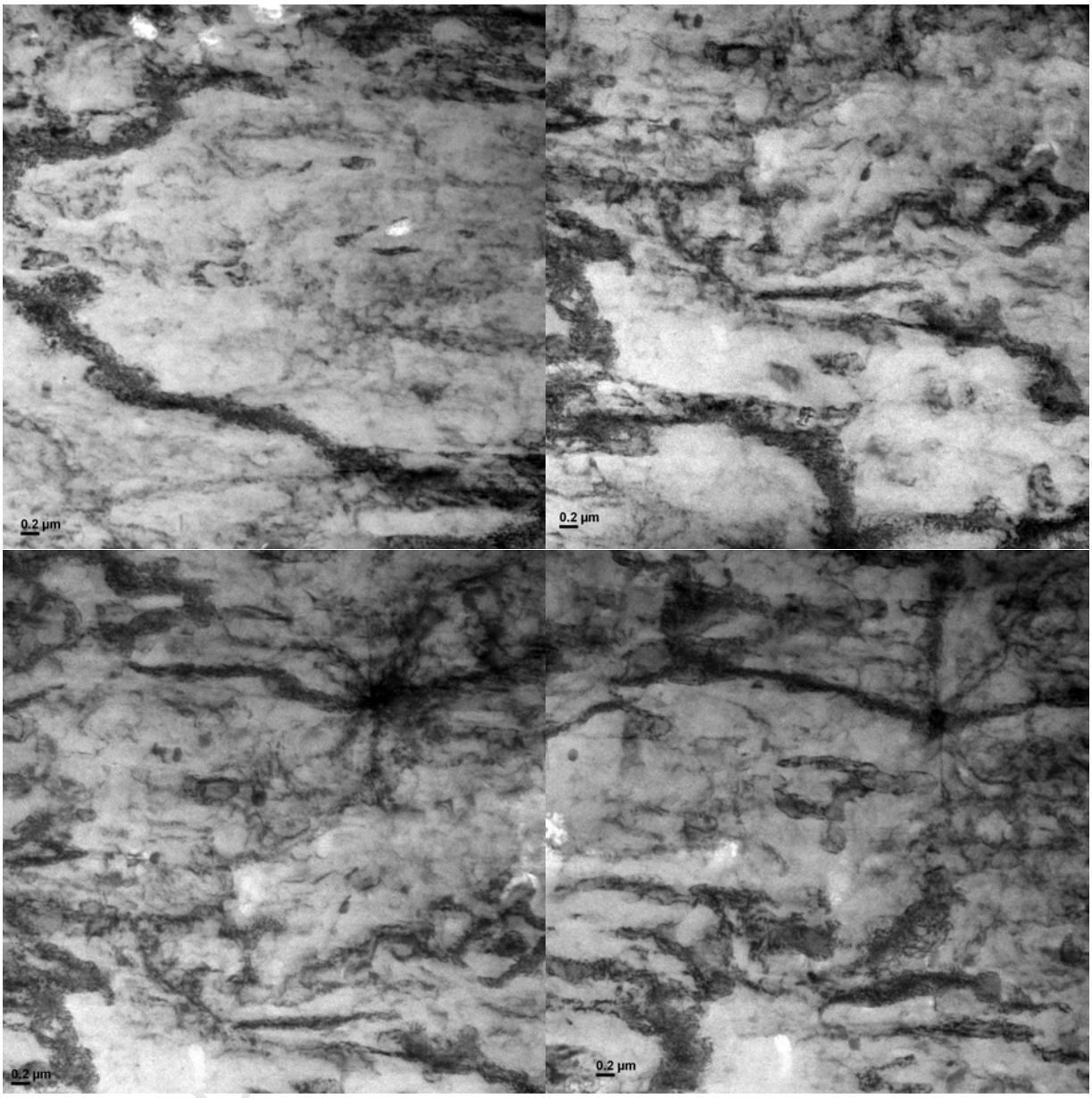

Figure 7.5: TEM micrographs of CSHT samples with SCCP for 4 minutes.

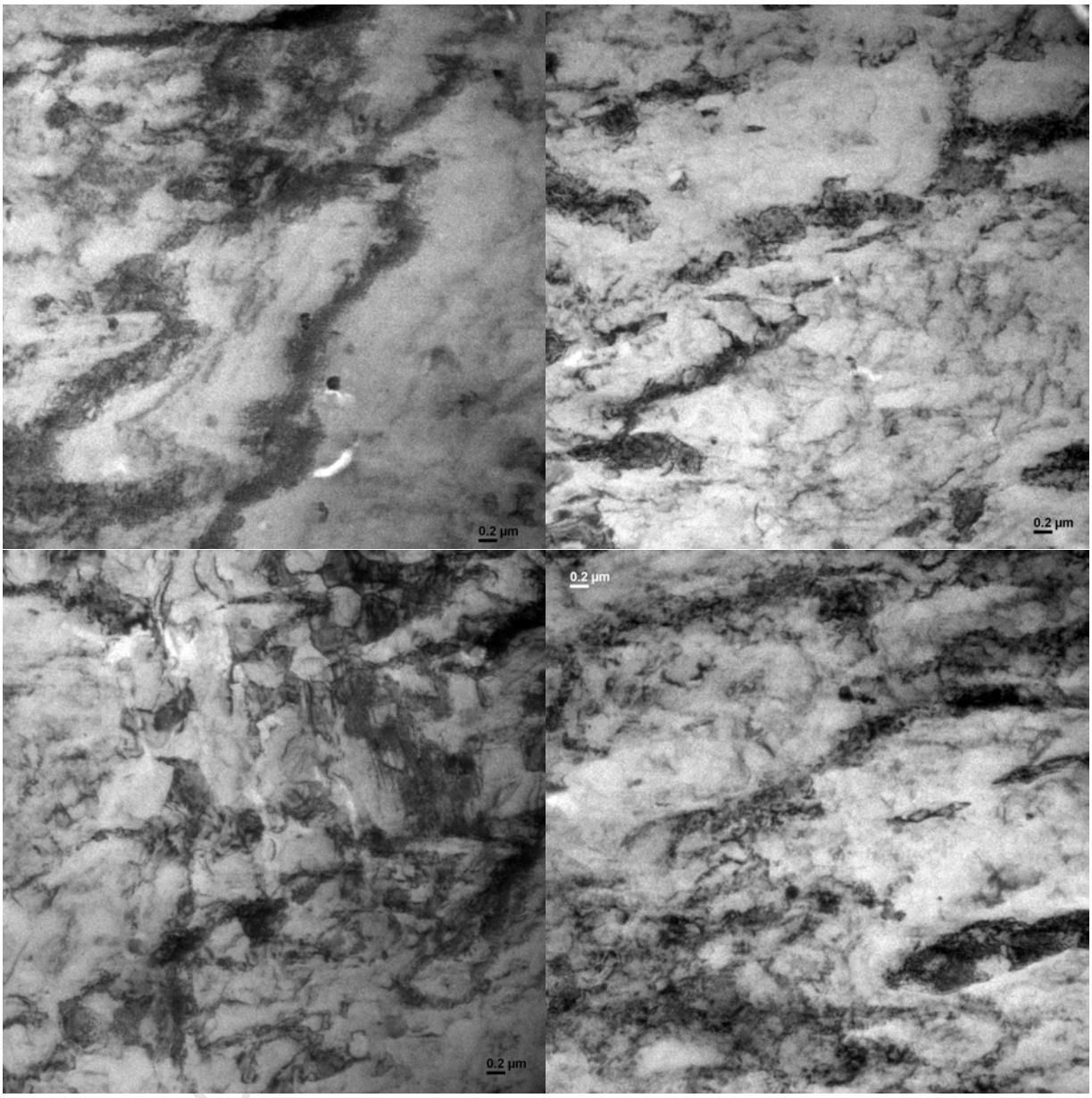

Figure 7.6: TEM micrographs of CSHT samples with SCCP for 30 minutes.

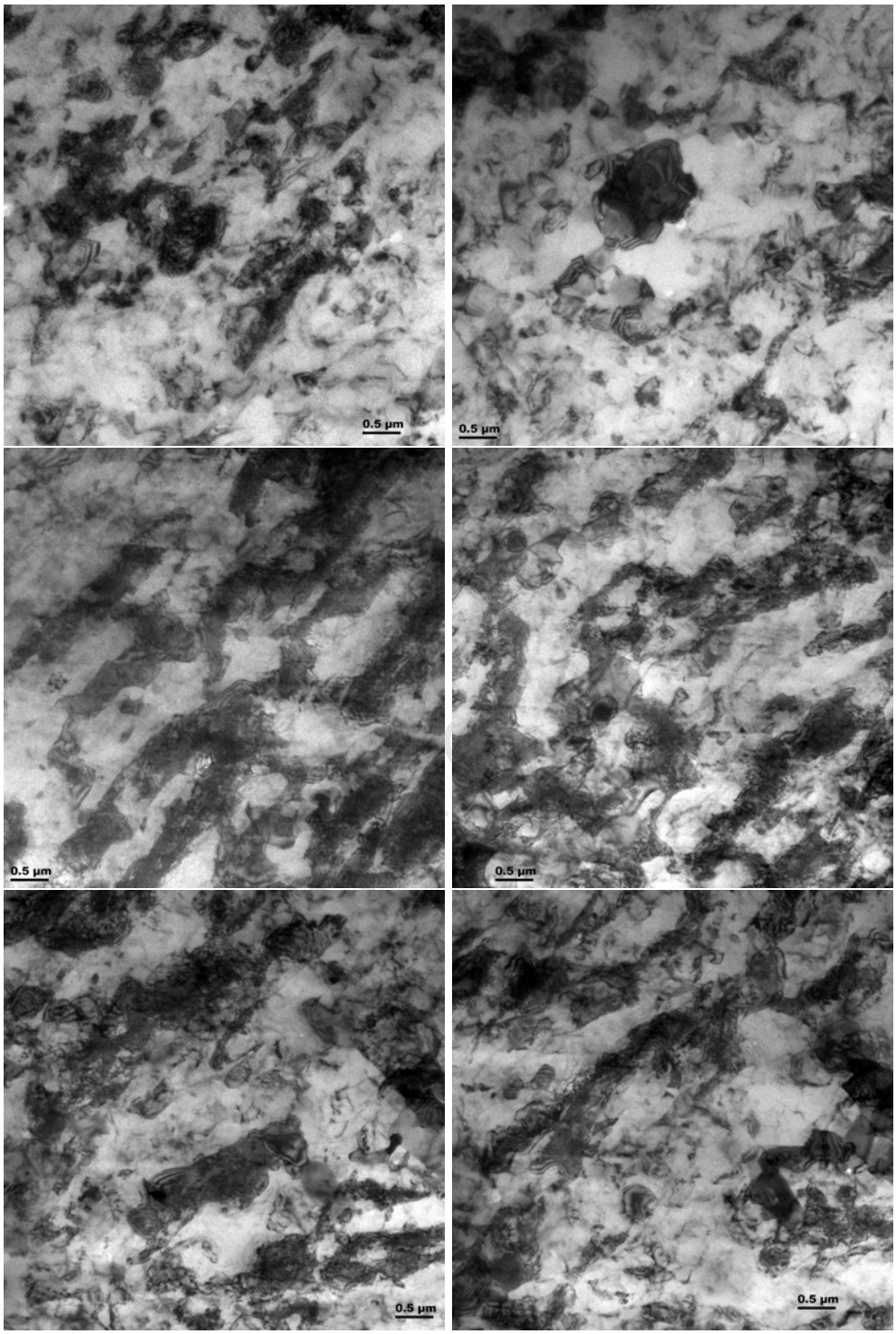

Figure 7.7: TEM micrographs of CSHT samples with SCCP for 4 hours.

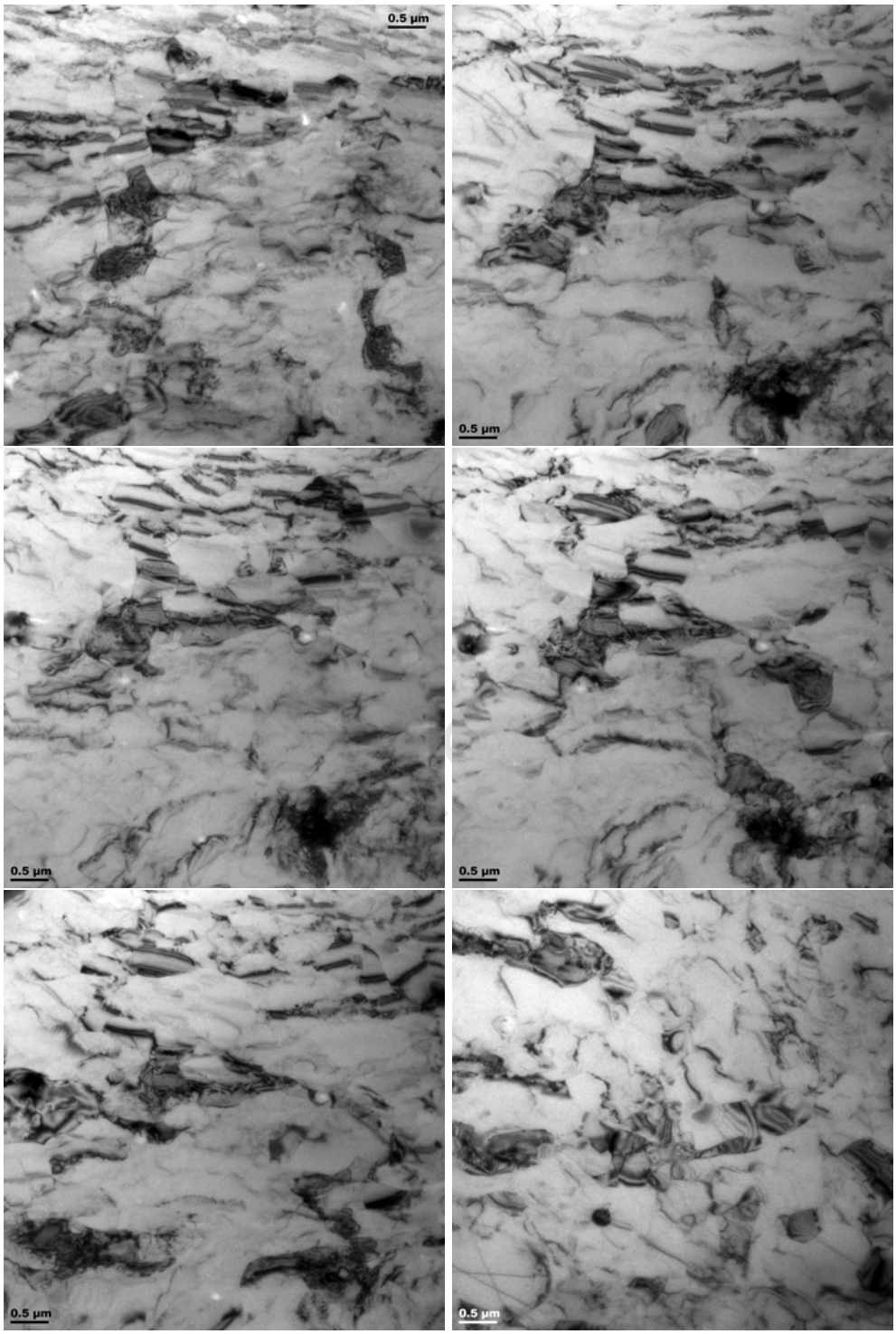

Figure 7.8: TEM micrographs of as-CR samples with SCCP for 4 hours.